Is instantaneous quantum Internet possible?

Mario Mastriani

ORCID Id: 0000-0002-5627-3935

Abstract - Instantaneous teleportation - the transmission and reconstruction over arbitrary distances of an unknown state without any type of disambiguation based on classical bits - is demonstrated, supporting the fact that instantaneous information transfer via an Einstein-Podolsky-Rosen channel is definitely possible. In other words, quantum correlations can be used to send signals, reinforcing the existence of an action at a distance, hence, paving the way for a better understanding of quantum entanglement and its consequent impact on Quantum Internet, as well as, on a realistic relationship between Special Relativity and Quantum Mechanics.

1. Introduction

Quantum entanglement [1-3] is at the center of a great controversy, which consists of the apparent violation of the local realism and causality [4, 5]. As a simple example of this, if we make a local measurement of the state of one of two entangled particles (e.g., the orientation of its spin) there is an instant notification to its counterpart, which adopts the opposite state of the first one (i.e., spin in the opposite orientation), even when both are at a distance where said notification required a trip at a faster-than-light speed [6, 7] to be instantaneous. According to Special Relativity [8] this is impossible. Such disagreement gives rise to the main cause of conflict between Quantum Mechanics [9] and Special Relativity [2, 5, 10]. As a result, there is a general consensus among scientists that this link cannot be used to transmit useful information at a superluminal speed [11-14]. However, an exception seems to represent a procedure known as quantum teleportation [15-19], which requires two classical bits of disambiguation to locally reconstruct the teleported state. This is done at the expense of a classical channel, therefore, the complete teleportation procedure itself is subject to the speed of the transmission for this channel, which, as it is evident, is the speed of light. In summary, teleportation does not represent a faster-than-light quantum communication procedure [15] at all.

Two no-go theorems, No-Signaling [20-24] and No-Communication [6, 25], establish that it is impossible to obtain an instantaneous notification about the result of a local measurement regarding the state of one of the two entangled particles between observers separated by distances such that said notification should travel to a faster-than-light speed. An instant notification would contradict the local realism [4] and causality [5] established in the EPR paradox (Einstein-Podolsky-Rosen) [26] which is absolutely consistent with Special Relativity [8]. In this context, the EPR paradox interprets the entanglement as a spooky action at a distance by virtue of the violation of the locality [27, 28], and it can only justify it by means of the existence of local hidden variables [29]. Bell's Theorem [30] and its later improvement through the Clauser-Horne-Shimony-Holt (CHSH) procedure [31] give an experimental framework to pass the problem to the initial locality hypotheses which will be tested in the light of subsequent experiments. These theorems establish unequal paths that if experimentally violated would prove the non-existence of local hidden variables and, at the same time, the non-locality nature of entanglement. However, this violation does not say anything about the possible existence of non-local hidden variables as established by several theories in this regard [32, 33], in particular, one of them of a deterministic nature [34].

The creators of the teleportation protocol [15] in the first lines of their paper's Introduction, literally, say: *The existence of long range correlations between Einstein-Podolsky-Rosen (EPR) [26] pairs of particles raises the question of their use for information transfer. Einstein himself used the word "telepathically" in this context [35]. It is known that instantaneous information transfer is definitely impossible [36]. Here, we show that EPR correlations can nevertheless assist in the "teleportation" of an intact quantum state from one place to another, by a sender who knows neither the state to be teleported nor the location of the intended receiver.*

If we delve further into the literature that deals with the subject of quantum teleportation, then we can see that all the conclusions about the impossibility of sending useful information through an EPR channel revolve, directly or indirectly, around quantum measurement [37, 38]. This is evident, since as a consequence of what is measured on one side, we are, apparently, faced with the impossibility of reconstructing the correct information instantaneously on the other side. This apparent impossibility in relation to entanglement will be put to the test in this work. In fact, it seems incredible that all the literature on this subject has not yet explained how a random phenomenon can be synchronized between two elements in a completely indifferent way to the distance that separates them, since what is important here is that nature communicates instantaneously and how this happens, no matter, whether or not, man can take advantage of these principles in a system for an instant communication. As a species, we face the same kind of problem that we have always faced: being in front of a wonderful force of nature and trying to control it for our benefit, and this is the keyword: control, which will be covered in depth from Section 3 onwards.

Showing up next, a setup with all the inexcusable tools needed to analyze this problem in depth is outlined in Section 2. In Section 3, we introduce the supporting experiments of Section 2 respect to quantum entanglement and quantum teleportation. In Section 4, we provide additional experiments, which constitute applications related to quantum internet. Section 5 is exclusively reserved to two techniques of quantum repeaters and a third technique resulting from the combination of the previous ones, and called hybridization. Finally, Section 6 provides a conclusion and future work proposals.

2. Entropic analysis

Although in the previous section we put quantum measurement at the center of the problem, what we are really talking about is information, given that while we do not measure the elements of the entangled pair, they are found in a combination of states, but when we measure them, i.e., we try to inform ourselves of its situation, the first particle randomly takes one of the following determined states: *spin-up* or *spin-down*, which is accompanied by the end of the entanglement. Once the state of the first particle is established, the state of the second one is deterministic and instantaneously determined as the opposite of the first one, regardless of the distance between them. Since, we are dealing with information, the best tools to use are Entropy and Mutual Information [1], through which we will carry out an entropic analysis of the problem posed in the previous section.

For a better understanding of all the concepts to be developed from now on, we will organize this section through the following subsections:
2.1 **Setup**: we will enunciate the minimum amount of necessary Quantum Information Processing tools [39], and we will define the concepts of Entropy and Mutual Information [1] on the basis of which we will develop the entropic analysis, which will be applied according to the degree of correlation between the particles, in the following subsections:
2.2 **Completely independent particles**,
2.3 **Classically-correlated particles**, and
2.4 **Entangled particles**.
2.5 **Consequences on Quantum Communications**: we will make important preliminary conclusions regarding the previous case.

Finally, before proceeding to the exhaustive entropic analysis of the problem raised in Section 1, we need to make some considerations:

1. From what was mentioned above, we can recognize the importance of organizing the analysis according to the existence of three well-defined populations in relation to the degree of correlation between particles. So that, if we go from the lowest to the highest degree of correlation, we will have independent, classically-correlated, and entangled particles [1]. As is evident, for all three cases, every known physical quantity must be conserved, namely: spin, mass, energy, moment of spin or torque, etc. As we will see, the three mentioned populations will hold their condition (i.e., independent, classically-correlated, and entangled) regardless of the distance between the particles. However, the third population (i.e., entangled particles) carries an added attribute, which consists of an effect of maximum correlation between said particles involved, with an instantaneous synchronization between them, and which is maintained even when the distance separating these entangled particles is infinite. Therefore, in order for the entanglement to be concomitant with this situation, we must raise a couple of hypotheses:

   a. If an effect is independent of distance, even if it is infinite, it is because something (or many things) related to that effect (i.e., some other physical entities) also accompanies the distance in that infinite potential increase of range in order to sustain said effect. This is evident, since the space in Physics is always linked with everything else: time, energy, etc.

   b. Everything must be conserved, without exception, because if something potentially infinite is involved, then that something must be compensated so that with each entanglement the universe is not unbalanced.

   These two items are in themselves a principle of exclusion, given that nothing in Physics can get out of range alone and decompensated without having serious consequences. While in the other two cases (independent, and classically-correlated) there is no need to make the effort to sustain any effect, therefore nothing needs to accompany a distance out of range.

2. Consistent with entropy, we will use a scalar notation based on spins in order to preserve a greater correspondence between the tools associated with entropy (as in the case of Mutual Information) and the spins themselves.

2.1. Setup

We will begin with the definition of the minimum amount of tools that are essential in this section. For pure states, that is, states on the Bloch's sphere [39-41] of **Figure 1**, any wave-function

$$|\psi\rangle = \alpha|0\rangle + \beta|1\rangle \tag{1}$$

arises from the superposition of the so-called Computational Basis States (CBS) and qubit basis states $\{|0\rangle, |1\rangle\}$, which are located at the poles of the already mentioned sphere with $|\alpha|^2 + |\beta|^2 = 1$, such that $\alpha \wedge \beta \in \mathbb{C}$ of a Hilbert's space [39]. Strictly, the complete wave-function will be

$$|\psi\rangle = e^{i\gamma}\left(cos\frac{\theta}{2}|0\rangle + e^{i\phi} sin\frac{\theta}{2}|1\rangle\right) = e^{i\gamma}\left(cos\frac{\theta}{2}|0\rangle + \left(cos\,\phi + i\,sin\,\phi\right)sin\frac{\theta}{2}|1\rangle\right) \tag{2}$$

where $0 \leq \theta \leq \pi$, $0 \leq \phi < 2\pi$ [39]. However, we can ignore the factor $e^{i\gamma}$ of Eq.(2), because it has no observable effects [40], and for that reason we can effectively write

$$|\psi\rangle = cos\frac{\theta}{2}|0\rangle + e^{i\phi} sin\frac{\theta}{2}|1\rangle \tag{3}$$

with $\alpha = cos\left(\theta/2\right)$ and $\beta = e^{i\phi} sin\left(\theta/2\right)$, being then equal to the Eq.(2). The numbers θ and ϕ define a point on the unit three-dimensional sphere, as shown in **Figure 1**.
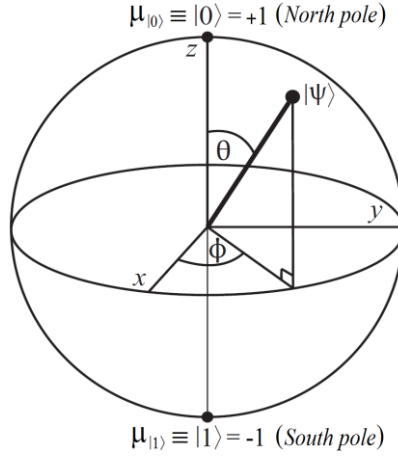
Figure 1 Bloch's Sphere.

Now, we can represent the mentioned poles in different ways. In fact, we introduce an alternative and very useful version for the task to be developed, which is a scalar way to represent the poles based on the orientation of the spins:

$$\left(Spin\ up = |\uparrow\rangle = |0\rangle = \begin{bmatrix} 1 \\ 0 \end{bmatrix} = North\ pole \right) \equiv \left(\mu_{|0\rangle} = 1 \right) \tag{4}$$

$$\left(Spin\ down = |\downarrow\rangle = |1\rangle = \begin{bmatrix} 0 \\ 1 \end{bmatrix} = South\ pole \right) \equiv \left(\mu_{|1\rangle} = -1 \right) \tag{5}$$

being $\mu_{|0\rangle}$ and $\mu_{|1\rangle}$ the scalar versions of the *spin up* $|0\rangle$ and the *spin down* $|1\rangle$, respectively, in such a way that the sum of both spins that represent the poles is null (i.e., it is conserved): $\mu_{|0\rangle} + \mu_{|1\rangle} = 0$, similarly to the case when a spinless particle decays in two new entangled particles with opposite spins [1, 2, 39]. We can see both spins (*up* and *down*) in the poles of **Figure 1**. The scalar notation based on μ is arithmetically more ductile than the Dirac's notation [39] based on <bra| and |ket> and allows us to work better with magnitudes and signs which will be fundamental in the analysis that we will do. In fact, in this notation, we associate the sign of μ with the mentioned spin orientation or polarization of the different particles. These μ's will have as much generality as the Dirac's notation in regards to its validity for all types of particles. Therefore, in this work, the letter μ will represent this concept, exclusively, and does not necessarily mean muon. Moreover, and based on CBS, we can define another basis, which will be very useful for the rest of this work as well as for quantum information in general [39], and quantum teleportation and superdense coding in particular [1, 15-19, 39, 42, 43]. Taking into account the interaction of two subsystems A and B, considering that their components are pure states and using their scalar versions here too, we will obtain,

$$\left(|0^A\rangle \otimes |0^B\rangle = |0^A\rangle|0^B\rangle = |0^A, 0^B\rangle = |0^A 0^B\rangle \right) \equiv \left(\mu_{|0^A 0^B\rangle} = \mu_{|0^{A,B}\rangle}^2 = 1 \right) \tag{6a}$$

$$\left(|1^A\rangle \otimes |1^B\rangle = |1^A\rangle|1^B\rangle = |1^A, 1^B\rangle = |1^A 1^B\rangle \right) \equiv \left(\mu_{|1^A 1^B\rangle} = -\mu_{|1^{A,B}\rangle}^2 = -1 \right) \tag{6b}$$

where $\otimes$ is the Kronecker's product, and $\mu_{|0^A 0^B\rangle}$ and $\mu_{|1^A 1^B\rangle}$ are the scalar version of $|0^A 0^B\rangle$ and $|1^A 1^B\rangle$, respectively, with $\mu_{|0^A 0^B\rangle} + \mu_{|1^A 1^B\rangle} = 0$, i.e., here also the spin is conserved between $\mu_{|0^A 0^B\rangle}$ and $\mu_{|1^A 1^B\rangle}$.

The rule of the signs that support the equivalences and equalities seen so far is very simple, however, extremely strict and important. Consequently with this, and being

$$|00\rangle = \begin{bmatrix} 1 \\ 0 \end{bmatrix} \otimes \begin{bmatrix} 1 \\ 0 \end{bmatrix} = \begin{bmatrix} 1 \\ 0 \\ 0 \\ 0 \end{bmatrix}, \quad |11\rangle = \begin{bmatrix} 0 \\ 1 \end{bmatrix} \otimes \begin{bmatrix} 0 \\ 1 \end{bmatrix} = \begin{bmatrix} 0 \\ 0 \\ 0 \\ 1 \end{bmatrix}, \quad |01\rangle = \begin{bmatrix} 1 \\ 0 \end{bmatrix} \otimes \begin{bmatrix} 0 \\ 1 \end{bmatrix} = \begin{bmatrix} 0 \\ 0 \\ 1 \\ 0 \end{bmatrix}, \quad |10\rangle = \begin{bmatrix} 0 \\ 1 \end{bmatrix} \otimes \begin{bmatrix} 1 \\ 0 \end{bmatrix} = \begin{bmatrix} 0 \\ 1 \\ 0 \\ 0 \end{bmatrix} \tag{7}$$

we are going to use them to build the famous Bell's bases [1-3], with 2-qubit vectors, the combined Hilbert space will be $H^{A\cup B} = H_2^A \otimes H_2^B$, and then we will have the following four vectors,

$$|\beta_{00}\rangle = |\Phi^+\rangle = \frac{1}{\sqrt{2}}(|00\rangle + |11\rangle), \quad |\beta_{10}\rangle = |\Phi^-\rangle = \frac{1}{\sqrt{2}}(|00\rangle - |11\rangle),$$
$$|\beta_{01}\rangle = |\Psi^+\rangle = \frac{1}{\sqrt{2}}(|01\rangle + |10\rangle), \quad |\beta_{11}\rangle = |\Psi^-\rangle = \frac{1}{\sqrt{2}}(|01\rangle - |10\rangle). \tag{8}$$

Moreover and considering that a maximally entangled pair emerges from a spinless particle, it is evident that the bases of the Eq.(8) must also comply with the conservation of the spin. Thus, for $|\beta_{00}\rangle$ and $|\beta_{10}\rangle$ we have

$$\frac{1}{\sqrt{2}}\left(|0^A 0^B\rangle \pm |1^A 1^B\rangle\right) \rightarrow \left(\mu_{|0^A\rangle} + \mu_{|0^B\rangle} + \mu_{|1^A\rangle} + \mu_{|1^B\rangle} = 0\right), \tag{9}$$

while that for $|\beta_{01}\rangle$ and $|\beta_{11}\rangle$ we will have,

$$\frac{1}{\sqrt{2}}\left(|0^A 1^B\rangle \pm |1^A 0^B\rangle\right) \rightarrow \left(\mu_{|0^A\rangle} + \mu_{|1^B\rangle} + \mu_{|1^A\rangle} + \mu_{|0^B\rangle} = 0\right), \tag{10}$$

which confirms the conservation of the spin for maximally entangled states. Finally, we must note that the negative sign in the middle of the simple bases $|0^A 0^B\rangle$ and $|1^A 1^B\rangle$ of Eq.(9) do not matter, nor do the negative sign in the middle of the simple bases $|0^A 1^B\rangle$ and $|1^A 0^B\rangle$ of Eq.(10).

Next, the concepts necessary for a better understanding of the next subsections will be developed. These concepts are: density matrix, entropy and mutual information [1]. The last one is important as a metric to ponder the degree of correlation between two subsystems. In this way, we recognize three levels of correlation between two subsystems: completely independent, classically-correlated and entangled subsystems. Besides, and as we have already said, we definitively opt for the scalar notation over the Dirac's notation based on <bra| and |ket> [39] since the former respects orientation (thanks to the sign of μ), magnitude (thanks to the value of μ) and is much more practical and flexible from the arithmetic point of view. Although we will refer to both types of notations (Dirac and scalar), deductions about the next subsections will be exclusively carried out through scalar notation from now on. Besides, since both entropy and mutual information are scalar magnitudes [1, 44], the use of scalar notation will be closer to an elegant treatment of the problem posed. Consequently, we are going to begin with the density matrix of the subsystems treated individually,

$$\rho^A = \rho^B = \frac{1}{2}\left(|0\rangle\langle 0| + |1\rangle\langle 1|\right) = \frac{1}{2}I = \frac{1}{2}\begin{bmatrix} 1 & 0 \\ 0 & 1 \end{bmatrix}, \tag{11}$$

where the scalar version of this operator, but based on the above defined μ, will be

$$r^A = r^B = \frac{1}{2}\left(\frac{\mu_{|0\rangle}^2 + \mu_{|1\rangle}^2}{\eta}\right) = \frac{1}{2}\left(\frac{\mu_{|0\rangle}^2 + \mu_{|1\rangle}^2}{2}\right), \tag{12}$$

where $\eta = 2$ is an adjustment parameter necessary to compensate the misadjustments existing between the traditional and scalar versions of the density matrix. We must note that $r^A = r^B = \frac{1}{2}$, which is consequent with the matrix nature of Eq.(11), in particular, in the context of the entropy that we will see later. However, with respect to the case of the system composed of two subsystems, its density matrix will depend on whether or not these subsystems are entangled. Therefore, for the non-entangled case, we will have:

$$\rho^{A\cup B} = \rho^A \otimes \rho^B , \tag{13}$$

but for the entangled case, the density matrix will be,

$$\rho^{A\cup B} \neq \rho^A \otimes \rho^B . \tag{14}$$

This operator will depend on each of the 3 cases that will be analyzed in the next subsections. Now, with respect to the entropy, we begin with the traditional definition [1], that is,

$$S^A = S^B = -tr\left[\rho^A log\left(\rho^A\right)\right] = -tr\left[\rho^B log\left(\rho^B\right)\right], \tag{15}$$

then, replacing Eq.(11) into Eq.(15), yields,

$$S^A = S^B = -tr\left[\frac{1}{2}\begin{bmatrix}1 & 0\\0 & 1\end{bmatrix} log\left(\frac{1}{2}\begin{bmatrix}1 & 0\\0 & 1\end{bmatrix}\right)\right] = 1, \tag{16}$$

while the scalar version of the entropy is,

$$S^A = S^B = -\kappa\left[r^A log\left(r^A\right)\right] = -\kappa\left[r^B log\left(r^B\right)\right], \tag{17}$$

where, κ is another adjustment parameter. Therefore, replacing Eq.(12) into Eq.(17), and remembering that: $\mu_{|0\rangle} = -\mu_{|1\rangle} = 1$, we will have a $\kappa = 2$, which yields,

$$S^A = S^B = -2\left[\frac{1}{2}\left(\frac{\mu_{|0\rangle}^2 + \mu_{|1\rangle}^2}{2}\right) log\left(\frac{1}{2}\left(\frac{\mu_{|0\rangle}^2 + \mu_{|1\rangle}^2}{2}\right)\right)\right] = -2\left[\frac{1}{2} log\left(\frac{1}{2}\right)\right] = 1 . \tag{18}$$

In the same way, for a composed system, the entropy is,

$$S^{A\cup B} = -tr\left[\rho^{A\cup B} log\left(\rho^{A\cup B}\right)\right] = -\kappa\left[r^{A\cup B} log\left(r^{A\cup B}\right)\right] . \tag{19}$$

In this case, κ depends on the degree of correlation (completely independent, classically-correlated, and entangled subsystems) between both subsystems. Moreover, in both worlds: the classical and the quantum, the correlations between the subsystems are those established by the additional information.

In the case of composite quantum systems, the mutual information $S^{A\cap B}$ is introduced to quantify that additional information, allowing us to obtain the degree of correlation between both subsystems [1],

$$S^{A\cap B} = S^A + S^B - S^{A\cup B} \geq 0 . \tag{20}$$

Therefore, the entropy of the composite system $S^{A\cap B}$ indicates that the uncertainty of a state $\rho^{A\cup B}$ is less than the two subsystems S^A and S^B added together. In other words, $S^{A\cap B}$ tells us how much

more information the composite system can store compared to the individual subsystems that compose it. Besides, $S^{A \cap B}$ measures the distance between the state $\rho^{A \cup B}$ and the non-entangled state $\rho^A \otimes \rho^B$ [1]. If states like Eq.(13) are separable states, then the reduced density matrices of Eq.(11) are pure states, thus the entropy of the state is zero. The nonzero value of the entropy of the reduced density matrix therefore is an indication of the possible existence of entanglement.

The entropy of the subsystems S^A and S^B is equal to one in all cases (i.e., $S^A = S^B = 1$); while the entropy of the composite system $S^{A \cup B}$ will have different values for each and every of the three cases. For the sake of simplicity, the subsystems are firstly expressed in qubits, to then be replaced by their corresponding spins. Making use of Eq.(20), the main idea is to relate correlations and entanglement to the entropy, and in particular, to the mutual information $S^{A \cap B}$. Then, in the next subsections, we will present the mutual information of the three types of subsystems: completely independent, classically correlated, and entangled, where the last one is critical for the development of subsequent subsections.

2.2. Completely independent subsystems

In this case, both subsystems have absolute and complete independence between them, i.e., $\rho^{A \cup B}$ is a Kronecker's product of density matrices like Eq.(13). We can clearly see this independence in **Figure 2**. Therefore, there are no correlations between such subsystems.
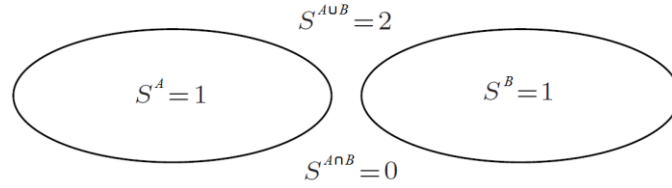

Figure 2 Completely independent subsystems.

In the computational basis of $H^A \otimes H^B$, $\rho^{A \cup B}$ takes the following form,

$$\rho^{A \cup B} = \frac{1}{4}\left(\left|0^A,0^B\right\rangle\left\langle 0^A,0^B\right| + \left|0^A,1^B\right\rangle\left\langle 0^A,1^B\right| + \left|1^A,0^B\right\rangle\left\langle 1^A,0^B\right| + \left|1^A,1^B\right\rangle\left\langle 1^A,1^B\right| \right) = \frac{1}{4}I, \quad (21)$$

where I is a 4x4 identity matrix. Then, replacing Eq.(21) into Eq.(19), $S^{A \cup B}$ will be

$$S^{A \cup B} = -tr\left\{ \frac{1}{4}\begin{bmatrix} 1 & 0 & 0 & 0 \\ 0 & 1 & 0 & 0 \\ 0 & 0 & 1 & 0 \\ 0 & 0 & 0 & 1 \end{bmatrix} \log\left(\frac{1}{4}\begin{bmatrix} 1 & 0 & 0 & 0 \\ 0 & 1 & 0 & 0 \\ 0 & 0 & 1 & 0 \\ 0 & 0 & 0 & 1 \end{bmatrix} \right) \right\} = 2. \quad (22)$$

Now, introducing the results of Eq.(18) and (22) into Eq.(20), we will have,

$$S^{A \cap B} = S^A + S^B - S^{A \cup B} = 1 + 1 - 2 = 0. \quad (23)$$

The result of Eq.(23) endorses the complete independence of the subsystems. In fact, if we remember the equivalences of Subsection 2.1, where $|0\rangle \equiv \mu_{|0\rangle}$, $|1\rangle \equiv \mu_{|1\rangle}$, $\left|0^A0^B\right\rangle \equiv \mu_{|0^A0^B\rangle}$, and $\left|1^A1^B\right\rangle \equiv \mu_{|1^A1^B\rangle}$, then, the scalar version of Eq.(21) will be,

$$r^{A\cup B} = \frac{1}{4}\left(\frac{\mu_{|0^A0^B\rangle}\mu_{|0^A0^B\rangle} + \mu_{|0^A1^B\rangle}\mu_{|0^A1^B\rangle} + \mu_{|1^A0^B\rangle}\mu_{|1^A0^B\rangle} + \mu_{|1^A1^B\rangle}\mu_{|1^A1^B\rangle}}{\eta}\right)$$

$$= \frac{1}{4}\left(\frac{\mu_{|0^{A,B}\rangle}^2\mu_{|0^{A,B}\rangle}^2 + \left(\mu_{|0^A\rangle}\mu_{|1^B\rangle}\right)\left(\mu_{|0^A\rangle}\mu_{|1^B\rangle}\right) + \left(\mu_{|1^A\rangle}\mu_{|0^B\rangle}\right)\left(\mu_{|1^A\rangle}\mu_{|0^B\rangle}\right) + \left(-\mu_{|1^{A,B}\rangle}^2\right)\left(-\mu_{|1^{A,B}\rangle}^2\right)}{4}\right) \qquad (24)$$

$$= \frac{1}{4}\left(\frac{\mu_{|0^{A,B}\rangle}^4 + \mu_{|0^A\rangle}^2\mu_{|1^B\rangle}^2 + \mu_{|1^A\rangle}^2\mu_{|0^B\rangle}^2 + \mu_{|1^{A,B}\rangle}^4}{\eta}\right) = \left(\frac{\mu_{|0^{A,B}\rangle}^4 + 2\mu_{|0^{A,B}\rangle}^2\mu_{|1^{A,B}\rangle}^2 + \mu_{|1^{A,B}\rangle}^4}{4^2}\right) = \left(\frac{\mu_{|0^{A,B}\rangle}^2 + \mu_{|1^{A,B}\rangle}^2}{4}\right)^2$$

where $\eta = 4$ for the purpose of adjusting its subsequent use into entropy. Besides, we must make the following deduction considering that: $\mu_{|0^{A,B}\rangle}^2 = \mu_{|1^{A,B}\rangle}^2 = 1$. Then, replacing Eq.(24) into the scalar version of Eq.(19) with $\kappa = 4$, and $S^{A\cup B} = 2$ from Eq.(22), we will have,

$$S^{A\cup B} = 2 = -\kappa\left[r^{A\cup B}\log\left(r^{A\cup B}\right)\right] = -4\left[\left(\frac{\mu_{|0^{A,B}\rangle}^2 + \mu_{|1^{A,B}\rangle}^2}{4}\right)^2\log\left(\left(\frac{\mu_{|0^{A,B}\rangle}^2 + \mu_{|1^{A,B}\rangle}^2}{4}\right)^2\right)\right] \qquad (25)$$

Then, we begin a series of actions on Eq.(25): simplifications, additions on both sides of the equal sign, selective passages of terms and replacements considering that $\mu_{|0^{A,B}\rangle}^2 = \mu_{|1^{A,B}\rangle}^2 = 1$,

$$\frac{4}{\left(\mu_{|0^{A,B}\rangle}^2 + \mu_{|1^{A,B}\rangle}^2\right)^2} = -\log\left(\frac{\mu_{|0^{A,B}\rangle}^2 + \mu_{|1^{A,B}\rangle}^2}{4}\right) \qquad (26)$$

$$\frac{4}{\left(\mu_{|0^{A,B}\rangle}^2 + \mu_{|1^{A,B}\rangle}^2\right)^2} + \log\left(\frac{\mu_{|0^{A,B}\rangle}^2}{2}\right) + \log\left(\frac{\mu_{|1^{A,B}\rangle}^2}{2}\right) = -\log\left(\frac{\mu_{|0^{A,B}\rangle}^2 + \mu_{|1^{A,B}\rangle}^2}{4}\right) + \log\left(\frac{\mu_{|0^{A,B}\rangle}^2}{2}\right) + \log\left(\frac{\mu_{|1^{A,B}\rangle}^2}{2}\right) \qquad (27)$$

$$1-1-1 = \log\left(\frac{\frac{\mu_{|0^{A,B}\rangle}^2}{2}\frac{\mu_{|1^{A,B}\rangle}^2}{2}}{\frac{\mu_{|0^{A,B}\rangle}^2 + \mu_{|1^{A,B}\rangle}^2}{4}}\right) \qquad (28)$$

$$-1 = \log\left(\frac{\mu_{|0^{A,B}\rangle}^2\mu_{|1^{A,B}\rangle}^2}{\mu_{|0^{A,B}\rangle}^2 + \mu_{|1^{A,B}\rangle}^2}\right) \qquad (29)$$

Finally,

$$\mu_{|\Uparrow^A\Uparrow^B\rangle} = \mu_{|\Uparrow^{A,B}\rangle}^2 = \frac{\mu_{|0^{A,B}\rangle}^2\mu_{|1^{A,B}\rangle}^2}{\mu_{|0^{A,B}\rangle}^2 + \mu_{|1^{A,B}\rangle}^2} = \frac{\mu_{|0^A0^B\rangle}\left(-\mu_{|1^A1^B\rangle}\right)}{\mu_{|0^A0^B\rangle} + \left(-\mu_{|1^A1^B\rangle}\right)} = \frac{\mu_{|0^A0^B\rangle}\mu_{|0^A0^B\rangle}}{\mu_{|0^A0^B\rangle} + \mu_{|0^A0^B\rangle}} = \frac{\mu_{|0^A0^B\rangle}}{2} = \frac{-\mu_{|1^A1^B\rangle}}{2} = 2^{-1} = \frac{1}{2} \qquad (30)$$

From Eq.(30), we can see that an entropic reflex appears as a consequence of this analysis, which, in reality, comes in a pair:

$$\left(\mu_{\left| \Uparrow^A \Uparrow^B \right\rangle} = \mu^2_{\left| \Uparrow^{A,B} \right\rangle} \right) = \left(-\mu_{\left| \Downarrow^A \Downarrow^B \right\rangle} = -\mu^2_{\left| \Downarrow^{A,B} \right\rangle} \right) \tag{31}$$

Equation (30) does not immediately expose the twin entropic reflex since this analysis was based on mutual information instead of complete information. Moreover, from here on, we can refer to these entropic reflexes as spectra, ghosts, shadows, alter-egos, or avatars. We choose avatars. Those avatars represented by Eq.(31) are second-degree-equivalent spins, i.e., second-degree avatars, for completely independent subsystems with a value of ½. As we will see later, there will also be first-degree avatars. It is evident that it would have been impossible to deduce the avatars with the Dirac's notation based on <bra| and |ket> or the tensor analysis [51]. **Figure 3** represents the graphic interpretation of Eq.(30).

Figure 3 Original second-degree spins and their corresponding second-degree-equivalent spins (μ^2) or second-degree avatars for completely independent particles. Besides, we can see the distances between them.

Figure 3 shows that $\mu_{\left| 0^A 0^B \right\rangle}$ is in position A, and $-\mu_{\left| 1^A 1^B \right\rangle}$ is in position B, where, the intersection of both light green lines allows us to determine the value of both second-degree avatars of Eq.(31), according to Eq.(30). But, what about their positions? To answer this question we will resort to the conservation of torque between the present spins of **Figure 3** and their corresponding lever arms,

$$\sum_{\forall i} \mu_i \times d_i = 0 = \mu_{\left| \Uparrow^A \Uparrow^B \right\rangle} \times d_{A'} + \mu_{\left| 0^A 0^B \right\rangle} \times d_A - \mu_{\left| 1^A 1^B \right\rangle} \times d_B - \mu_{\left| \Downarrow^A \Downarrow^B \right\rangle} \times d_{B'} \tag{32}$$

A direct consequence of the conservation of torque is that the avatars are the entropic expression of the originals, i.e., for the entropic analysis performed, the originals behave entropically as if they were the avatars, in fact, each original particle has its own avatar,

$$\mu_{\left| 0^A 0^B \right\rangle} \times d_A = \mu_{\left| \Uparrow^A \Uparrow^B \right\rangle} \times d_{A'} \tag{33a}$$

$$\mu_{\left| 1^A 1^B \right\rangle} \times d_B = \mu_{\left| \Downarrow^A \Downarrow^B \right\rangle} \times d_{B'} \tag{33b}$$

thus,

$$d_{A'} = \frac{\mu_{\left| 0^A 0^B \right\rangle}}{\mu_{\left| \Uparrow^A \Uparrow^B \right\rangle}} d_A = \frac{\mu_{\left| 0^A 0^B \right\rangle}}{\mu_{\left| 0^A 0^B \right\rangle} / 2} d_A = 2 \, d_A \tag{34a}$$

$$d_{B'} = \frac{\mu_{\left|1^A 1^B\right\rangle}}{\mu_{\left|\Downarrow^A \Downarrow^B\right\rangle}} d_B = \frac{\mu_{\left|1^A 1^B\right\rangle}}{\mu_{\left|1^A 1^B\right\rangle}/2} d_B = 2\, d_B \tag{34b}$$

From the entropic point of view, it is the avatars which will actually get involved in some degree of correlation. As we can see, the avatars are smaller than the originals and are further away from each other than the originals are. Therefore, the avatars are even more independent between them that the originals are between themselves and are more disconnected than them. In other words, the entropic analysis further deepens the independence situation between the particles, highlighting an absolute degree of decorrelation between them.

Now, based on **Figure 4**, if we move $-\mu_{\left|1^A 1^B\right\rangle}$ from position B to $\underline{B}$, and we leave $\mu_{\left|0^A 0^B\right\rangle}$ in its original position A$\equiv$$\underline{A}$, and reapply Eq.(30) to this new configuration, we will see that a new $\mu_{\left|\Uparrow^A \Uparrow^B\right\rangle} = \mu_{\left|\Uparrow^{A,B}\right\rangle}^2$ appears as a result of the two new intersected light green lines, passing from position A' to A", which has a value of ½ again, i.e., similar to the previous case of **Figure 3**, while $-\mu_{\left|\Downarrow^A \Downarrow^B\right\rangle} = \mu_{\left|\Downarrow^{A,B}\right\rangle}^2$ will move from position B' to B".

Figure 4 Completely independent subsystems with an increase in the separation of the original spins.

We can see this new result in **Figure 4**, where, the pink lines are parallel to the thick black line of the base and perpendicular to the arrows representing the spins. In other words, the pink lines indicate that the heights of the arrows that represent the spins $\mu_{\left|\Uparrow^A \Uparrow^B\right\rangle}$ are preserved regardless of the distance between both original particles ($\mu_{\left|0^A 0^B\right\rangle}, -\mu_{\left|1^A 1^B\right\rangle}$) on which Eq.(30) is applied. This indicates that the entropic reflexes or avatars are completely insensitive to the distance between the two original spins. Now, if we apply square root to both sides of Eq.(30), we will obtain the first-degree-equivalent spins or first-degree avatars,

$$\left[\mu_{\left|\Uparrow^{A,B}\right\rangle}, \mu_{\left|\Downarrow^{A,B}\right\rangle}\right] = \pm\sqrt{\mu_{\left|\Uparrow^A \Uparrow^B\right\rangle}} = \pm\sqrt{\mu_{\left|\Uparrow^{A,B}\right\rangle}^2} = \pm\sqrt{\frac{\mu_{\left|0^{A,B}\right\rangle}^2 \mu_{\left|1^{A,B}\right\rangle}^2}{\mu_{\left|0^{A,B}\right\rangle}^2 + \mu_{\left|1^{A,B}\right\rangle}^2}} = \frac{\pm\mu_{\left|0^{A,B}\right\rangle}}{\sqrt{1 + \left(\frac{\mu_{\left|0^{A,B}\right\rangle}}{\mu_{\left|1^{A,B}\right\rangle}}\right)^2}} = \pm\mu_{\left|0^{A,B}\right\rangle} \zeta = \pm\frac{\sqrt{2}}{2} \tag{35}$$

where

$$\zeta = \frac{1}{\sqrt{1 + \left(\dfrac{\mu_{|0^{A,B}\rangle}}{\mu_{|1^{A,B}\rangle}}\right)^2}} \tag{36}$$

is an scale factor [45-47], which is absolutely consequent with the contraction that suffers the avatars respect to the originals,

$$\mu_{|\Uparrow^{A,B}\rangle} = \mu_{|0^{A,B}\rangle}\,\zeta$$
$$\mu_{|\Downarrow^{A,B}\rangle} = \mu_{|1^{A,B}\rangle}\,\zeta \tag{37}$$

Moreover, the upper part of **Figure 5** shows the second-degree spins (μ^2), while the lower part of the same figure shows the first-degree spins (μ).

Figure 5 Upper part shows the second-degree spins (μ^2), while, lower part shoes the first-degree spins (μ), including distances for completely independent subsystems.

The lower part of **Figure 5** shows us the first-degree spins. The entropic analysis allows us to look inside what happens in a couple of subsystems, in fact, it is like taking an X-ray photograph inside them which will be more or less correlated.

11

In the case of the two original particles located in A and B, the lower part of **Figure 5** contemplates the two possible states that both original particles can take, i.e., *spin-up* or *spin-down*. If we apply a quantum measurement by detectors on some of these particles, then its orientation will be defined by one of both possibilities. Something similar is seen when we measure an entangled particle, with the difference that when measuring is made, then nature will randomly decide by one of the two possible orientations, and no matter which one it is, its entangled counterpart will take the opposite state.

Finally, avatars are only a reflex of the entropic behavior of the original spins, as well as a main witness of the degree of correlation of these, thanks to the conservation of torque, spins, energy, and everything else.

2.3. Classically-correlated subsystems

In this case, it is possible to create correlations without obtaining entanglement for $S^{A \cap B} \neq 0$ (**Figure 6**). For example, let us do this with the *separable mixture* of pure product states,

$$\rho^{A \cup B} = \frac{1}{2} \left(\left| 0^A, 0^B \right\rangle \left\langle 0^A, 0^B \right| + \left| 1^A, 1^B \right\rangle \left\langle 1^A, 1^B \right| \right). \tag{38}$$

Figure 6 Classically-correlated subsystems.

As we can see, $\rho^{A \cup B}$ of Eq.(38) contains fewer terms than the completely independent case of Eq.(21). In the computational basis of $H^A \otimes H^B$, $\rho^{A \cup B}$ will be:

$$\rho^{A \cup B} = \frac{1}{2} \begin{bmatrix} 1 & 0 & 0 & 0 \\ 0 & 0 & 0 & 0 \\ 0 & 0 & 0 & 0 \\ 0 & 0 & 0 & 1 \end{bmatrix}. \tag{39}$$

Therefore, replacing Eq.(39) into Eq.(19), $S^{A \cup B}$ will be

$$S^{A \cup B} = -tr \left\{ \frac{1}{2} \begin{bmatrix} 1 & 0 & 0 & 0 \\ 0 & 0 & 0 & 0 \\ 0 & 0 & 0 & 0 \\ 0 & 0 & 0 & 1 \end{bmatrix} \log \left(\frac{1}{2} \begin{bmatrix} 1 & 0 & 0 & 0 \\ 0 & 0 & 0 & 0 \\ 0 & 0 & 0 & 0 \\ 0 & 0 & 0 & 1 \end{bmatrix} \right) \right\} = 1. \tag{40}$$

Next, introducing the results of Equations (18) and (40) into Eq.(20), yields the following

$$S^{A \cap B} = S^A + S^B - S^{A \cup B} = 1 + 1 - 1 = 1. \tag{41}$$

This result brings out a certain degree of correlation between the subsystems. Then, if we remember the equivalences of Eq.(6), the scalar version of Eq.(38) will be,

$$r^{A \cup B} = \frac{1}{2}\left(\frac{\mu_{|0^A 0^B\rangle}\mu_{|0^A 0^B\rangle} + \mu_{|1^A 1^B\rangle}\mu_{|1^A 1^B\rangle}}{\eta} \right) = \frac{1}{2}\left(\frac{\mu^2_{|0^{A,B}\rangle}\mu^2_{|0^{A,B}\rangle} + \left(-\mu^2_{|1^{A,B}\rangle}\right)\left(-\mu^2_{|1^{A,B}\rangle}\right)}{4} \right)$$

$$= \frac{1}{2}\left(\frac{\mu^4_{|0^{A,B}\rangle} + \mu^4_{|1^{A,B}\rangle}}{4} \right) = \frac{\mu^4_{|0^{A,B}\rangle} + \mu^4_{|1^{A,B}\rangle}}{8}$$

(42)

where $\eta = 4$ for the same reasons as for the completely independent case, where we also consider: $\mu^4_{|0^{A,B}\rangle} = \mu^4_{|1^{A,B}\rangle} = 1$. Then, replacing Eq.(42) into the scalar version of Eq.(19) with $\kappa = 2$, and $S^{A \cup B} = 1$ from Eq.(40), we will have,

$$S^{A \cup B} = 1 = -\kappa\left[r^{A \cup B} log\left(r^{A \cup B}\right) \right] = -2\left(\frac{\mu^4_{|0^{A,B}\rangle} + \mu^4_{|1^{A,B}\rangle}}{8} \right) log\left(\frac{\mu^4_{|0^{A,B}\rangle} + \mu^4_{|1^{A,B}\rangle}}{8} \right).$$

(43)

Then, we begin a series of actions on Eq.(43): simplifications, additions on both sides of the equal sign, selective passages of terms and replacements considering that $\mu^4_{|0^{A,B}\rangle} = \mu^4_{|1^{A,B}\rangle} = 1$,

$$\frac{4}{\left(\mu^4_{|0^{A,B}\rangle} + \mu^4_{|1^{A,B}\rangle} \right)} = -log\left(\frac{\mu^4_{|0^{A,B}\rangle} + \mu^4_{|1^{A,B}\rangle}}{8} \right)$$

(44)

$$= -\left[log\left(\mu^4_{|0^{A,B}\rangle} + \mu^4_{|1^{A,B}\rangle} \right) - log\left(2^3\right) \right] = -log\left(\mu^4_{|0^{A,B}\rangle} + \mu^4_{|1^{A,B}\rangle} \right) + 3$$

$$\frac{4}{\left(\mu^4_{|0^{A,B}\rangle} + \mu^4_{|1^{A,B}\rangle} \right)} - 3 + log\left(\mu^4_{|0^{A,B}\rangle} \right) + log\left(\mu^4_{|1^{A,B}\rangle} \right) = -log\left(\mu^4_{|0^{A,B}\rangle} + \mu^4_{|1^{A,B}\rangle} \right) + log\left(\mu^4_{|0^{A,B}\rangle} \right) + log\left(\mu^4_{|1^{A,B}\rangle} \right)$$

(45)

$$2 - 3 + 0 + 0 = -1 = log\left(\frac{\mu^4_{|0^{A,B}\rangle}\mu^4_{|1^{A,B}\rangle}}{\mu^4_{|0^{A,B}\rangle} + \mu^4_{|1^{A,B}\rangle}} \right)$$

(46)

Finally,

$$\mu^2_{|\Uparrow^A \Uparrow^B\rangle} = \mu^4_{|\Uparrow^{A,B}\rangle} = \frac{\mu^4_{|0^{A,B}\rangle}\mu^4_{|1^{A,B}\rangle}}{\mu^4_{|0^{A,B}\rangle} + \mu^4_{|1^{A,B}\rangle}} = \frac{\mu^4_{|0^{A,B}\rangle}\mu^4_{|0^{A,B}\rangle}}{\mu^4_{|0^{A,B}\rangle} + \mu^4_{|0^{A,B}\rangle}} = \frac{\mu^4_{|0^{A,B}\rangle}}{2} = 2^{-1} = \frac{1}{2}$$

(47)

Anew, this would have remained hidden if not for this type of treatment: the scalar notation.

On the other hand, if we did a graphic representation of Eq.(47), as the one done in the previous case for Eq.(30) (i.e., completely independent), such graphical representation would show us, here also, that the avatars are completely insensitive to the distance between the original spins, both for the second and first-degree spins.

Now, if we apply the fourth root to both sides of Eq.(47), we obtain the final values of the first-degree avatars.

$$\left[\mu_{\Uparrow^{A,B}},\mu_{\Rightarrow^{A,B}},\mu_{\Downarrow^{A,B}},\mu_{\Leftarrow^{A,B}}\right]=\sqrt[4]{\mu_{\left|\Uparrow^{A,B}\right\rangle}^{4}}\left[+1,+i,-1,-i\right]=\sqrt[4]{\frac{\mu_{\left|0^{A,B}\right\rangle}^{4}\mu_{\left|1^{A,B}\right\rangle}^{4}}{\mu_{\left|0^{A,B}\right\rangle}^{4}+\mu_{\left|1^{A,B}\right\rangle}^{4}}}\left[+1,+i,-1,-i\right]$$

$$=\frac{\mu_{\left|0^{A,B}\right\rangle}\left[+1,+i,-1,-i\right]}{\sqrt[4]{1+\left(\dfrac{\mu_{\left|0^{A,B}\right\rangle}}{\mu_{\left|1^{A,B}\right\rangle}}\right)^{4}}}=\mu_{\left|0^{A,B}\right\rangle}\varsigma\left[+1,+i,-1,-i\right]$$

(48)

being

$$\varsigma=\frac{1}{\sqrt[4]{1+\left(\dfrac{\mu_{\left|0^{A,B}\right\rangle}}{\mu_{\left|1^{A,B}\right\rangle}}\right)^{4}}}=\frac{1}{\sqrt[4]{2}}$$

(49)

Here too, the avatars suffer a contraction with respect to the original spins in a factor ς

$$\mu_{\Uparrow^{A,B}}=\mu_{\left|0^{A,B}\right\rangle}\varsigma$$
$$\mu_{\Rightarrow^{A,B}}=i\,\mu_{\left|0^{A,B}\right\rangle}\varsigma$$
$$\mu_{\Downarrow^{A,B}}=-\mu_{\left|0^{A,B}\right\rangle}\varsigma=\mu_{\left|1^{A,B}\right\rangle}\varsigma$$
$$\mu_{\Leftarrow^{A,B}}=-i\,\mu_{\left|0^{A,B}\right\rangle}\varsigma=i\,\mu_{\left|1^{A,B}\right\rangle}\varsigma$$

(50)

while, the avatars' positions can also be calculated thanks to the torque conservation, with a set of equations similar to (32), (33), and (34).

Finally, we will not go into detail with this degree of correlation because it does not align with the central idea of this work.

2.4. Entangled subsystems

This is undoubtedly the most important case of the three, because of its projection on quantum communications, which will have a separate subsection later on, for its preliminary conclusions.

For this case, we are going to resort to **Figure 7**. First, we will take one of Bell's states of Eq.(8) and as an example, specifically $\left|\beta_{00}\right\rangle=\left|\Phi^{+}\right\rangle$, with $\rho^{A\cup B}$ from Eq.(51),

$$\rho^{A\cup B}=\frac{1}{4}\left(\left|0^{A},0^{B}\right\rangle\left\langle0^{A},0^{B}\right|+\left|0^{A},0^{B}\right\rangle\left\langle1^{A},1^{B}\right|+\left|1^{A},1^{B}\right\rangle\left\langle0^{A},0^{B}\right|+\left|1^{A},1^{B}\right\rangle\left\langle1^{A},1^{B}\right|\right).$$
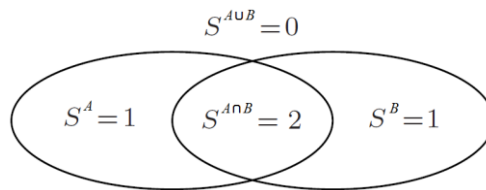
(51)

Figure 7 Entangled subsystems.

Besides, given that for this case $S^{A \cup B} = 0$, we are going to introduce this value and the results of Eq.(16) into Eq.(20). Consequently, we will obtain the following:

$$S^{A \cap B} = S^A + S^B - S^{A \cup B} = 1 + 1 - 0 = 2 .$$

(52)

On the other hand, as in the other two cases (completely independent and classically correlated), we will use, the scalar notation where the polarizations or orientations of the spins (μ and μ^2) are represented by the sign of a scalar: *spin-up* $\equiv$ +1 and *spin-down* $\equiv$ -1. We will start with the calculation of $r^{A \cup B}$,

$$
\begin{aligned}
r^{A \cup B} &= \frac{1}{4} \left(\frac{\mu_{\left|0^A 0^B\right\rangle} \mu_{\left|0^A 0^B\right\rangle} + \mu_{\left|0^A 0^B\right\rangle} \mu_{\left|1^A 1^B\right\rangle} + \mu_{\left|1^A 1^B\right\rangle} \mu_{\left|0^A 0^B\right\rangle} + \mu_{\left|1^A 1^B\right\rangle} \mu_{\left|1^A 1^B\right\rangle}}{\eta} \right) \\
&= 4 \left(\frac{\mu_{\left|0^{A,B}\right\rangle}^2 \mu_{\left|0^{A,B}\right\rangle}^2 + \mu_{\left|0^{A,B}\right\rangle}^2 \left(-\mu_{\left|1^{A,B}\right\rangle}^2\right) + \left(-\mu_{\left|1^{A,B}\right\rangle}^2\right) \mu_{\left|0^{A,B}\right\rangle}^2 + \left(-\mu_{\left|1^{A,B}\right\rangle}^2\right)\left(-\mu_{\left|1^{A,B}\right\rangle}^2\right)}{4} \right), \\
&= \frac{1}{4} \left(\frac{\mu_{\left|0^{A,B}\right\rangle}^4 - 2\mu_{\left|0^{A,B}\right\rangle}^2 \mu_{\left|1^{A,B}\right\rangle}^2 + \mu_{\left|1^{A,B}\right\rangle}^4}{4} \right) = \left(\frac{\mu_{\left|0^{A,B}\right\rangle}^2 - \mu_{\left|1^{A,B}\right\rangle}^2}{4} \right)^2
\end{aligned}
$$

(53)

where we need to use $\eta = 4$ for the same reasons that we had in the previous cases. In fact, η has always the same value, where we must remember that: $\mu_{\left|0^{A,B}\right\rangle}^2 = \mu_{\left|1^{A,B}\right\rangle}^2 = 1$. Then, replacing Eq.(53) into the scalar version of Eq.(19) with $\kappa = 4$, we will have,

$$
\begin{aligned}
S^{A \cup B} = 0 = -\kappa \left[r^{A \cup B} log\left(r^{A \cup B} \right) \right] &= -4 \left[\left(\frac{\mu_{\left|0^{A,B}\right\rangle}^2 - \mu_{\left|1^{A,B}\right\rangle}^2}{4} \right)^2 log\left(\left(\frac{\mu_{\left|0^{A,B}\right\rangle}^2 - \mu_{\left|1^{A,B}\right\rangle}^2}{4} \right)^2 \right) \right] \\
&= -\frac{1}{2} \left(\mu_{\left|0^{A,B}\right\rangle}^2 - \mu_{\left|1^{A,B}\right\rangle}^2 \right)^2 log\left(\frac{\mu_{\left|0^{A,B}\right\rangle}^2 - \mu_{\left|1^{A,B}\right\rangle}^2}{4} \right)
\end{aligned}
$$

(54)

Passing the term outside logarithm on the right side of Eq.(54) to denominator on the left side, then

$$\frac{0}{\frac{1}{2}\left(\mu_{\left|0^{A,B}\right\rangle}^2 - \mu_{\left|1^{A,B}\right\rangle}^2 \right)^2} = \infty = -log\left(\frac{\mu_{\left|0^{A,B}\right\rangle}^2 - \mu_{\left|1^{A,B}\right\rangle}^2}{4} \right).$$

(55)

That is to say, on the left side of Eq.(55), the denominator tends to zero with more power than the numerator. In fact, the right side verifies it, because, -log(0) = ∞. From Eq.(55), we begin a series of simplifications, additions on both sides of the equal sign, selective passages of terms and replacements that do not alter the equation,

$$\infty + log\left(\frac{\mu_{\left|0^{A,B}\right\rangle}^2}{2} \right) + log\left(\frac{\mu_{\left|1^{A,B}\right\rangle}^2}{2} \right) = -log\left(\frac{\mu_{\left|0^{A,B}\right\rangle}^2 - \mu_{\left|1^{A,B}\right\rangle}^2}{4} \right) + log\left(\frac{\mu_{\left|0^{A,B}\right\rangle}^2}{2} \right) + log\left(\frac{\mu_{\left|1^{A,B}\right\rangle}^2}{2} \right).$$

(56)

Making use of the selective replacements, we will have,

15

$$\infty - 1 - 1 = log\left(\dfrac{\dfrac{\mu^2_{|0^{A,B}\rangle}}{2} \dfrac{\mu^2_{|1^{A,B}\rangle}}{2}}{\dfrac{\mu^2_{|0^{A,B}\rangle} - \mu^2_{|1^{A,B}\rangle}}{4}}\right) = log\left(\dfrac{\mu^2_{|0^{A,B}\rangle}\mu^2_{|1^{A,B}\rangle}}{\mu^2_{|0^{A,B}\rangle} - \mu^2_{|1^{A,B}\rangle}}\right) = log\left(\mu_{|\Uparrow^A\Uparrow^B\rangle}\right) = log\left(\mu^2_{|\Uparrow^{A,B}\rangle}\right), \tag{57}$$

Finally, the second-degree avatars will be

$$\mu_{|\Uparrow^A\Uparrow^B\rangle} = \mu^2_{|\Uparrow^{A,B}\rangle} = \dfrac{\mu^2_{|0^{A,B}\rangle}\mu^2_{|1^{A,B}\rangle}}{\mu^2_{|0^{A,B}\rangle} - \mu^2_{|1^{A,B}\rangle}} = \dfrac{\mu_{|0^A0^B\rangle}\left(-\mu_{|1^A1^B\rangle}\right)}{\mu_{|0^A0^B\rangle} - \left(-\mu_{|1^A1^B\rangle}\right)} = \dfrac{-\mu_{|0^A0^B\rangle}\mu_{|1^A1^B\rangle}}{\mu_{|0^A0^B\rangle} + \mu_{|1^A1^B\rangle}} = 2^\infty = +\infty \tag{58}$$

The graphic interpretation of Eq.(58) can be seen in **Figure 8**, which shows that $\mu_{|0^A0^B\rangle}$ is in position B, and $\mu_{|1^A1^B\rangle}$ is in position A, where, the intersection of both light green lines allows us to determine the spin values, according to Eq.(58),

Figure 8 Graphic representation of entangled subsystems with scalar notation.

Actually, Eq.(58) has two possible values, i.e., $\pm\infty$, which can be observed at both ends of **Figure 8**, where both light green lines are cut. Such light green lines connect the top of $\mu_{|0^A0^B\rangle}$ with the tail of $\mu_{|1^A1^B\rangle}$ and the top of $\mu_{|1^A1^B\rangle}$ with the tail of $\mu_{|0^A0^B\rangle}$. These results are shown in the Eq.(59)

$$\left[\mu_{|\Uparrow^A\Uparrow^B\rangle}, \mu_{|\Downarrow^A\Downarrow^B\rangle}\right] = \left[\mu^2_{|\Uparrow^{A,B}\rangle}, -\mu^2_{|\Downarrow^{A,B}\rangle}\right] = \left[+\infty, -\infty\right] \tag{59}$$

Before analyzing the positions of the second-degree avatars of Eq.(59), we must remember that in every entanglement process there are two entangled particles (at least) as those mentioned in Eq.(8), e.g., a pair of $|\beta_{00}\rangle$, i.e., we have a duplication of the graph of **Figure 8** as shown in **Figure 9**.

Figure 9 Graphic representation of an entangled subsystem for an EPR pair.

As we will see below, the second-degree avatars are exactly in the middle of the original particles. The set of particles located in **A** represent the entangled particle $|\beta_{00}\rangle$ in Alice's hands, while the set of particles located in **B** represent the other entangled particle $|\beta_{00}\rangle$ of the EPR pair in Bob's hands. Their avatars are in the middle, all together in a single point, i.e., **O**, although in **Figure 9**, we have separated them a bit so as not to complicate the drawing.

Figure 10 represents the entropic analysis for an EPR pair showing in detail how the cross-groupings of Alice's and Bob's elements represent the entanglement according to this analysis. In fact, from the entropic point of view, there is a shared rearrangement between a half of each EPR in Alice's hands and the other half of each EPR in Bob's hands, which constitutes the link cross-wise.

Figure 10 Cross-groupings of Alice's and Bob's elements to represent the entanglement.

Now, if we move $\mu_{|0^A 0^B\rangle}$ from position **B** to position **$\underline{B}$**, we will have $\mu_{|\Uparrow^A \Uparrow^B\rangle} = +\infty$ and $\mu_{|\Downarrow^A \Downarrow^B\rangle} = -\infty$ again. Besides, as in the case of completely independent subsystems, **Figure 11** shows that $\mu_{|\Uparrow^A \Uparrow^B\rangle}$ and $\mu_{|\Downarrow^A \Downarrow^B\rangle}$ are absolutely insensitive to the distance between the original spins, as long as $\mu_{|0^A 0^B\rangle}$ and $\mu_{|1^A 1^B\rangle}$ do not change neither in modulus nor in its orientation (polarization). Regardless how much the original spins separate from each other, such displacement does not alter the final result; i.e., the avatars: $\mu_{|\Downarrow^A \Downarrow^B\rangle} = -\infty$ and $\mu_{|\Uparrow^A \Uparrow^B\rangle} = +\infty$. This confirms the success of Eq.(58) since it attempts to model the entanglement, and as we know from several laboratory experiences, entanglement does not seem to care about the distance between the entangled particles [48, 49].

Figure 11 Scalar notation for entangled subsystems with an increase in the separation between the original spins.

On the other hand, if we properly apply square root to both sides of Eq.(58) and considering Eq.(59), then, we will obtain the four first-degree avatars. Then,

$$\mu^2_{|\Uparrow^{A,B}\rangle} = \frac{\mu^2_{|0^{A,B}\rangle} \mu^2_{|1^{A,B}\rangle}}{\mu^2_{|0^{A,B}\rangle} - \mu^2_{|1^{A,B}\rangle}} \quad \Rightarrow \quad \mu_{|\Uparrow^{A,B}\rangle} = \pm \sqrt{\frac{\mu^2_{|0^{A,B}\rangle} \mu^2_{|1^{A,B}\rangle}}{\mu^2_{|0^{A,B}\rangle} - \mu^2_{|1^{A,B}\rangle}}} \tag{60a}$$

$$-\mu^2_{|\Downarrow^{A,B}\rangle} = -\frac{\mu^2_{|0^{A,B}\rangle} \mu^2_{|1^{A,B}\rangle}}{\mu^2_{|0^{A,B}\rangle} - \mu^2_{|1^{A,B}\rangle}} \quad \Rightarrow \quad \mu_{|\Downarrow^{A,B}\rangle} = \pm \sqrt{\frac{\mu^2_{|0^{A,B}\rangle} \mu^2_{|1^{A,B}\rangle}}{\mu^2_{|0^{A,B}\rangle} - \mu^2_{|1^{A,B}\rangle}}} \tag{60b}$$

Equations (60a) and (60b) are identical, and from them we will obtain four solutions

$$\mu_{|\Uparrow^A\rangle} = \sqrt{\frac{\mu_{|0^{A,B}\rangle}^2 \, \mu_{|1^{A,B}\rangle}^2}{\mu_{|0^{A,B}\rangle}^2 - \mu_{|1^{A,B}\rangle}^2}} = \frac{\mu_{|0^A\rangle}}{\sqrt{1 - \left(\dfrac{\mu_{|1^{A,B}\rangle}}{\mu_{|0^{A,B}\rangle}}\right)^2}} = \mu_{|0^A\rangle} \ \gamma = +\infty \tag{61a}$$

$$\mu_{|\Downarrow^A\rangle} = -\sqrt{\frac{\mu_{|0^{A,B}\rangle}^2 \, \mu_{|1^{A,B}\rangle}^2}{\mu_{|0^{A,B}\rangle}^2 - \mu_{|1^{A,B}\rangle}^2}} = \frac{-\mu_{|0^A\rangle}}{\sqrt{1 - \left(\dfrac{\mu_{|1^{A,B}\rangle}}{\mu_{|0^{A,B}\rangle}}\right)^2}} = -\mu_{|0^A\rangle} \ \gamma = \mu_{|1^A\rangle} \ \gamma = -\infty \tag{61b}$$

$$\mu_{|\Uparrow^B\rangle} = \sqrt{\frac{\mu_{|0^{A,B}\rangle}^2 \, \mu_{|1^{A,B}\rangle}^2}{\mu_{|0^{A,B}\rangle}^2 - \mu_{|1^{A,B}\rangle}^2}} = \frac{\mu_{|0^B\rangle}}{\sqrt{1 - \left(\dfrac{\mu_{|1^{A,B}\rangle}}{\mu_{|0^{A,B}\rangle}}\right)^2}} = \mu_{|0^B\rangle} \ \gamma = +\infty \tag{61c}$$

$$\mu_{|\Downarrow^B\rangle} = -\sqrt{\frac{\mu_{|0^{A,B}\rangle}^2 \, \mu_{|1^{A,B}\rangle}^2}{\mu_{|0^{A,B}\rangle}^2 - \mu_{|1^{A,B}\rangle}^2}} = \frac{-\mu_{|0^B\rangle}}{\sqrt{1 - \left(\dfrac{\mu_{|1^{A,B}\rangle}}{\mu_{|0^{A,B}\rangle}}\right)^2}} = -\mu_{|0^B\rangle} \ \gamma = \mu_{|1^B\rangle} \ \gamma = -\infty \tag{61d}$$

where

$$\gamma = \frac{1}{\sqrt{1 - \left(\dfrac{\mu_{|1^{A,B}\rangle}}{\mu_{|0^{A,B}\rangle}}\right)^2}} = \frac{1}{\sqrt{1 - \left(\dfrac{\mu_{|0^{A,B}\rangle}}{\mu_{|1^{A,B}\rangle}}\right)^2}} = \frac{1}{\sqrt{1 - \left(\dfrac{v}{c}\right)^2}} \tag{62}$$

is the Lorentz factor [50], and since $\mu_{|0^{A,B}\rangle}^2 = \mu_{|1^{A,B}\rangle}^2$, being v a generic speed, and c the speed of light, if $v = c$ (as it happens in this case) then $\gamma = \infty$. This shows us the relativistic nature of the avatars of Eq.(61), or in other words, the relativistic nature of entanglement. This could imply two things: the avatars do not have mass (then and according to Special Relativity [8], they should move at the speed of light), or else they have mass of different sign, which would mutually annul each other in a single point where all the avatars meet and that we will proceed to calculate, in which case, the avatars would be related to the wormholes' traversability resulting from the entanglement of two black holes, or a black hole and a white hole [51-54]. We are talking about a very particular traversability, in fact, a traversability insensitive to the relative distance between both black holes. We are inclined to the second option, since obviously the avatars do not move. Effectively, as we can see, Eq.(58) does not have a component or parameter with the positions of the original spins, in fact, this equation is insensitive to these locations; as a result, the second-degree spins (μ^2) are not present where the light green lines are cut. Those crosses only allow us to determine their magnitudes. This is evident, since a spin cannot have any projection on an axis of another nature as in the case of the axis of distance (d).

As in the previous two cases (completely independent and classically correlated), we will resort again to the conservation of torque between the present spins of **Figure 9** and their corresponding lever arms. Resorting to said figure, we will begin with the following equivalences:

$$d_A = d_{|0^A0^B\rangle_A} = d_{|1^A1^B\rangle_A} \tag{63a}$$

$$d_B = d_{|0^A0^B\rangle_B} = d_{|1^A1^B\rangle_B} \tag{63b}$$

$$d_O = d_{|\Uparrow^A\Uparrow^B\rangle_A} = d_{|\Downarrow^A\Downarrow^B\rangle_A} = d_{|\Uparrow^A\Uparrow^B\rangle_B} = d_{|\Downarrow^A\Downarrow^B\rangle_B} \tag{63c}$$

Then, the conservation of torque will be:

$$\sum_{\forall i} \mu_i \times d_i = 0 = \mu_{|0^A0^B\rangle_A} \times d_{|0^A0^B\rangle_A} + \mu_{|1^A1^B\rangle_A} \times d_{|1^A1^B\rangle_A} + \mu_{|0^A0^B\rangle_B} \times d_{|0^A0^B\rangle_B} + \mu_{|1^A1^B\rangle_B} \times d_{|1^A1^B\rangle_B}$$
$$\mu_{|\Uparrow^A\Uparrow^B\rangle_A} \times d_{|\Uparrow^A\Uparrow^B\rangle_A} + \mu_{|\Downarrow^A\Downarrow^B\rangle_A} \times d_{|\Downarrow^A\Downarrow^B\rangle_A} + \mu_{|\Uparrow^A\Uparrow^B\rangle_B} \times d_{|\Uparrow^A\Uparrow^B\rangle_B} + \mu_{|\Downarrow^A\Downarrow^B\rangle_B} \times d_{|\Downarrow^A\Downarrow^B\rangle_B} \tag{64}$$

If we did not consider the complete EPR pair with its two components, but only a half of each entangled particle as in the case of **Figure 8** then the torque of Eq.(64) would not be conserved.

A direct consequence of the conservation of torque is that the avatars are the entropic expression of the original spins, i.e., for the entropic analysis performed, the original spins behave as if they were the avatars; in other words, each original particle has its own avatar from the entropic point of view,

$$\mu_{|0^A0^B\rangle_A} \times d_{|0^A0^B\rangle_A} = \mu_{|\Uparrow^A\Uparrow^B\rangle_A} \times d_{|\Uparrow^A\Uparrow^B\rangle_A} \tag{65a}$$

$$\mu_{|1^A1^B\rangle_A} \times d_{|1^A1^B\rangle_A} = \mu_{|\Downarrow^A\Downarrow^B\rangle_A} \times d_{|\Downarrow^A\Downarrow^B\rangle_A} \tag{65b}$$

$$\mu_{|0^A0^B\rangle_B} \times d_{|0^A0^B\rangle_B} = \mu_{|\Uparrow^A\Uparrow^B\rangle_B} \times d_{|\Uparrow^A\Uparrow^B\rangle_B} \tag{65c}$$

$$\mu_{|1^A1^B\rangle_B} \times d_{|1^A1^B\rangle_B} = \mu_{|\Downarrow^A\Downarrow^B\rangle_B} \times d_{|\Downarrow^A\Downarrow^B\rangle_B} \tag{65d}$$

Then, taking into account Eq.(61), we will have,

$$\mu_{|\Uparrow^A\Uparrow^B\rangle_A} = \mu_{|0^A0^B\rangle_A} \gamma^2 \tag{66a}$$

$$\mu_{|\Downarrow^A\Downarrow^B\rangle_A} = \mu_{|1^A1^B\rangle_A} \gamma^2 \tag{66b}$$

$$\mu_{|\Uparrow^A\Uparrow^B\rangle_B} = \mu_{|0^A0^B\rangle_B} \gamma^2 \tag{66c}$$

$$\mu_{|\Downarrow^A\Downarrow^B\rangle_B} = \mu_{|1^A1^B\rangle_B} \gamma^2 \tag{66d}$$

Consequently,

$$d_{|\Uparrow^A\Uparrow^B\rangle_A} = \frac{\mu_{|0^A0^B\rangle_A}}{\mu_{|\Uparrow^A\Uparrow^B\rangle_A}} d_{|0^A0^B\rangle_A} = \frac{\mu_{|0^A0^B\rangle_A}}{\mu_{|0^A0^B\rangle_A} \gamma^2} d_{|0^A0^B\rangle_A} = \frac{d_{|0^A0^B\rangle_A}}{\gamma^2} = 0 \tag{67a}$$

$$d_{|\Downarrow^A\Downarrow^B\rangle_A} = \frac{\mu_{|1^A1^B\rangle_A}}{\mu_{|\Downarrow^A\Downarrow^B\rangle_A}} d_{|1^A1^B\rangle_A} = \frac{\mu_{|1^A1^B\rangle_A}}{\mu_{|1^A1^B\rangle_A} \gamma^2} d_{|1^A1^B\rangle_A} = \frac{d_{|1^A1^B\rangle_A}}{\gamma^2} = 0 \tag{67b}$$

$$d_{|\Uparrow^A\Uparrow^B\rangle_A} = \frac{\mu_{|0^A0^B\rangle_A}}{\mu_{|\Uparrow^A\Uparrow^B\rangle_A}} d_{|0^A0^B\rangle_A} = \frac{\mu_{|0^A0^B\rangle_A}}{\mu_{|0^A0^B\rangle_A} \gamma^2} d_{|0^A0^B\rangle_A} = \frac{d_{|0^A0^B\rangle_A}}{\gamma^2} = 0 \tag{67c}$$

$$d_{\left|\Downarrow^A \Downarrow^B\right\rangle_B} = \frac{\mu_{\left|1^A 1^B\right\rangle_B}}{\mu_{\left|\Downarrow^A \Downarrow^B\right\rangle_B}} d_{\left|1^A 1^B\right\rangle_B} = \frac{\mu_{\left|1^A 1^B\right\rangle_B}}{\mu_{\left|1^A 1^B\right\rangle_B} \gamma^2} d_{\left|1^A 1^B\right\rangle_B} = \frac{d_{\left|1^A 1^B\right\rangle_B}}{\gamma^2} = 0 \qquad (67d)$$

The result of Eq.(67) has a dramatic meaning in Quantum Communications given that the avatars are together at an intermediate point determined by such equation, while the original spins are, in general, extremely far apart from each other. In fact, the exact locations of the original spins do not matter, what does matter is that the avatars will always be between original spins. Summing-up, we can say that the avatars see the universe as if it was a point.

Low part of **Figure 12** shows the interiors of the EPR pairs at points **A** and **B**, i.e., of the entangled particles held by Alice and Bob, respectively. It is an X-ray photograph inside both EPRs while the entanglement is alive (prior to the quantum measurement), and all thanks to the entropic analysis.

Figure 12 Second and first-degree originals and avatars, including distances for entangled subsystems.

On the other hand, in the same way that the conservation of the spin for the originals is fulfilled, it is evident that this also happens for the avatars, see **Figure 12**. Otherwise, with each entanglement the universe would be unbalanced,

$$\mu_{\left|0^A 0^B\right\rangle_A} + \mu_{\left|1^A 1^B\right\rangle_A} + \mu_{\left|0^A 0^B\right\rangle_B} + \mu_{\left|1^A 1^B\right\rangle_B} = 0 \tag{68a}$$

$$\mu_{\left|\Uparrow^A \Uparrow^B\right\rangle_A} + \mu_{\left|\Downarrow^A \Downarrow^B\right\rangle_A} + \mu_{\left|\Uparrow^A \Uparrow^B\right\rangle_B} + \mu_{\left|\Downarrow^A \Downarrow^B\right\rangle_B} = 0 \tag{68b}$$

Moreover, the original spins and their avatars form an original-avatar pair. In this case, the avatars are the shadows of the original spins projected on the (μ^2) axis with the same morphology (in this case, the orientation or polarization of the spins) and with infinite magnitude. The original-avatar pairs can be seen in Eq.(66). Unlike the case of Eq.(37) for the completely independent case where each original spin is contracted in a ζ factor inasmuch as $\zeta = \sqrt{2}/2 < 1$, in the entangled case, Eq.(61), each original spin is dilated in a proportion equal to the Lorentz factor [50] for $v = c$, i.e., $\gamma = \infty$.

The upper part of **Figure 12** shows us the second-degree avatars for entangled subsystems. We can highlight Eq.(61) and (66) of this figure, while the lower part of **Figure 12** shows the first-degree avatars with the same polarization and color of the original spin they represent, strictly according to each case of Eq.(61). An important aspect to highlight is that there are four second-degree avatars (Eq.66 and upper part of **Figure 12**) and four first-degree avatars (Eq.61 and lower part of **Figure 12**). Here also, the avatars have identity and correspondence, that is, they are unambiguously associated with their corresponding original spin forming an indivisible original-avatar pair. Moreover, the original spins are inaccessible (since they are immersed in an integrating context such as a Bell base), therefore, the avatars are too. If we do a quantum measurement on one of the two original EPRs, then the entanglement is destroyed and the avatars of Eq.(61) and (66) disappear, where another type of avatars appears, i.e., those of the completely independent or classically-correlated cases. The point here is that avatars are equivalent to the original spins from the operational point of view. This will be seen in detail in the next subsection.

2.5. Consequences on Quantum Communications

This subsection will revolve around the consequences of Eq.(67) which will have an unimaginable scope. The concentration of avatars at point **O** of **Figure 12** tells us that, for these, everything looks as if the universe was a point, that is, the whole universe is still a point, like the primal moment of the Big Bang. In addition, such concentration in only one point tells us other things that impact Quantum Communications fully:

1. Wormholes, that is, tunnels created by two entangled black holes have null length, i.e., they are punctual, and therefore, they have absolute traversability.

2. What about the locality and non-locality? If we return, to one of Eq.(65), e.g., Eq.(65a) and replace the Eq.(67a) in it, then,

$$\mu_{\left|0^A 0^B\right\rangle_A} \times d_{\left|0^A 0^B\right\rangle_A} = \mu_{\left|\Uparrow^A \Uparrow^B\right\rangle_A} \times d_{\left|\Uparrow^A \Uparrow^B\right\rangle_A}$$

$$\mu_{\left|0^A 0^B\right\rangle_A} \times d_{\left|0^A 0^B\right\rangle_A} = \mu_{\left|\Uparrow^A \Uparrow^B\right\rangle_A} \times \left(\frac{d_{\left|0^A 0^B\right\rangle_A}}{\gamma^2} \right) \tag{69}$$

$$\mu_{\left|0^A 0^B\right\rangle_A} \times \left(d_{\left|0^A 0^B\right\rangle_A} \gamma^2 \right) = \mu_{\left|\Uparrow^A \Uparrow^B\right\rangle_A} \times d_{\left|0^A 0^B\right\rangle_A}$$

where

$\left(\dfrac{d_{|0^A 0^B\rangle_A}}{\gamma^2} \right)$ represents the locality contraction, or locality range of avatars, while,

$\left(d_{|0^A 0^B\rangle_A} \gamma^2 \right)$ represents the locality dilation, or the no-locality of the originals, which covers any separation that mediates between them and that undoubtedly is equivalent to the non-locality we know [5] in relation to them from the experiments related to Bell's theorem [30] and CHSH [31].

We can see that, while Eq.(67) represents the contraction in the separation between avatars, i.e., the contraction of their range of locality, at the same time said contraction of locality is equivalent to the dilation in the locality of the original spins, which is undoubtedly equivalent to the non-locality of these [11, 22], i.e.:

(***Non-locality of original spins*** = ***Locality dilatation of original spins***) ≡ (***Locality of avatars***)

In other words, the original spins communicate in a non-local way, but, from the entropic point of view, this is equivalent to a local communication between avatars.

3. What about the Bohr's complementarity principle [55, 56]? In particular, the wave-particle duality [57], which gives rise to another question: how is it possible that during any experiment (e.g., that of the double slit) when observing the acting elements, they stop acting as a wave and start acting as a particle? What interests us, in the context of this work, is the analysis of the complementarity principle of the wave-particle in relation to the Bohr's rule [58], which establishes that $|\psi|^2$ is the probability of the position of the particle leading to the conclusion that co-location of particle and wavefunction is not possible unless the wavefunction is a Dirac's delta function.

   Invoking the wavefunction-spin relation [59] and given that the avatars have spins with a magnitude equal to infinite, then we assume they have a wavefunction with an amplitude equal to infinite, precisely that of the Dirac's delta type, located at a point with a null range of locality, i.e., the co-location between particle and wavefunction works well for the avatars.

   The EPRs, instead, have a unified but deconcentrated wavefunction of dilated locality which can potentially spread throughout the universe (it dilates in order to be continent with the entangled particles fulfilling the non-locality), contrary to the concentrated wavefunction the avatars possess. That is, co-location does not work for EPRs according to Bohr's complementarity principle.

4. From an entropic point of view, the avatars are plenipotentiary representatives of the original spins. It is as if the originals behaved entropically as the avatars do, which are the ones that actually communicate. The entire channel is reduced to the point where the avatars are, with a transit time for an eventual message that we will extract from the second row of Eq.(69)

$$l_{ch} = \frac{d_{|0^A 0^B\rangle_A}}{\gamma^2} = \frac{\left(v_m\, t_{|0^A 0^B\rangle_A} \right)}{\gamma^2} = v_m \left(\frac{t_{|0^A 0^B\rangle_A}}{\gamma^2} \right) = 0 \tag{70}$$

$$t_{ch} = \frac{t_{|0^A 0^B\rangle_A}}{\gamma^2} = 0 \tag{71}$$

Where v_m is the speed at which a message travels on the channel, l_{ch} is the cannel length, and t_{ch} is the transit time of the message through the channel. According, to Eq.(70) and (71), l_{ch} and t_{ch} are respectively contracted, and this contraction is equivalent to the locality range of the avatars.

The absence of channel between avatars has dramatic consequences on quantum communications, since, if the channel is reduced to a point, then:

a) what a transmitter deposits at that point is perfectly and exactly equal to what a receiver receives from that point, i.e., *what you put* at that point is equal to *what you get* from that point (WYPWYG), then, that channel has infinite bandwidth and null latency (anything that crosses it will do it instantaneously). In the space of avatars, we are not talking about transmitting but about sharing information in that punctual channel,
b) there is no channel noise in a channel that does not exist,
c) a channel with infinite bandwidth and zero noise has an infinite channel capacity [60], and
d) finally: *it is impossible to attack, intercept or hack a channel that does not exist*, because it is impossible to attack the nothing.

In spite of what has been said, if we put the entanglement in a practical context, for example, we involve it in a quantum teleportation [15-19, 61], then, the gates with which the teleportation protocol is implemented insert different types of noise, reducing significantly the attributes of the protocol as a whole.

5. Equations (70) and (71) have depth implications on the old and tempestuous relationship between Special Relativity [8] and Quantum Mechanics [9] because of the quantum entanglement [26]. For example, let us consider a turtle trying to travel a null-length path, at a speed within the next range $v_m = 0.13\text{-}0.30$ mph, which is clearly much smaller than the speed of light $c = 670,600,000$ mph, however, the turtle will travel the route instantaneously without resorting to any superluminal speed [11-14]. In other words, the paradox EPR [26] is disabled, as well as the No-Go theorems of No-Signaling [20-24] and No-Communications [25].

Evidently, based on everything said so far, there is no collision or contradiction between Special Relativity [8] and Quantum Mechanics [9] because of the quantum entanglement [26]. In fact, Special Relativity does not contradict Quantum Mechanics, on the contrary, it supports Quantum Mechanics thanks to Eq.(61, 67, 69, 70, 71) so that the latter does not violate Special Relativity.

This concubinage between both theories based on the entropic analysis has other implications. Equation (6) corresponding to the original spins has its counterpart in the avatars world, e.g., for the EPR in Alice's hands, we will find,

$$\left(\left| \Uparrow^A \Uparrow^B \right\rangle = \left| 0^A 0^B \right\rangle^{\otimes \gamma} \right) \equiv \left(\mu_{\left| \Uparrow^A \Uparrow^B \right\rangle} = \mu_{\left| 0^A 0^B \right\rangle} \gamma^2 = \mu^2_{\left| \Uparrow^{A,B} \right\rangle} \gamma^2 = +\infty \right)$$

$$\left(\left| \Downarrow^A \Downarrow^B \right\rangle = \left| 1^A 1^B \right\rangle^{\otimes \gamma} \right) \equiv \left(\mu_{\left| \Downarrow^A \Downarrow^B \right\rangle} = \mu_{\left| 1^A 1^B \right\rangle} \gamma^2 = -\mu^2_{\left| \Downarrow^{A,B} \right\rangle} \gamma^2 = -\infty \right)$$

(72)

in the same way as a typical element of an EPR pair, i.e.,

$$\left| \beta_{00} \right\rangle = \frac{\left| 0^A 0^B \right\rangle + \left| 1^A 1^B \right\rangle}{\left\| \left| 0^A 0^B \right\rangle + \left| 1^A 1^B \right\rangle \right\|_2} = \frac{\left| 0^A 0^B \right\rangle + \left| 1^A 1^B \right\rangle}{\sqrt{2}}$$

(73)

also has its counterpart,

$$\left| \beta_{\Uparrow\Uparrow} \right\rangle = \frac{\left| \Uparrow^A \Uparrow^B \right\rangle + \left| \Downarrow^A \Downarrow^B \right\rangle}{\left\| \left| \Uparrow^A \Uparrow^B \right\rangle + \left| \Downarrow^A \Downarrow^B \right\rangle \right\|_\gamma} = \frac{\left| 0^A 0^B \right\rangle^{\otimes \gamma} + \left| 1^A 1^B \right\rangle^{\otimes \gamma}}{\left\| \left| 0^A 0^B \right\rangle^{\otimes \gamma} + \left| 1^A 1^B \right\rangle^{\otimes \gamma} \right\|_\gamma}$$

(74)

Even though the Lorentz factor (γ) [50] comes from Eq.(62) and it is clearly a continuous variable, such that $\gamma \in ¡$, its use in Eq.(72) and (74) gives dimension to vectors thanks to the tensorial notation, indicating its entire character. Strictly speaking, we are talking about a $\gamma \in ¥$, i.e., of a quantization of the Lorentz factor [50].

Equations (61), (72) and (74) highlight the degree of symbiosis between Special Relativity and Quantum Mechanics, which could only be evidenced by the entropic analysis of entanglement and scalar notation based on spins. Besides, Eq.(72) and (74) tell us about inflation in the Bloch's sphere, while reaffirming that entanglement is a purely relativistic phenomenon.
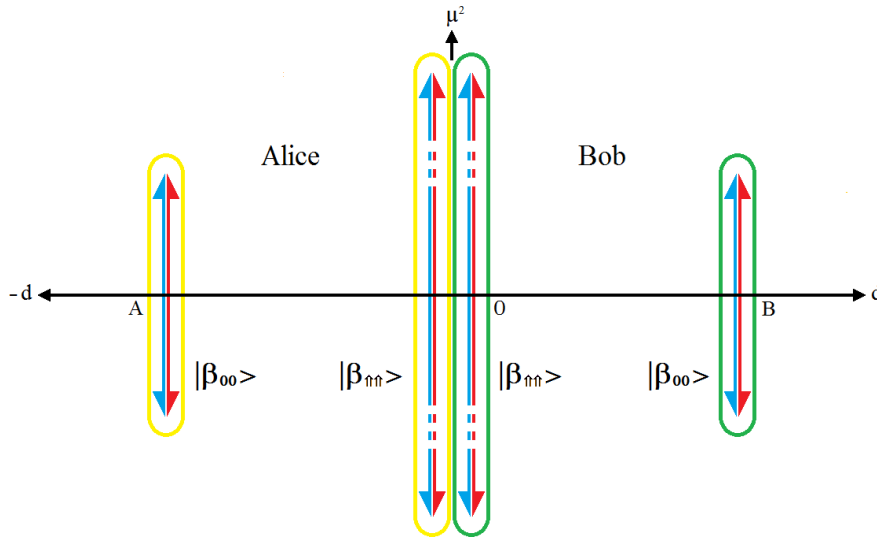

Figure 13 The yellow cartridges contain $\left|\beta_{00}\right\rangle$ and $\left|\beta_{\Uparrow\Uparrow}\right\rangle$ relative to Alice, while the green cartridges contain those related to Bob.

Of the five items exposed in this subsection, we conclude that:

a) the avatars are the hinge between Quantum Mechanics and Special Relativity, hinting at a possible path to a Theory of Everything [62],
b) without the spine-based scalar notation the avatars would have never been revealed,
c) the traditional symbolic logic based on the Dirac's notation takes us away instead of approaching a Theory of Everything,
d) now, we understand how nature instantly notifies the state of one of the elements of an EPR pair to the other one after being measured,
e) in principle, there is not the slightest hint of impediment for an instantaneous transmission via an EPR channel,
f) it is incredible that the literature has made such a statement about the impossibility of transmitting information instantaneously on an EPR channel without deepening enough in the use of the tools of Information Theory [60],
g) given that the eventual impediment of the previous item that the literature talks about so much is not in a confrontation between Quantum Mechanics and Special Relativity, then the problem, if it really exists, must be somewhere else.

But, if the problem of the instantaneous transmission of information does not lie in the previous items, then, where is it? The answer to this question is easier than it seems. Let us picture the following situation: three people in a room, **A**, **B** and **C**. **A** is murdered and we just proved that **B** could not be the murderer because he was unconscious before **A** was killed. Ergo, the killer has to be **C**. Then, the problem has to be in the same act of measuring. With quantum measurement everything is left to randomness [37, 38]. The detectors commonly used are passive, they report the state of what they detect without exercising any kind of control over what they measure. There is no control, so it is impossible to transmit useful information instantly, which is logical because it is impossible to exercise some control with passive elements such as single photon detectors (SPD) used in quantum teleportation [15-19, 39, 61], i.e., we cannot do a controlled disambiguation but only measure and transmit the measured so that on the other side of the channel that information is used in the reconstruction. Therefore, it is not necessary to measure but to control. We will implement some experiments to verify this hypothesis in the following section.

3. Quantum measurement vs quantum control

As we have mentioned in Section 1, by measuring one of the components of an EPR pair (which is constituted internally as indicated by Eq.(73) and that can be observed in the lower part of **Figure 12**), a *spin-up* or a *spin-down* will result randomly, in such a way that the other component of the EPR pair will adopt the opposite orientation instantly. It is evident that we have no control over the result of the measure, what we can only do is to report the result obtained from that measure. The only way to control the result is to resort to an *in pectore* selection of this result, and this can only be done by a technique well known in quantum technology and known as qubit reset procedure [63].

Fast, deterministic and active qubit reset to a target state [64] is a key operation in many quantum algorithms, and particularly in error correction codes [65]. Besides, it is a powerful tool to reuse subsequently the same qubit [66]. There are two types of qubit reset: passive and active [67], however, the active version is up to ~ 100 times faster than the passive initialization [68]. On the other hand, the initial state preparation (and reset) of the registers on the physical quantum computer will generate entropy due to Landauer's erasure principle [69]. For a qubit preparation, a qubit reset and a quantum measurement, incoherent operations are required [70]. Fast and reliable reset of a qubit is a key prerequisite for any quantum technology [71], where faster qubit reset is almost a synonymous of smaller errors. Currently, there are several techniques [68, 72, 73] and protocols [74-76], including its simulated version on several platforms [77-83] to obtain this. In fact, Rigetti [82] is the only company that allows us to use a qubit reset on their quantum processing unit (QPU) but only at the beginning of the process in order to prepare the different qubits to be used.

Next, we will analyze the intervention in a comparative way of quantum measurement [37-39] vs qubit reset [63] for two cases: EPR pairs [1-3] and quantum teleportation [15-19, 39, 61].

3.1. EPR pair

3.1.1 *Quantum measurement*

Let us suppose that we have two corrals with one cow in each, as shown in **Figure 14**. Each corral only has two gates: a *spin-up* and a *spin-down*. We open both gates in both corrals. The experiment begins with the corral on the left, where we have a 50% chance of the cow coming out of any of the gates.

Figure 14 The experiment begins with the corral on the left. That cow has a 50% chance of leaving through any of both gates. When that cow decides to leave, e.g., through the *spin-up* gate, then the cow from the corral on the right will exit through the *spin-down* gate with a 100 % of certainty.

Now, experience tells us that if the cow in the corral on the left exits through the *spin-up* gate, then the cow from the corral on the right will exit through the *spin-down* gate with 100% certainty. At the beginning, we have an uncertainty of 50% regarding which gate the cow will use to leave the corral on the left, but absolute certainty about the gate the cow will use to leave the corral on the right once we find out where the first cow exits from. That is, the decision of the cow on the left conditions the departure of the cow on the right, that is, we have no control over the outcome of the experiment. It is clear that we yield the control of the result of experiment to the cow on the left, instead of us.

The same experiment can be implemented on the Quirk platform [78] and is represented in **Figure 15**. We have chosen this platform because it is the most pedagogical and has the best graphic expression of all simulators, however, this experiment can be reproduced with identical results on an optical table.

Figure 15 Quirk implementation, where, D0 detects a *spin-up*, then instantaneously D1 detects a *spin-down*, both with vertical polarization. Entanglement dies as a consequence of the detection process.

Figure 15 shows two qubits (q[0] and q[1]) and the generation of an EPR pair thanks to the combination of a Hadamard's gate (**H**) and a CNOT gate. D0 and D1 represent a pair of detectors with vertical polarization. Detector D0 represents the pair of eyes of the corral on the left of **Figure 14**, while detector D1 represents the pair of eyes of the corral on the right of the same figure. DM means density matrix, Po|1> means percent of |1>, and BS means Bloch's sphere. It is evident that the three witnesses at the output of EPR generation block, i.e., DM, Po|1> and BS show behavior in both qubits q[0] and q[1] typical of an EPR pair. Then, if D0 detects (continuing with the example of **Figure 14**) a *spin-up* |0> for q[0], then q[1] resulting from detector D1 is absolutely defined as a *spin-dow* |1>, as this is evidenced by DM, Po|1> and BS at the output of both detectors. All the laboratory experiments carried out during the last decades support this result.

3.1.2 *Quantum control via qubit reset*

This experiment revolves around **Figure 16**, where we again have two corrals with a cow in each of them. Here, too, the experiment begins with the corral on the left, however, now we only open the *spin-up* gate. Instantly, the cow on the right, which has both gates open, will go out through the *spin-up* gate with 100% certainty. We do not need to measure, detect or transmit anything. It is us who are in total control of the experiment, instead of the animal. **Figure 17** shows us the implementation of this experiment on Quirk platform. It is evident that the qubit reset gate [|0>] is neither reversible nor unitary, in fact, this gate, according to IBM Q [79], will be,

$$\left[|0\rangle\right]\begin{bmatrix}\alpha\\\beta\end{bmatrix}\rightarrow\begin{bmatrix}|\alpha|+|\beta|\,j\\0\end{bmatrix}\sim\begin{bmatrix}1\\0\end{bmatrix} \tag{75}$$

converts any arbitrary qubit in the ground state |0>. While, its counterpart,

$$\left[|1\rangle\right]\begin{bmatrix}\alpha\\\beta\end{bmatrix}\rightarrow\begin{bmatrix}0\\|\alpha|+|\beta|\,j\end{bmatrix}\sim\begin{bmatrix}0\\1\end{bmatrix} \tag{76}$$

converts any arbitrary qubit in |1>. This will be used in **Figure 18**.

Figure 16 Here too, the experiment begins with the corral on the left. We open the *spin-up* gate only, then the only possibility that that cow has is to exit through that gate. The cow on the right has both gates open, however, it will exit through the *spin-up* gate with a 100 % of certainty.
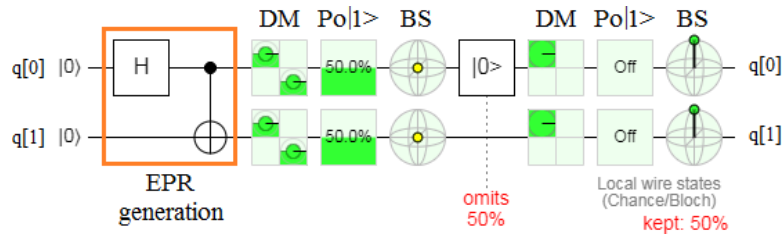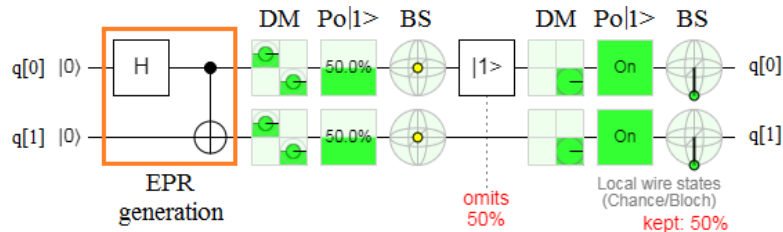

Figure 17 Quirk implementation, where, the qubit reset gate [|0>] converts qubit q[0] in *spin-up*, then instantaneously qubit q[1] imitates it. Entanglement also dies as a consequence of this gate.

While qubit reset gate [|0>] of **Figure 17** puts the qubit q[0] in *spin-up* and instantaneously the qubit q[1] results in the same orientation, **Figure 18** shows that the action of the qubit reset gate [|1>] on the qubit q[0], puts it in *spin-down* and as a consequence of this, instantaneously q[1] adopts the same orientation.

Figure 18 Quirk implementation, where, the qubit reset gate [|1>] converts qubit q[0] in *spin-down*, then instantaneously qubit q[1] imitates it. Entanglement also dies as a consequence of this gate.

There is a fourth possibility, although this is not control but simply an annulment of the entanglement and the subsequent recovery of the original ground states |0>. This can be seen in **Figure 19**. The block highlighted in light blue is exactly the counterpart of its namesake in orange. However, for the purposes of this work, this possibility has no major significance.

28

Figure 19 Quirk implementation, where, the light blue block is the counterpart of the orange block, which is responsible of the EPR generation. Then, the light blue block only recovers the original ground states |0>, i.e., it does not represent any type of control.

Additional implementations in other platforms also with cloud services give the same results obtained with Quirk. **Figure 20** shows the results of experiment of **Figure 17** on IBM Q platform [79], where the implementation was carried out under the following parameters: shots = 100, and seed = random.

Figure 20 IBM Q implementation of experiment of **Figure 17**. Quantum circuit on the left represents the *drag & drop* structure, while, the graph on the right represents the probability bar, which confirms the results obtained with Quirk.

Figure 21 shows the captured screen for the implementation on Rigetti's quantum virtual machine (QVM) [82], where, the probabilities match those in **Figure 20** for IBM Q. **Figure 22** shows an implementation on Quantum Programming Studio platform [80], which gives identical results to the previous platforms, which can be seen in the Bloch's spheres on the right of **Figure 22**.

Figure 21 Captured screen with amplitudes and probabilities on Rigetti's platform [82].

Figure 22 Implementation of the experiment of **Figure 17** on Quantum Programming Studio. Quantum circuit on the left represents the *drag & drop* structure, while, the graph on the right represents the set of angles, Probabilities of |1> and the Bloch's spheres, which also confirms the results obtained with Quirk.

29

3.2. Quantum teleportation

In this subsection, we will see if what has been demonstrated for the case of the EPR pair, with and without control, is maintained by putting entanglement in its most famous context: Quantum Teleportation protocol [15-19, 39, 61]. In fact, we will consider two types of protocols:

- Uncontrolled quantum teleportation: the traditional non-instantaneous protocol, and
- Controlled quantum teleportation: the improved and instantaneous protocol.

3.2.1. Uncontrolled quantum teleportation

We will describe this protocol in a procedural way based on **Figure 23**. First, an EPR pair is created and distributed between Alice and Bob.

Figure 23 Uncontrolled quantum teleportation using two classical bits for disambiguation.

The horizontal green line of **Figure 23** separates Alice's and Bob's sides, and it can represent any arbitrary distance between them [15-19, 39, 61]. Besides, in **Figure 23** *SPD* block means single photon detector set, $\{X, Z\}$ are Pauli's matrices activated by the bits $\{b_2, b_1\}$ respectively [1, 15-19], and EPR is the source of the entangled particles of Eq.(8). In fact, any of the EPRs of the Bell's basis complete set [1, 39] can be chosen, however, we will use $|\beta_{00}\rangle = |\Phi^+\rangle$.

Alice's side:

1) Alice gets an arbitrary and unknown state to be teleported,

$$|\psi\rangle = \alpha|0\rangle + \beta|1\rangle = [\alpha \quad \beta]^T \tag{77}$$

where $(\bullet)^T$ means *transpose of* $(\bullet)$, and remembering from Section 2.1: $|\alpha|^2 + |\beta|^2 = 1$ and $\alpha \wedge \beta \in \pounds$ of a Hilbert's space [39].

2) $|\psi\rangle = \alpha|0\rangle + \beta|1\rangle$ and $|\beta_{00}\rangle$ enter to a Bell State Measurement (BSM) block constitutes by a *CNOT* gate, a *Hadamard's* (H) gate and the *SPD*, then, a 3-partite state results in,

$$
\begin{aligned}
|\psi_0\rangle &= |\psi\rangle \otimes |\beta_{00}\rangle = |\psi\rangle|\beta_{00}\rangle = (\alpha|0\rangle + \beta|1\rangle)\,\tfrac{1}{\sqrt{2}}(|00\rangle + |11\rangle) \\
&= \tfrac{1}{\sqrt{2}}\big[\alpha|0\rangle(|00\rangle + |11\rangle) + \beta|1\rangle(|00\rangle + |11\rangle)\big] = \tfrac{1}{\sqrt{2}}\big[\alpha|000\rangle + \alpha|011\rangle + \beta|100\rangle + \beta|111\rangle\big] \\
&= \big[\tfrac{\alpha}{\sqrt{2}} \quad \tfrac{\beta}{\sqrt{2}} \quad 0 \quad 0 \quad 0 \quad 0 \quad \tfrac{\alpha}{\sqrt{2}} \quad \tfrac{\beta}{\sqrt{2}}\big]^T
\end{aligned}
\tag{78}
$$

30

where "$\otimes$" is the Kronecker's product [39]. For simplicity [1-3, 39-41], from now on, we will adopt $|x\rangle \otimes |y\rangle = |x\rangle |y\rangle$ in a generic form.

3) A *CNOT* gate is applied to $|\psi_0\rangle$,

$$|\psi_1\rangle = \frac{1}{\sqrt{2}}\left[\alpha|000\rangle + \alpha|011\rangle + \beta|110\rangle + \beta|101\rangle\right]$$

$$= \left[\frac{\alpha}{\sqrt{2}} \quad 0 \quad 0 \quad \frac{\beta}{\sqrt{2}} \quad 0 \quad \frac{\beta}{\sqrt{2}} \quad \frac{\alpha}{\sqrt{2}} \quad 0\right]^T$$

(79)

4) A *Hadamard's* (H) gate is applied to $|\psi_1\rangle$,

$$|\psi_2\rangle = \frac{1}{2}\left[|00\rangle X^0 Z^0 |\psi\rangle + |01\rangle X^1 Z^0 |\psi\rangle + |10\rangle X^0 Z^1 |\psi\rangle + |11\rangle X^1 Z^1 |\psi\rangle\right]$$

$$= \frac{1}{2}\left[|\Phi^+\rangle X^0 Z^0 |\psi\rangle + |\Phi^-\rangle X^1 Z^0 |\psi\rangle + |\Psi^+\rangle X^0 Z^1 |\psi\rangle + |\Psi^-\rangle X^1 Z^1 |\psi\rangle\right]$$

$$= \left[\frac{\alpha}{2} \quad \frac{\alpha}{2} \quad \frac{\beta}{2} \quad \frac{-\beta}{2} \quad \frac{\beta}{2} \quad \frac{-\beta}{2} \quad \frac{\alpha}{2} \quad \frac{\alpha}{2}\right]^T$$

$$= \left[\frac{\alpha}{2} \quad 0 \quad \frac{\beta}{2} \quad 0 \quad 0 \quad 0 \quad 0 \quad 0\right]^T \rightarrow |\Phi^+\rangle \rightarrow |00\rangle \rightarrow 00 \rightarrow X^0 Z^0$$

$$+ \left[0 \quad \frac{\alpha}{2} \quad 0 \quad \frac{-\beta}{2} \quad 0 \quad 0 \quad 0 \quad 0\right]^T \rightarrow |\Psi^+\rangle \rightarrow |10\rangle \rightarrow 10 \rightarrow X^0 Z^1$$

$$+ \left[0 \quad 0 \quad 0 \quad 0 \quad \frac{\beta}{2} \quad 0 \quad \frac{\alpha}{2} \quad 0\right]^T \rightarrow |\Phi^-\rangle \rightarrow |01\rangle \rightarrow 01 \rightarrow X^1 Z^0$$

$$+ \left[0 \quad 0 \quad 0 \quad 0 \quad 0 \quad \frac{-\beta}{2} \quad 0 \quad \frac{\alpha}{2}\right]^T \rightarrow |\Psi^-\rangle \rightarrow |11\rangle \rightarrow 11 \rightarrow X^1 Z^1$$

(80)

From the last four rows of Eq.(80), we can draw the following conclusions:
a) they represent the quantum measurement carried out by Alice and the suggestion that she makes to Bob by transmitting the classical bits of disambiguation, by a classical channel, to reconstruct the teleported state [15-19],
b) the result of quantum measurement arises randomly and the four possible results are equally likely to appear,
c) the projections of the four bases are overlapping in relation to the detectors of the SPD [84], and
d) given that the teleportation protocol begins with the distribution of an EPR pair, the quantum measurement kills the entanglement (i.e., it destroys the original arbitrary state on Alice's side) so as not to violate the No-Cloning Theorem [85], which implies that in order to teleport another state it must again distribute another EPR pair, and thus, the process continues indefinitely.

Table I synthesizes the complete quantum teleportation protocol.

Table I *Alice's side*: measurement of the base, classical transmission of bits, and the collapse of states.
Bob's side: classical reception of bits, gates application for the final recovery of the arbitrary state.

Alice's measurement	Alice transmits	This happens with probability	Collapsed state	Bob applies $X^{b_2} Z^{b_1}$
$|\Phi^+\rangle \rightarrow 00$	$b_2 b_1 = 00$	$\left\|\frac{1}{2} X^0 Z^0 |\psi\rangle\right\|^2 = \frac{1}{4}$	$|\Phi^+\rangle X^0 Z^0 |\psi\rangle$	$X^0 Z^0 |\psi\rangle = |\psi\rangle$
$|\Psi^+\rangle \rightarrow 01$	$b_2 b_1 = 01$	$\left\|\frac{1}{2} X^0 Z^1 |\psi\rangle\right\|^2 = \frac{1}{4}$	$|\Psi^+\rangle X^0 Z^1 |\psi\rangle$	$X^0 Z^1 |\psi\rangle = Z|\psi\rangle$
$|\Phi^-\rangle \rightarrow 10$	$b_2 b_1 = 10$	$\left\|\frac{1}{2} X^1 Z^0 |\psi\rangle\right\|^2 = \frac{1}{4}$	$|\Phi^-\rangle X^1 Z^0 |\psi\rangle$	$X^1 Z^0 |\psi\rangle = X|\psi\rangle$
$|\Psi^-\rangle \rightarrow 11$	$b_2 b_1 = 11$	$\left\|\frac{1}{2} X^1 Z^1 |\psi\rangle\right\|^2 = \frac{1}{4}$	$|\Psi^-\rangle X^1 Z^1 |\psi\rangle$	$X^1 Z^1 |\psi\rangle = X Z|\psi\rangle$

With the same pedagogical commitment as in the case of the EPR pair of Subsection 3.1.1, we will analyze quantum measurement in the context of quantum teleportation through the example of the cow in the corral. We begin the experiment by leaving the four gates of the corral in **Figure 24** open. The cow will have an identical probability of exiting by any of the four gates. Once the cow decides on a gate, e.g., |00>, Alice observes it and transmits the result to Bob in the form of two classical bits ($b_1 = 0$, and $b_2 = 0$) sent by a classical channel, so that Bob can reconstruct the teleported state.

Figure 24 The corral has the four gates open. The cow has the same chance of exiting through any of the four gates. When the cow decides to leave, e.g., through the |00> gate, then Alice observes and transmits the result to Bob in the form of two classical bits, in this case, $b_1 = 0$, and $b_2 = 0$.

It is evident that the last four rows of Eq.(80), **Table I** and **Figure 24** are related to the point that the three, finally, represent the same thing, which consists that we exclusively have a state of observation without control over the experiment. As it will be seen in the next subsection, this is the reason for the need for a classical connection between Alice and Bob in addition to the EPR channel.

Meanwhile, we will implement the protocol of **Figure 23** on two platforms, e.g., Quirk [78] and IBM Q [79], in order to verify what has been said, although this protocol has been tested with total success during the last two decades [16-18]. For both platforms, we choose the same state to be teleported, in order to compare outcomes, which results from:

$$q[0] = H\,T\,H\,S\,q[0] = \frac{\begin{bmatrix} 1 & 1 \\ 1 & -1 \end{bmatrix}}{\sqrt{2}} \sqrt[4]{\begin{bmatrix} 1 & 0 \\ 0 & -1 \end{bmatrix}} \frac{\begin{bmatrix} 1 & 1 \\ 1 & -1 \end{bmatrix}}{\sqrt{2}} \sqrt[2]{\begin{bmatrix} 1 & 0 \\ 0 & -1 \end{bmatrix}} \begin{bmatrix} 1 \\ 0 \end{bmatrix} = \left(85.3553\%\,|0\rangle, 14.6447\%\,|1\rangle\right) \tag{81}$$

with

$$H = \frac{\begin{bmatrix} 1 & 1 \\ 1 & -1 \end{bmatrix}}{\sqrt{2}}, \; T = \sqrt[4]{\begin{bmatrix} 1 & 0 \\ 0 & -1 \end{bmatrix}} = \sqrt[4]{Z}, \; S = \sqrt[2]{\begin{bmatrix} 1 & 0 \\ 0 & -1 \end{bmatrix}} = \sqrt[2]{Z}, \; q[0] = \begin{bmatrix} 1 \\ 0 \end{bmatrix} \tag{82}$$

Figure 25 shows the implementation of the uncontrolled (standard) quantum teleportation protocol of **Figure 23** on Quirk simulator [78]. The blocks in color mean: orange for EPR generation, light blue for qubit generation (to be teleported), pink for BSM, gray for classical channel, and light green for the

unitary transforms to be applied by Bob to recover the teleported state. The complete coincidence between both sets of witness tools shows that the state is perfectly teleported.

Figure 25 Uncontrolled (standard) quantum teleportation implemented on Quirk [X] simulator.

Figure 26 is the quantum circuits for the same experiment but on IBM Q simulator [79]. The results can be seen in the probability bars of **Figure 27**, where, we have obtained: 0.250+0.220+0.170+0.150 = 0.790 for |0> and 0.060+0.060+0.060+0.030 = 0.210 for |1>, which differs from the values of Eq.(81) because of decoherence [38]. It is important to emphasize that this implementation was done on the IBM Q [79] simulator since its quantum processing unit (QPU) or physical quantum machine cannot implement the *if-then-else* statement. In fact, this is something that Rigetti's QPU cannot do either [82]. The implementation was carried out under the following parameters: shots = 1024, and seed = random. Finally, the barrier in **Figure 26**, between qubit preparation and BSM blocks, serves to avoid *per se* optimizations of the simulator.

Figure 26 Uncontrolled (standard) quantum teleportation implemented on IBM Q [79] simulator.

Figure 27 Probability bars for the experiment of **Figure 26**.

Additional confirmations on other platforms such as Rigetti [82], Quantum Programming Studio [80], or Intel & QuTech's Inspire [83] are obviously unnecessary.

33

3.2.2. Controlled quantum teleportation

We will describe this protocol highlighting the critical differences with the standard (uncontrolled) version of **Figure 23**. **Figure 28** represents the controlled protocol of quantum teleportation, which also begins with the creation and distribution of an EPR pair between Alice and Bob.

Figure 28 Controlled quantum teleportation using two qubit reset [|0>] gates.

On Alice's side, the *CNOT*, Hadamard's (*H*) and both qubit reset [|0>] gates form the Bell State Control (BSC) block, which is the first important difference with the standard (uncontrolled) version. The action of both qubit reset [|0>] gates eliminates the last three lines of the Eq.(80) and also the entanglement. A direct and instantaneous consequence of such action is that Bob does not require any kind of message from Alice to know which unitary transformation he must prepare to reconstruct the teleported state given that it will always be the same due to both qubit reset [|0>] gates. Consequently, the unitary transformation is reduced to the identity matrix. Besides, as we will see later, the elimination of the last three lines of Eq.(80) allows the controlled version to have greater robustness respect to the decoherence compared to the uncontrolled version.

Figure 29 shows how the BSC works. Alice and Bob agree (before the experiment) that the gate |00> will always open exclusively. Then, since the cow can only exit through said gate, Alice does not need to observe or transmit to Bob the gate, i.e., the random (uncontrolled) was replaced by the control.

Figure 29 The corral only has the gate |00> open. Then, the cow can only exit by that gate with a 100 % of probability. Alice does not observe or transmit anything to Bob since it is not necessary because it is prearranged in an anti-causal way (controlled) so the cow will always go out through it.

Next, we are going to implement the controlled protocol of quantum teleportation of **Figure 28** on the following three quantum platforms with services on the cloud: Quirk [78], IBM Q [79], and Rigetti [82]. However, before implementations, we will clarify some things:

1. Quirk [78] simulator is a formidable tool for the graphical implementation of quantum circuits, in fact, it is the most pedagogical one with the best graphical interface, which allows us to make drag and drops operations without any type of coding, however, and as we saw in the previous case, Quirk does not consider decoherence. This is the reason why in **Figure 25**, both of them: the qubit to be teleported (prepared) and the reconstructed qubit (teleported) are identical. Clearly, this is not what happened on the IBM Q platform [79], since the probability bars of **Figure 27** are a little different to the percentages of Eq.(81).

2. IBM Q [79] has not implemented the qubit reset gate even on its physical quantum machine or Quantum Processing Unit (QPU) yet, therefore, we will resort to its simulator. On the other hand, all its topologies (of 5, 9, 14, 21, 32, or more qubits) perform qubit reset in a *per se* way at the beginning of the process and transparent to the user, in order to quickly put to ground state all the qubits to be used, as soon as possible, and in this way make the most of the coherence time. Both the previous implementations and the one we will do next, were encoded in Quantum Assembly language (qasm). In fact, even if IBM Q implemented the qubit reset gate on its QPU, there would be no need to resort to Quantum Information Science Kit (qiskit), because we only need three qubits, then we could take advantage of the 5 qubits topologies like Tenerife or Yorktown [79]. It is important to clarify that IBM Q [63] has the technology to be able to implement the qubit reset gate on its QPUs [paper Jay Gambetta and Chow], which should only be put into service.

3. A similar case to that of IBM Q happens with Rigetti [82], that is, the qubit reset gate cannot be freely used on any part of the quantum circuit in all its lattices [82] but only at the beginning. Therefore, here we will also resort to its QVM instead of its QPU. Apparently, Rigetti would also possess the technology to do so in a future.

4. There is a slight difference between the mathematical value of the qubit to be prepared in Eq.(81) $q[0] = (85.3553\% |0\rangle, 14.6447\% |1\rangle)$, and that we can see in the qubit prepared by Quirk [78] (**Figure 30**) $q[0] = (85.4\% |0\rangle, 14.6\% |1\rangle)$, and that prepared by IBM Q (**Figure 31**) $q[0] = (86\% |0\rangle, 14\% |1\rangle)$. The difference is minimal, however, we must highlight it because the experiment is by comparison between the simulators. This is not something that we can control, because it is the interpretation that each simulator makes for that combination of matrices.

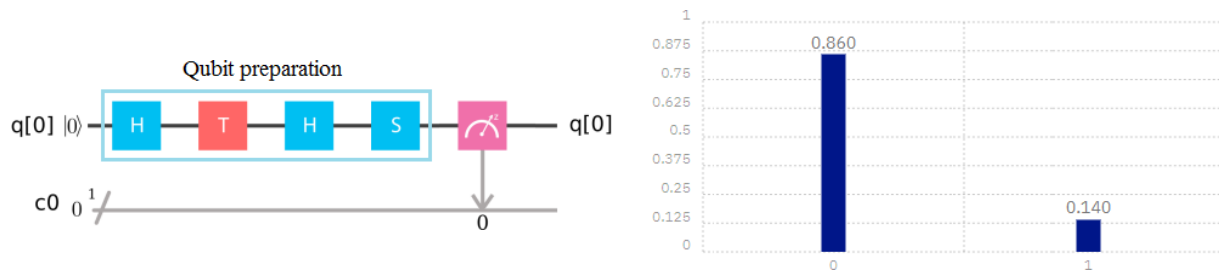**Figure 30** Qubit preparation of Eq.(81) on Quirk [78].

Figure 31 Qubit preparation of Eq.(81) on IBM Q [79]. Execution parameters: shots = 1024, seed = 7.

As happened in the previous cases, we are going to give to Quirk [78] the possibility of implementing the protocol of **Figure 28** first.
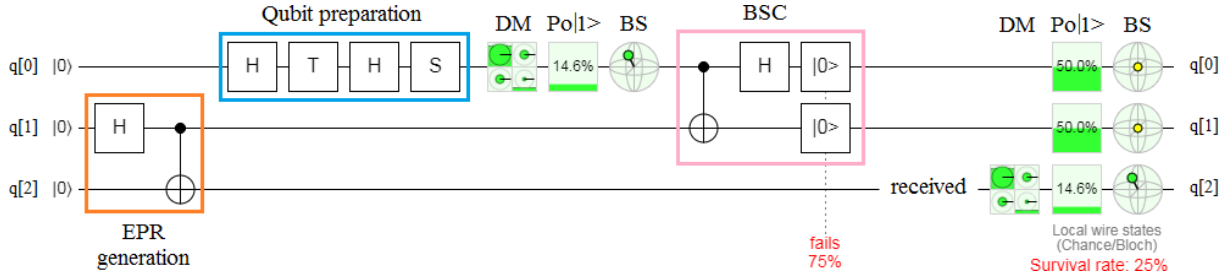

Figure 32 Controlled quantum teleportation protocol implemented on Quirk [X] simulator.

Figure 32 shows the Quirk [78] implementation of the controlled quantum teleportation protocol of **Figure 28**. The coincidence between the state of q[0] after qubit preparation block and q[2], at the end of protocol, is total. In fact, the three metrics (DM, Po|1>, and BS) in both points, are similar, which indicates that the teleportation was successful. Both qubits reset gates of BSC eliminates the 75 % of the projections that come out from BSC, establishing a survival rate of 25 %, which can be seen on the right-down corner of **Figure 32**. Although Quirk's qubit preparation values differ from those of the purely mathematical version of Eq.(81), the important thing here, is that the qubit to be teleported q[0] and the teleported qubit q[2] are identical. Obviously, decoherence and/or gates' noise is not taken into account on this platform.

The IBM Q [79] implementation of **Figure 28** protocol can be seen in **Figure 33**. IBM Q only allows measurements at the end of a process (as indeed all simulators do with a strong practical commitment), then, between the blocks of qubit preparation and Bell State Control (BSC) there is only a barrier, instead of the metrics for the qubit's status evaluation to be teleported which was in the same place for the Quirk case. **Figure 34** represents the probability bars for this experiment, which are identical to the output of qubit preparation block on the right of **Figure 31**. The execution parameters were: shots = 1024 and seed = 7.

Figure 33 Controlled quantum teleportation protocol implemented on IBM Q [79] simulator.

Figure 34 Probability bars for the experiment of **Figure 33**.

Next, we analyze the results obtained on Rigetti's platform [82], which can be seen in **Figure 35**, and they are: wavefunction, amplitudes, and probabilities.


```
----------WAVEFUNCTION----------
(0.9238795325+0.3826834324j)|000>
----------AMPLITUDES----------
[0.92387953+0.38268343j 0.        +0.j     0.        +0.j
 0.        +0.j         0.        +0.j     0.        +0.j
 0.        +0.j         0.        +0.j     ]
----------PROBABILITIES----------
Key Prob
000 0.1464466094067262
001 0.0
010 0.853553390593274
011 0.0
100 0.0
101 0.0
110 0.0
111 0.0
----------RESULTS----------
[[0]]
```

Figure 35 Captured screen with wavefunction, amplitudes, and probabilities on Rigetti platform [82].

The first relevant aspect that we can observe from **Figure 35** consists of the absolute coincidence between the values delivered by this platform and those of the Eq.(81) due to the purely mathematical version. The relationship between the wavefunction, the density matrix and the probabilities is exposed in Equations (83), (84) and (85).

$$|\psi\rangle = \alpha|0\rangle + \beta|1\rangle = \alpha\begin{bmatrix}1\\0\end{bmatrix} + \beta\begin{bmatrix}0\\1\end{bmatrix} = \begin{bmatrix}\alpha\\\beta\end{bmatrix} = \begin{bmatrix}0.9238795325\\0.3826834324\end{bmatrix} \tag{83}$$

$$|\psi\rangle\langle\psi| = \begin{bmatrix}\alpha\\\beta\end{bmatrix}\begin{bmatrix}\alpha^* & \beta^*\end{bmatrix} = \begin{bmatrix}|\alpha|^2 & \alpha\beta\\\beta\alpha & |\beta|^2\end{bmatrix}$$
$$= \begin{bmatrix}0.9238795325\\0.3826834324\end{bmatrix}\begin{bmatrix}0.9238795325 & 0.3826834324\end{bmatrix} = \begin{bmatrix}0.8535533905 & 0.3573883144\\0.3573883144 & 0.1464466094\end{bmatrix} \tag{84}$$

$$Po|0\rangle = 0.8535533905$$
$$Po|1\rangle = 0.1464466094 \tag{85}$$

where $(\bullet)^*$ means conjugate transpose of $(\bullet)$, $Po|0>$ means *Probability of* $|0>$, and $Po|1>$ means *Probability of* $|1>$. Therefore, we can say that the original qubit of Eq.(81) has been prepared and impeccably teleported on Rigetti's platform [82] as in any other platform.

3.3. Some preliminary reflections

It is evident that from an uncontrolled process like quantum measurement any signaling activity is impossible. It is simply a mechanism of observation of nature, which does not allow the control or use of any attribute of said nature as the instant communication between entangled particles. We saw this, in detail, both for the case of EPR pair in Subsection 3.1.1 and for the uncontrolled (standard) quantum teleportation protocol in Subsection 3.2.1.

Although all the implementations were carried out on simulators, both gate noise and decoherence do not affect the instantaneity of the controlled quantum teleportation protocol, given that, as we have seen in Subsections 2.4 and 2.5, this instantaneity is somewhat innate of the very nature of quantum

entanglement, that is, of the characteristics of avatars and their location. However, and returning for a moment to Subsection 2.5, if we put the entanglement in a practical context such as the quantum teleportation, due to the implementation of the latter through noisy gates, this non-zero noise interacts with the infinite bandwidth of the entanglement to give a finite channel capacity [60], that is, the noise degraded the attributes of the link, as it could not be otherwise.

The Bell State Measurement (BSM) block used by the uncontrolled (standard) quantum teleportation protocol produces an ambiguity, which is expressed as a purely random and equiprobable process. Quantum measurement starts the disambiguation process from which two bits arise that will be transmitted to Bob through a classical channel and at the same time destroys the entanglement. These two classical bits indicate on which of the four bases the qubit to be teleported is projected, i.e., by which of the four gates the cow of **Figure 24** came out. Besides, the same quantum measurement process avoids the violation of No-Cloning Theorem [85], since when the entanglement dies and therefore all the projections of the treated qubit die too, the only surviving qubit will be on Bob's side when applying the corresponding unitary transformations according to the instructions sent by Alice.

On the other hand, in the case of the controlled version of quantum teleportation protocol, the *in pectore* action of the qubit reset gates, *ad referendum* of the Bell State Control (BSC), does not generate ambiguity and does not violate the No-Cloning Theorem. The intervention of the qubit reset gates is equivalent to always leaving the gate |00> of **Figure 29** open exclusively, eliminating the entanglement and establishing a control over the experiment by which Bob knows in advance which gate the cow comes out of, i.e., what unitary transformation applies, which in this case is equal to the identity matrix, thus, Bob does not need to do anything to recover the teleported state.

Finally, we should not confuse the controlled quantum teleportation protocol presented in this work, which allows an instantaneous communication, with that made by Valivarthi *et al* [86] and what was implemented in [87], since the latter implies a statistical analysis after the experiment was ended using a gate present in Quirk [78] and known as "*post-select* |0><0|". This experiment does not imply an instantaneous teleportation at all, in fact, it is slower than the uncontrolled or standard version (that disambiguates via classic channel), since, the result is achieved once the experiment is finished. Then, there is no teleportation whatsoever but a conclusion. Alice and Bob finally exchange results using another channel (or meet at the end of the experiment) and everything is reduced to a statistical analysis, because, if Alice and Bob did not share data, then Bob would have to guess Alice's statistical results.

4. Other experiments

Next, we will evaluate a series of Quantum Communication tools, some of which will incorporate the control concept seen so far and that will help us to face the technology necessary for an efficient implementation of Quantum Internet [88-94].

4.1. Robust quantum teleportation

In this subsection, we will analyze the following cases of quantum teleportation, namely:

- Noiseless non-robust uncontrolled quantum teleportation: this case was seen in Subsection 3.2.1,
- Noiseless non-robust controlled quantum teleportation: this case was seen in Subsection 3.2.2,
- Noisy non-robust uncontrolled quantum teleportation: this case will be seen in the Subsection 4.1.1,
- Noisy non-robust controlled quantum teleportation: this case will be seen in the Subsection 4.1.2,
- Noiseless robust uncontrolled quantum teleportation: this case will be seen in the Subsection 4.1.3,
- Noiseless robust controlled quantum teleportation: this case will be seen in the Subsection 4.1.4,
- Noisy robust uncontrolled quantum teleportation: this case will be seen in the Subsection 4.1.5, and
- Noisy robust controlled quantum teleportation: this case will be seen in the Subsection 4.1.6.

When we say *noisy*, we actually refer to foreseeing the presence of noise from the very deduction of the quantum teleportation protocol.

4.1.1. Noisy non-robust uncontrolled quantum teleportation

So far, we have talked about the noise introduced by the gates used by the quantum teleportation protocols, but we have not mentioned them in particular. Specifically, there are three types of noise:

- Bit flip,
- Phase flip (or phase damping), and
- Bit-phase flip

However, we will model all the noise present in the protocols associated with the EPR pair, that is, $|\beta_{00}\rangle$, since the entangled pair is present at each point of said protocols. Therefore, based on **Figure 23**, we will consider a noise of the type,

$$|\beta_{00}\rangle_n = A|00\rangle + B|11\rangle \tag{86}$$

where subscript n means *noise*, and

$$|A|^2 + |B|^2 = 1, \tag{87}$$

with $A \neq B$. Then, repeating Eq.(78) but with $|\beta_{00}\rangle_n$ instead of $|\beta_{00}\rangle$, we will have

$$
\begin{aligned}
|\psi_0\rangle = |\psi\rangle|\beta_{00}\rangle_n &= (\alpha|0\rangle + \beta|1\rangle)(A|00\rangle + B|11\rangle) \\
&= \alpha A|000\rangle + \beta A|100\rangle + \alpha B|011\rangle + \beta B|111\rangle
\end{aligned} \tag{88}
$$

Now, a CNOT gate is applied to Eq.(88), resulting in

$$|\psi_1\rangle = \alpha A|000\rangle + \beta A|110\rangle + \alpha B|011\rangle + \beta B|101\rangle \tag{89}$$

Then, we apply a Hadamard's gate to the elements of Eq.(89),

$$\tag{90}$$

$$
\begin{aligned}
|\psi_2\rangle &= \frac{1}{\sqrt{2}}\Big[\alpha A|000\rangle + \alpha A|100\rangle + \beta A|010\rangle - \beta A|110\rangle + \alpha B|011\rangle + \alpha B|111\rangle + \beta B|001\rangle - \beta B|101\rangle\Big] \\
&= \frac{A}{\sqrt{2}}|00\rangle\alpha|0\rangle + \frac{B}{\sqrt{2}}|00\rangle\beta|1\rangle + \frac{A}{\sqrt{2}}|10\rangle\alpha|0\rangle - \frac{B}{\sqrt{2}}|10\rangle\beta|1\rangle + \frac{A}{\sqrt{2}}|01\rangle\beta|0\rangle + \frac{B}{\sqrt{2}}|01\rangle\alpha|1\rangle + \frac{B}{\sqrt{2}}|11\rangle\alpha|1\rangle - \frac{A}{\sqrt{2}}|11\rangle\beta|0\rangle \\
&= \frac{1}{\sqrt{2}}\Big[|00\rangle(A\alpha|0\rangle + B\beta|1\rangle) + |10\rangle(A\alpha|0\rangle - B\beta|1\rangle) + |01\rangle(B\alpha|1\rangle + A\beta|0\rangle) + |11\rangle(B\alpha|1\rangle - A\beta|0\rangle)\Big] \\
&= \frac{1}{\sqrt{2}}\Big[|00\rangle(\alpha|0_n\rangle + \beta|1_n\rangle) + |10\rangle(\alpha|0_n\rangle - \beta|1_n\rangle) + |01\rangle(\alpha|1_n\rangle + \beta|0_n\rangle) + |11\rangle(\alpha|1_n\rangle - \beta|0_n\rangle)\Big] \\
&= \frac{1}{\sqrt{2}}\Big[|00\rangle X^0 Z^0|\psi_n\rangle + |10\rangle X^1 Z^0|\psi_n\rangle + |01\rangle X^0 Z^1|\psi_n\rangle + |11\rangle X^1 Z^1|\psi_n\rangle\Big] \\
&= \frac{1}{\sqrt{2}}\Big[|\Phi^+\rangle X^0 Z^0|\psi_n\rangle + |\Phi^-\rangle X^1 Z^0|\psi_n\rangle + |\Psi^+\rangle X^0 Z^1|\psi_n\rangle + |\Psi^-\rangle X^1 Z^1|\psi_n\rangle\Big] \\
&= \begin{bmatrix} \frac{\alpha_n}{2} & \frac{\alpha_n}{2} & \frac{\beta_n}{2} & -\frac{\beta_n}{2} & \frac{\beta_n}{2} & -\frac{\beta_n}{2} & \frac{\alpha_n}{2} & \frac{\alpha_n}{2} \end{bmatrix}^T \\
&= \begin{bmatrix} \frac{\alpha_n}{2} & 0 & \frac{\beta_n}{2} & 0 & 0 & 0 & 0 & 0 \end{bmatrix}^T \to |\Phi^+\rangle \to |00\rangle \to 00 \to X^0 Z^0 \\
&+ \begin{bmatrix} 0 & \frac{\alpha_n}{2} & 0 & -\frac{\beta_n}{2} & 0 & 0 & 0 & 0 \end{bmatrix}^T \to |\Psi^+\rangle \to |10\rangle \to 10 \to X^0 Z^1 \\
&+ \begin{bmatrix} 0 & 0 & 0 & 0 & \frac{\beta_n}{2} & 0 & \frac{\alpha_n}{2} & 0 \end{bmatrix}^T \to |\Phi^-\rangle \to |01\rangle \to 01 \to X^1 Z^0 \\
&+ \begin{bmatrix} 0 & 0 & 0 & 0 & 0 & -\frac{\beta_n}{2} & 0 & \frac{\alpha_n}{2} \end{bmatrix}^T \to |\Psi^-\rangle \to |11\rangle \to 11 \to X^1 Z^1
\end{aligned}
$$

where,

$$|0_n\rangle = A|0\rangle \qquad (91)$$

$$|1_n\rangle = B|1\rangle \qquad (92)$$

$$|\psi_n\rangle = \alpha|0_n\rangle + \beta|1_n\rangle \qquad (93)$$

$$\left(\alpha_n|0\rangle = \alpha|0_n\rangle\right) \Rightarrow \left(\alpha_n\langle0|0\rangle = \alpha\langle0|0_n\rangle\right) \Rightarrow \left(\alpha_n = \alpha\langle0|0_n\rangle = \alpha\langle0|A|0\rangle = \alpha A\langle0|0\rangle = \alpha A\right) \qquad (94)$$

$$\left(\beta_n|1\rangle = \beta|1_n\rangle\right) \Rightarrow \left(\beta_n\langle1|1\rangle = \beta\langle1|1_n\rangle\right) \Rightarrow \left(\beta_n = \beta\langle1|1_n\rangle = \beta\langle1|B|1\rangle = \beta B\langle1|1\rangle = \beta B\right) \qquad (95)$$

From here on, we will follow a similar procedure to that of Table I in Subsection 3.2.1 but taking into account how sensitively the state is affected by noise. In fact, seeing Eq.(90), it is evident that it is almost impossible to recover the state $|\psi\rangle$ in an exact way. This is what we have seen in **Figure 27** in Subsection 3.2.1, which shows the probability bars of IBM Q [79] implementation.

4.1.2. Noisy non-robust controlled quantum teleportation

Although in the three implementations of Subsection 3.2.2 there is no difference between the state to be teleported and the state received by Bob, the reality is that there is a difference, which is hidden because the implementations were made on simulators. This protocol involves eliminating the last three rows of Eq.(90), however, the line that remains, associated with the base $|\Phi^+\rangle$, is undoubtedly affected by the noise of α_n and β_n. Besides, the state to be teleported will not generally be on a sphere, much less a unitary sphere, because it will generally not be fulfilled:

$$|\alpha_n|^2 + |\beta_n|^2 = |\alpha A|^2 + |\beta B|^2 = 1 \qquad (96)$$

4.1.3. Noiseless robust uncontrolled quantum teleportation

In this new protocol, **Figure 36**, we produce $|\beta_{00}\rangle \otimes |\psi\rangle$ instead of $|\psi\rangle \otimes |\beta_{00}\rangle$ used in the previous versions. We must highlight as a fundamental contrast between this version of quantum teleportation and the previous one that the Kronecker product "$\otimes$" is not commutative [39], then,

$$\begin{aligned}
|\psi_0\rangle = |\beta_{00}\rangle|\psi\rangle &= \frac{1}{\sqrt{2}}\left(|00\rangle + |11\rangle\right)\left(\alpha|0\rangle + \beta|1\rangle\right) \\
&= \frac{1}{\sqrt{2}}\left[\alpha|000\rangle + \beta|001\rangle + \alpha|110\rangle + \beta|111\rangle\right] \\
&= \left[\alpha/\sqrt{2} \quad 0 \quad 0 \quad \alpha/\sqrt{2} \quad \beta/\sqrt{2} \quad 0 \quad 0 \quad \beta/\sqrt{2}\right]^T
\end{aligned} \qquad (97)$$

Figure 36 Robust uncontrolled quantum teleportation using two classical bits for disambiguation.

Now, a *CNOT* gate is applied to Eq.(97), and the result will be present on the Alice's lower branch, because in her upper branch will be $\left|\beta_{00}\right\rangle$,

$$|\psi_1\rangle = \frac{1}{\sqrt{2}}\left[\alpha|000\rangle + \beta|001\rangle + \alpha|100\rangle + \beta|101\rangle\right] = \frac{1}{\sqrt{2}}\left[|00\rangle(\alpha|0\rangle + \beta|1\rangle) + |10\rangle(\alpha|0\rangle + \beta|1\rangle)\right]$$

$$= \frac{1}{\sqrt{2}}(\alpha|0\rangle + \beta|1\rangle)\left[|00\rangle + |10\rangle\right] = (\alpha|0\rangle + \beta|1\rangle)\left[\frac{1}{\sqrt{2}}(|0\rangle + |1\rangle)\right]|0\rangle = |\psi\rangle|+\rangle|0\rangle \qquad (98)$$

It is evident from **Figure 36** that the Hadamard's gate only involves to the Alice's upper branch, then,

$$(I \otimes H)|\beta_{00}\rangle = \left(\begin{bmatrix} 1 & 0 \\ 0 & 1 \end{bmatrix} \otimes \frac{1}{\sqrt{2}}\begin{bmatrix} 1 & 1 \\ 1 & -1 \end{bmatrix}\right)\frac{1}{\sqrt{2}}(|00\rangle + |11\rangle)$$

$$= \frac{1}{2}(|00\rangle + |10\rangle + |01\rangle - |11\rangle) \qquad (99)$$

We can draw some conclusions based on Eq.(98):

- the qubit to be teleported only has projection on $|+\rangle|0\rangle$,
- there is not overlapping of bases (or projections) that happened in Eq.(80) and Eq.(90),
- although the cow can only exit through the gate |+0>, Alice must still measure to eliminate the entanglement and transmit that information to Bob. In this way, the No-Cloning Theorem is not violated when reconstructing the teleported state from Bob's side thanks to an unitary transform, and
- the previous items simplify the data collection on the SPD block of the BSM.

Figure 37 shows the implementation of this protocol on Quirk [78]. The absolute equivalence between the qubit to be teleported and the recovered one, can only be explained by working on a simulator that does not consider noise or decoherence.

Figure 37 Robust uncontrolled quantum teleportation protocol implemented on Quirk [78] simulator.

Figure 38 Robust uncontrolled quantum teleportation protocol implemented on IBM Q [79] simulator.

In contrast, **Figures 38** and **39** take decoherence into account, although they also come from a simulator, such as IBM Q [79]. In particular, the probability bars in **Figure 39** give us the following values: 0.222+0.206+0.205+0.200 = 0.833 for |0> and 0.050+0.041+0.041+0.035 = 0.167 for |1>, which differs slightly from the values of the prepared qubit, i.e., 0.86 for |0> and 0.14 for |1>. The execution parameters were: shots = 1024 and seed = 7.

Figure 39 Probability bars for the experiment of **Figure 38**.

Finally, **Figure 40** shows the implementation of the new protocol on Rigetti's platform [82]. As we can see, the captured screen of **Figure 40** shows very similar results to those of **Figure 35**. The future implementation of the qubit reset gate on the physical quantum machines (QPU) of Rigetti [82] and IBM Q [79] will allow us to evaluate the true impact of the decoherence on these protocols.

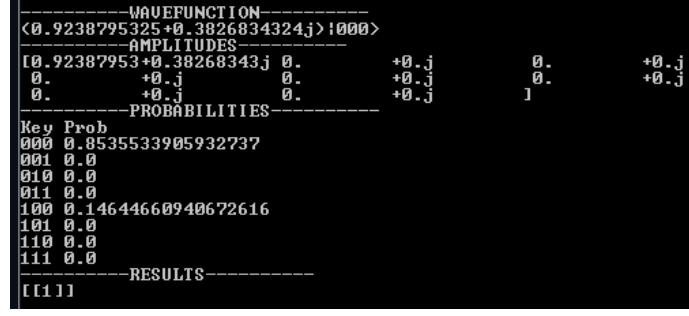**Figure 40** Captured screen with wavefunction, amplitudes, and probabilities on Rigetti platform [82].

4.1.4. Noiseless robust controlled quantum teleportation

The controlled version of the previous protocol is also based on the use of two qubit reset gates [|0>] at the output of the Bell's State Control (BSC) block (**Figure 41**) with identical criteria to the case of **Figure 28**.

Figure 41 Robust controlled quantum teleportation using two qubit reset [|0>] gates.

This protocol, like the previous case, is based on the last row of Eq.(99). The action of both qubit reset gates is equivalent to the control of the experiment at the output of the BSC, thus eliminating the need for any measurement or transfer of classical information from Alice to Bob. The same control process eliminates the entanglement. However, on Bob's side, the state recovers perfectly and instantaneously without the need to apply any unitary transformation.

Figure 42 represents the implementation of this protocol on Quirk platform [78]. The most notable difference with respect to the previous case is at the height of the BSC, where, despite that Eq.(99) only shows projection on a base, the action of both qubit reset gates eliminates 75% of the elements to the output of said BSC, which is shown in red as: fails 75%.

Figure 42 Robust controlled quantum teleportation protocol implemented on Quirk [78] simulator.

Figure 43 represents the quantum circuits of this protocol. As we can see, the details of the action of both qubit reset gates is not as graphic or explicit as in the case of Quirk, however, the probability bars of **Figure 44** tell us of an exact teleportation of the state, i.e., Bob gets: 0.86 for |0> and 0.14 for |1>, with the same execution parameters of the previous case: shots = 1024 and seed = 7.

Figure 43 Robust controlled quantum teleportation protocol implemented on IBM Q [79] simulator.

Figure 44 Probability bars for the experiment of **Figure 43**.

Captured screen of **Figure 45** shows us the wavefunction, amplitudes and probabilities on Rigetti's platform [82], which are practically the same values of **Figure 40** for the previous protocol.

43

Figure 45 Captured screen with wavefunction, amplitudes, and probabilities on Rigetti platform [82].

4.1.5. Noisy robust uncontrolled quantum teleportation

For this case, we will resort again to the base $\left|\beta_{00}\right\rangle_n$ of Eq.(86), to which, we assign the noise of the protocol as a whole, then,

$$
\begin{aligned}
\left|\psi_0\right\rangle = \left|\beta_{00}\right\rangle_n\left|\psi\right\rangle &= \left(A\left|00\right\rangle + B\left|11\right\rangle\right)\left(\alpha\left|0\right\rangle + \beta\left|1\right\rangle\right)\\
&= \alpha A\left|000\right\rangle + \beta A\left|001\right\rangle + \alpha B\left|110\right\rangle + \beta B\left|111\right\rangle\\
&= \begin{bmatrix} \alpha A & \beta A & 0 & 0 & 0 & 0 & \alpha B & \beta B\end{bmatrix}^T
\end{aligned}
\tag{100}
$$

Now, a *CNOT* gate is applied to Eq.(100), and the result will be present on the Alice's lower branch again, because in her upper branch will be $\left|\beta_{00}\right\rangle_n$,

$$
\begin{aligned}
\left|\psi_1\right\rangle &= A\alpha\left|000\right\rangle + B\alpha\left|100\right\rangle + A\beta\left|001\right\rangle + B\beta\left|101\right\rangle\\
&= A\left|00\right\rangle\left(\alpha\left|0\right\rangle + \beta\left|1\right\rangle\right) + B\left|10\right\rangle\left(\alpha\left|0\right\rangle + \beta\left|1\right\rangle\right)\\
&= \left(A\left|00\right\rangle + B\left|10\right\rangle\right)\left(\alpha\left|0\right\rangle + \beta\left|1\right\rangle\right) = \left(A\left|00\right\rangle + B\left|10\right\rangle\right)\left|\psi\right\rangle = C\left|\psi\right\rangle
\end{aligned}
\tag{101}
$$

where

$$
C = \left(A\left|00\right\rangle + B\left|10\right\rangle\right).
\tag{102}
$$

In this case again, the Hadamard's gate only involves to the Alice's upper branch, then,

$$
\begin{aligned}
\left(I \otimes H\right)\left|\beta_{00}\right\rangle_n &= \left(\begin{bmatrix} 1 & 0 \\ 0 & 1\end{bmatrix} \otimes \frac{1}{\sqrt{2}}\begin{bmatrix} 1 & 1 \\ 1 & -1\end{bmatrix}\right)\left(A\left|00\right\rangle + B\left|11\right\rangle\right)\\
&= \frac{1}{\sqrt{2}}\left(A\left|00\right\rangle + A\left|10\right\rangle + B\left|01\right\rangle - B\left|11\right\rangle\right)
\end{aligned}
\tag{103}
$$

In other words, the noise causes that the state to be teleported is projected on a pair of bases at the exit of the BSC, as opposed to the noiseless case that it did on a single base. On the other hand, the state recovered from Bob's side will always be on a sphere although not necessarily a unitary one.

4.1.6. Noisy robust controlled quantum teleportation

The action of the qubit reset gates at the output of the BSC on the third row of Eq.(102) does not modify the result between both versions. It only makes the controlled version instantaneous, compared to the speed limitations of the uncontrolled version because of the classical channel used between Alice and Bob. In other words, the transmission of classical bits of disambiguation on the classical channel is limited by the speed of light.

4.2. Interfaces

In the quantum internet context [88-94], we will need to teleport classical information too, in an instantaneous way, if it is possible. Then, we will need Classical-to-Quantum (Cl2Qu) and Quantum-to-Classical (Qu2Cl) interfaces, which must comply with a series of conditions, for an optimal treatment and recovery of data. For reasons of spatial and temporal sequentiality, we will be very demanding with the conditions to be met by the Cl2Qu interface, given that its performance strongly conditions the performance of the chosen teleportation protocol, as well as, the performance of the Qu2Cl interface, which finally retrieves the teleported data. Therefore, all Cl2Qu interface must meet, *sine qua non* conditions such as the following:

a) ***Traceability:*** every bit to be teleported must not lose the necessary traceability throughout the entire process, which will also be seen as an inexcusable link between the bit and its location in the organization of data at all times. What is the reason for such a mandatory condition? The reason is that no physical quantum computer allows intermediate instances of quantum measurement. In other words, if the outcomes are not what we expected, then there is no way to go back and identify the source of the problem in the process. This is clearly in tune with the fact that the quantum world and its implementation in gates that respond to the different Algebras [1, 39] (Clifford, Pauli, etc.) represents an eclectic environment.

b) ***Homotopical relation:*** every bit of the set to be teleported (digital, i.e., classical) must maintain a homotopical relation of type $bit \rightarrow [\,Cl2Qu\,] \rightarrow |bit\rangle \equiv qubit$ with its counterpart within the physical quantum computer, for the same reason mentioned above.

c) ***Automatic intake:*** every bit to be teleported (digital, i.e., classical) must be converted to its quantum counterpart in an automatic way. The reason is more than obvious, just picture, as an example, the possibility of transmitting a color image of 1920x1080 pixels (i.e., 1920x1080x3x8 bits), then, the data volume of qubits to be prepared would be approximately of 50 Million. Who can and/or wants to prepare 50 Million of qubits by hand?

d) ***Facilitation in the design of the Quantum-to-Classical (Qu2Cl) interface:*** this condition is evidently essential for a correct recovery of outcomes, considering the problem of quantum measurement [37, 38] and complementarity [55, 56], which only ensure a complete accuracy in the recovery of the measured qubits if they have projection on a single axis exclusively, as is the case of the CBS, i.e., {|0>,|1>}. In other words, if the three previous conditions are met, then the Qu2Cl interface (i.e., which recovers the outcomes) is extremely simple. In fact, a quantum measurement exclusively on the *z* axis of the Bloch's sphere (**Figure 1**) is precisely how the physical quantum computers currently in service work. See Rigetti [82] and IBM Q Experience [79].

The Cl2Qu interface that we will propose requires an EPR pair for each pair of bits to be converted into qubits. This may seem that we will not fulfill the previous (c) condition as efficiently as required, however, it is simply a first step in the right direction, given that at least for proof of concept, it has proven to have a remarkable performance.

On the other hand, and as is evident, the only way to comply with such demands is to work with CBS, i.e., {|0>,|1>}. Then, an alternative to which we can resort is the Superdense Coding (SDC) protocol [39], from which emerges an extraordinary pair of interfaces for a direct relationship between classical bits and CBS, and vice-versa. **Figure 46** shows the SDC protocol, which is composed of two well-defined blocks: one which is light blue and the other one pink. The light blue block works as a Cl2Qu interface, while the pink block works as a Qu2Cl interface. All this, of course, is exclusively defined to be used with classical bits, and in consequence, with CBS.

As we can see in **Figure 46**, the problem with this Cl2Qu interfaces is that it requires an EPR pair for each pair of classical bits to be converted into CBS. However, an improved version is being developed right now [95], which will allow us to dramatically increase the efficiency of this interface by requiring a single EPR pair to convert an unlimited number of classical bits (at first) in CBS.
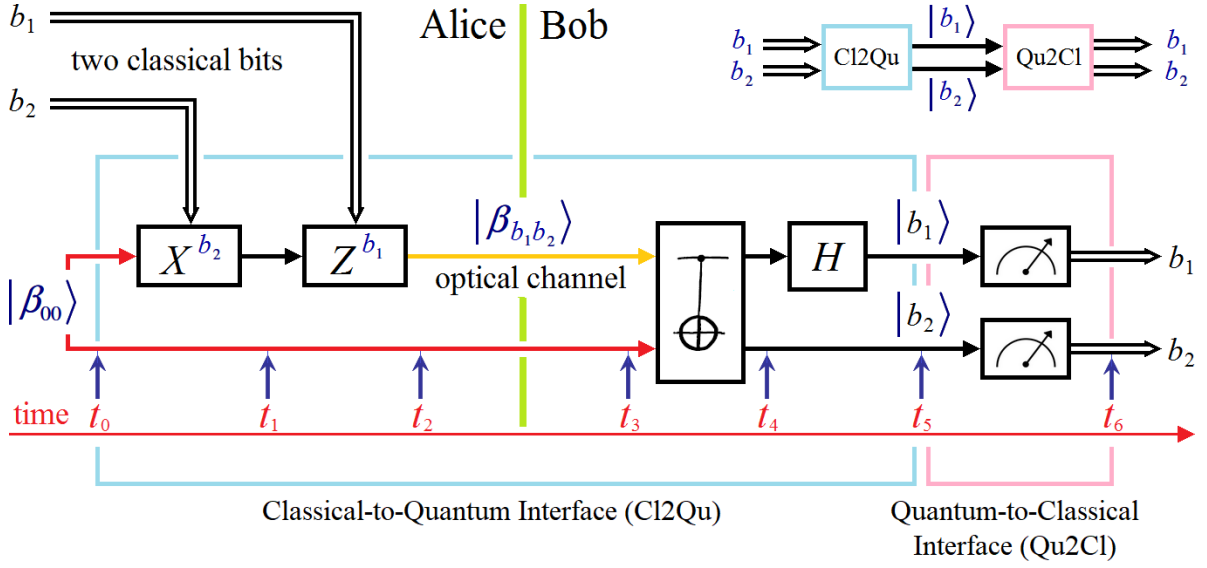
Figure 46 SDC protocol and the detail of both interfaces: Cl2Qu and Qu2Cl.

If we cut the SDC protocol, in such a way to extract the Cl2Qu interface, we will obtain **Figure 47**, which completely complies with all the conditions required by a Cl2Qu interface and that were previously enunciated.
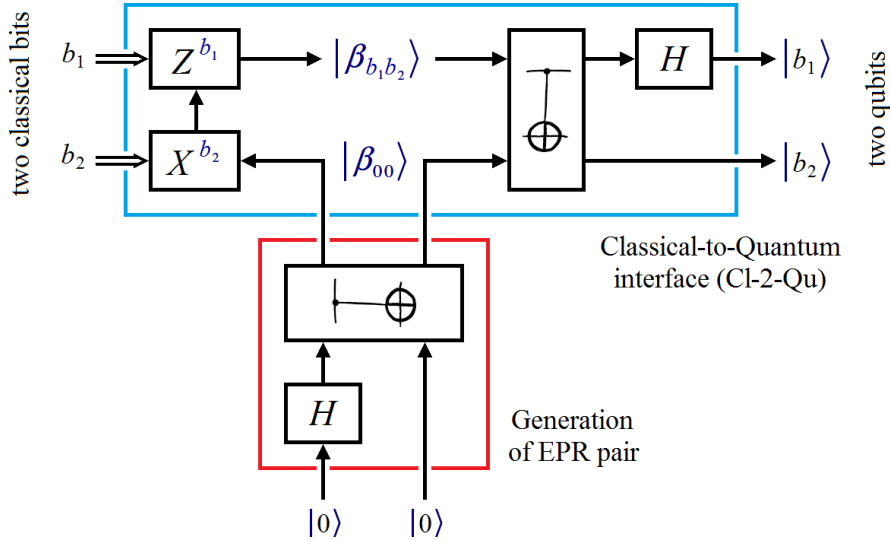

Figure 47 Classical-to-quantum (Cl2Qu) interface.

The Cl2Qu interface of **Figure 47** is derived from the SDC protocol and therefore can only convert two classical bits to its CBS counterpart, that is, $\{b_1, b_2\} \rightarrow Cl2Qu \rightarrow \{|b_1\rangle, |b_2\rangle\}$, being this a completely homotopic way, however, both the interface and its explanation are absolutely transferable to any number of bits, as it will happen in Subsection 5.2.

We create an EPR pair (i.e., two $|\beta_{00}\rangle$ entangled states) from two ground states |0>. Then, we have two possibilities according to b_2, i.e., 0 or 1. If $b_2 = 0$, then, at the output of the Pauli's gate X, we will have $|\beta_{00}\rangle$ again. See **Figure 47**. But, if $b_2 = 1$, then, at the output of the Pauli's gate X, we will have,

$$(\sigma_x \otimes I)|\beta_{00}\rangle = \left(\begin{bmatrix} 0 & 1 \\ 1 & 0 \end{bmatrix} \otimes \begin{bmatrix} 1 & 0 \\ 0 & 1 \end{bmatrix} \right) \begin{bmatrix} 1/\sqrt{2} \\ 0 \\ 0 \\ 1/\sqrt{2} \end{bmatrix} = \begin{bmatrix} 0 & 0 & 1 & 0 \\ 0 & 0 & 0 & 1 \\ 1 & 0 & 0 & 0 \\ 0 & 1 & 0 & 0 \end{bmatrix} \begin{bmatrix} 1/\sqrt{2} \\ 0 \\ 0 \\ 1/\sqrt{2} \end{bmatrix} = \begin{bmatrix} 0 \\ 1/\sqrt{2} \\ 1/\sqrt{2} \\ 0 \end{bmatrix} \tag{104}$$

If, at the output of the Pauli's gate Z, $b_2 = 0$ and $b_1 = 0$, then, we will obtain $|\beta_{00}\rangle$. But if $b_2 = 0$ and $b_1 = 1$, we will have,

$$(\sigma_z \otimes I)|\beta_{00}\rangle = \left(\begin{bmatrix} 1 & 0 \\ 0 & -1 \end{bmatrix} \otimes \begin{bmatrix} 1 & 0 \\ 0 & 1 \end{bmatrix} \right) \begin{bmatrix} 1/\sqrt{2} \\ 0 \\ 0 \\ 1/\sqrt{2} \end{bmatrix} = \begin{bmatrix} 1 & 0 & 0 & 0 \\ 0 & 1 & 0 & 0 \\ 0 & 0 & -1 & 0 \\ 0 & 0 & 0 & -1 \end{bmatrix} \begin{bmatrix} 1/\sqrt{2} \\ 0 \\ 0 \\ 1/\sqrt{2} \end{bmatrix} = \begin{bmatrix} 1/\sqrt{2} \\ 0 \\ 0 \\ -1/\sqrt{2} \end{bmatrix} \tag{105}$$

Now, if $b_2 = 1$ and $b_1 = 1$, we will use the result of Eq.(104) to obtain the state at the output of the Pauli's gate Z,

$$(\sigma_z \otimes I) \begin{bmatrix} 0 \\ 1/\sqrt{2} \\ 1/\sqrt{2} \\ 0 \end{bmatrix} = \left(\begin{bmatrix} 1 & 0 \\ 0 & -1 \end{bmatrix} \otimes \begin{bmatrix} 1 & 0 \\ 0 & 1 \end{bmatrix} \right) \begin{bmatrix} 0 \\ 1/\sqrt{2} \\ 1/\sqrt{2} \\ 0 \end{bmatrix} = \begin{bmatrix} 1 & 0 & 0 & 0 \\ 0 & 1 & 0 & 0 \\ 0 & 0 & -1 & 0 \\ 0 & 0 & 0 & -1 \end{bmatrix} \begin{bmatrix} 0 \\ 1/\sqrt{2} \\ 1/\sqrt{2} \\ 0 \end{bmatrix} = \begin{bmatrix} 0 \\ 1/\sqrt{2} \\ -1/\sqrt{2} \\ 0 \end{bmatrix} \tag{106}$$

Evidently, the result at the output of the Pauli's gate Z is the same as that one at the input of the *CNOT* gate in the upper right sector of **Figure 47**. The four obtained results, according to the values of b_2 and b_1, are attached to the entrance of the aforementioned *CNOT* gate under the generic name of $|\beta_{b_1 b_2}\rangle$, that is, at this point we have reached a first conversion of the type: $\{b_1, b_2\} \to |\beta_{b_1 b_2}\rangle$.

Now, applying *CNOT* gate to these results, we will obtain,

$$\begin{bmatrix} 1 & 0 & 0 & 0 \\ 0 & 1 & 0 & 0 \\ 0 & 0 & 0 & 1 \\ 0 & 0 & 1 & 0 \end{bmatrix} \begin{bmatrix} 1/\sqrt{2} \\ 0 \\ 0 \\ 1/\sqrt{2} \end{bmatrix} = \begin{bmatrix} 1/\sqrt{2} \\ 0 \\ 1/\sqrt{2} \\ 0 \end{bmatrix} \qquad \text{(for } b_2 = 0 \text{ and } b_1 = 0) \tag{107}$$

$$\begin{bmatrix} 1 & 0 & 0 & 0 \\ 0 & 1 & 0 & 0 \\ 0 & 0 & 0 & 1 \\ 0 & 0 & 1 & 0 \end{bmatrix} \begin{bmatrix} 1/\sqrt{2} \\ 0 \\ 0 \\ -1/\sqrt{2} \end{bmatrix} = \begin{bmatrix} 1/\sqrt{2} \\ 0 \\ -1/\sqrt{2} \\ 0 \end{bmatrix} \qquad \text{(for } b_2 = 0 \text{ and } b_1 = 1) \tag{108}$$

$$\begin{bmatrix} 1 & 0 & 0 & 0 \\ 0 & 1 & 0 & 0 \\ 0 & 0 & 0 & 1 \\ 0 & 0 & 1 & 0 \end{bmatrix} \begin{bmatrix} 0 \\ 1/\sqrt{2} \\ 1/\sqrt{2} \\ 0 \end{bmatrix} = \begin{bmatrix} 0 \\ 1/\sqrt{2} \\ 0 \\ 1/\sqrt{2} \end{bmatrix} \qquad \text{(for } b_2 = 1 \text{ and } b_1 = 0) \tag{109}$$

$$\begin{bmatrix} 1 & 0 & 0 & 0 \\ 0 & 1 & 0 & 0 \\ 0 & 0 & 0 & 1 \\ 0 & 0 & 1 & 0 \end{bmatrix} \begin{bmatrix} 0 \\ 1/\sqrt{2} \\ -1/\sqrt{2} \\ 0 \end{bmatrix} = \begin{bmatrix} 0 \\ 1/\sqrt{2} \\ 0 \\ -1/\sqrt{2} \end{bmatrix} \qquad \text{(for } b_2 = 1 \text{ and } b_1 = 1) \tag{110}$$

Now, we will apply the Hadamard's gate to the last set of equations according to **Figure 47** [1, 39], then, we will have

for $b_2 = 0$ and $b_1 = 0$:

$$(H \otimes I)\begin{bmatrix} 1/\sqrt{2} \\ 0 \\ 1/\sqrt{2} \\ 0 \end{bmatrix} = \left(\begin{bmatrix} 1/\sqrt{2} & 1/\sqrt{2} \\ 1/\sqrt{2} & -1/\sqrt{2} \end{bmatrix} \otimes \begin{bmatrix} 1 & 0 \\ 0 & 1 \end{bmatrix}\right)\begin{bmatrix} 1/\sqrt{2} \\ 0 \\ 1/\sqrt{2} \\ 0 \end{bmatrix} = \begin{bmatrix} 1/\sqrt{2} & 0 & 1/\sqrt{2} & 0 \\ 0 & 1/\sqrt{2} & 0 & 1/\sqrt{2} \\ 1/\sqrt{2} & 0 & -1/\sqrt{2} & 0 \\ 0 & 1/\sqrt{2} & 0 & -1/\sqrt{2} \end{bmatrix}\begin{bmatrix} 1/\sqrt{2} \\ 0 \\ 1/\sqrt{2} \\ 0 \end{bmatrix} \tag{111}$$

$$= \begin{bmatrix} 1 \\ 0 \\ 0 \\ 0 \end{bmatrix} = \begin{bmatrix} 1 \\ 0 \end{bmatrix} \otimes \begin{bmatrix} 1 \\ 0 \end{bmatrix} = |0\rangle \otimes |0\rangle = |00\rangle$$

for $b_2 = 0$ and $b_1 = 1$:

$$(H \otimes I)\begin{bmatrix} 1/\sqrt{2} \\ 0 \\ -1/\sqrt{2} \\ 0 \end{bmatrix} = \left(\begin{bmatrix} 1/\sqrt{2} & 1/\sqrt{2} \\ 1/\sqrt{2} & -1/\sqrt{2} \end{bmatrix} \otimes \begin{bmatrix} 1 & 0 \\ 0 & 1 \end{bmatrix}\right)\begin{bmatrix} 1/\sqrt{2} \\ 0 \\ -1/\sqrt{2} \\ 0 \end{bmatrix} = \begin{bmatrix} 1/\sqrt{2} & 0 & 1/\sqrt{2} & 0 \\ 0 & 1/\sqrt{2} & 0 & 1/\sqrt{2} \\ 1/\sqrt{2} & 0 & -1/\sqrt{2} & 0 \\ 0 & 1/\sqrt{2} & 0 & -1/\sqrt{2} \end{bmatrix}\begin{bmatrix} 1/\sqrt{2} \\ 0 \\ -1/\sqrt{2} \\ 0 \end{bmatrix} \tag{112}$$

$$= \begin{bmatrix} 0 \\ 0 \\ 1 \\ 0 \end{bmatrix} = \begin{bmatrix} 0 \\ 1 \end{bmatrix} \otimes \begin{bmatrix} 1 \\ 0 \end{bmatrix} = |1\rangle \otimes |0\rangle = |10\rangle$$

for $b_2 = 1$ and $b_1 = 0$:

$$(H \otimes I)\begin{bmatrix} 0 \\ 1/\sqrt{2} \\ 0 \\ 1/\sqrt{2} \end{bmatrix} = \left(\begin{bmatrix} 1/\sqrt{2} & 1/\sqrt{2} \\ 1/\sqrt{2} & -1/\sqrt{2} \end{bmatrix} \otimes \begin{bmatrix} 1 & 0 \\ 0 & 1 \end{bmatrix}\right)\begin{bmatrix} 0 \\ 1/\sqrt{2} \\ 0 \\ 1/\sqrt{2} \end{bmatrix} = \begin{bmatrix} 1/\sqrt{2} & 0 & 1/\sqrt{2} & 0 \\ 0 & 1/\sqrt{2} & 0 & 1/\sqrt{2} \\ 1/\sqrt{2} & 0 & -1/\sqrt{2} & 0 \\ 0 & 1/\sqrt{2} & 0 & -1/\sqrt{2} \end{bmatrix}\begin{bmatrix} 0 \\ 1/\sqrt{2} \\ 0 \\ 1/\sqrt{2} \end{bmatrix} \tag{113}$$

$$= \begin{bmatrix} 0 \\ 1 \\ 0 \\ 0 \end{bmatrix} = \begin{bmatrix} 1 \\ 0 \end{bmatrix} \otimes \begin{bmatrix} 0 \\ 1 \end{bmatrix} = |0\rangle \otimes |1\rangle = |01\rangle$$

for $b_2 = 1$ and $b_1 = 1$:

$$(H \otimes I)\begin{bmatrix} 0 \\ 1/\sqrt{2} \\ 0 \\ -1/\sqrt{2} \end{bmatrix} = \left(\begin{bmatrix} 1/\sqrt{2} & 1/\sqrt{2} \\ 1/\sqrt{2} & -1/\sqrt{2} \end{bmatrix} \otimes \begin{bmatrix} 1 & 0 \\ 0 & 1 \end{bmatrix}\right)\begin{bmatrix} 0 \\ 1/\sqrt{2} \\ 0 \\ -1/\sqrt{2} \end{bmatrix} = \begin{bmatrix} 1/\sqrt{2} & 0 & 1/\sqrt{2} & 0 \\ 0 & 1/\sqrt{2} & 0 & 1/\sqrt{2} \\ 1/\sqrt{2} & 0 & -1/\sqrt{2} & 0 \\ 0 & 1/\sqrt{2} & 0 & -1/\sqrt{2} \end{bmatrix}\begin{bmatrix} 0 \\ 1/\sqrt{2} \\ 0 \\ -1/\sqrt{2} \end{bmatrix} \tag{114}$$

$$= \begin{bmatrix} 0 \\ 0 \\ 0 \\ 1 \end{bmatrix} = \begin{bmatrix} 0 \\ 1 \end{bmatrix} \otimes \begin{bmatrix} 0 \\ 1 \end{bmatrix} = |1\rangle \otimes |1\rangle = |11\rangle$$

In this way, we obtained the equivalent qubits. Essentially, Cl2Qu interface is a block that performs a transfer of type $\{b_1, b_2\} \rightarrow \{|b_1\rangle, |b_2\rangle\}$ for CBS, i.e., $\{0,1\} \rightarrow \{|0\rangle, |1\rangle\}$. Moreover, since Cl2Qu works with said CBS, then the Quantum-to-Classical (Qu2Cl) interface is reduced to that of **Figure 48**, that is, a simple quantum measurement on the z axis of the Bloch's sphere.

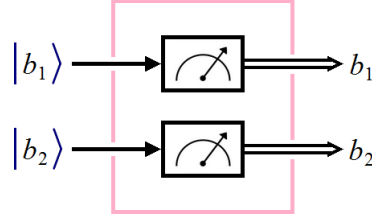Next, we will involve both interfaces in the quantum teleportation of classic information.

Figure 48 Quantum-to-Classical (Qu2Cl) interface.

4.3. Teleporting classical information

In this section, we will analyze the teleportation of classical information through an EPR channel in an instantaneous way. Specifically, this analysis will be especially oriented to the security of information. For this purpose, we will use the interfaces developed in the previous subsection.

4.3.1. Teleporting classical bits

Figure 49 shows on the left side 8 qubits ground state |0>. From q[0] and q[1] we construct b_1 and b_2. This possibility is exclusive to Quirk platform [78] which consists in using a quantum measurement on a CBS to obtain the corresponding bit. From q[2] to q[7] we have the ancilla states for the different EPR generation. We can clearly see four blocks in **Figure 49**:

- EPR and bits generation,
- Cl2Qu interface,
- Robust controlled quantum teleportation of both bits, and
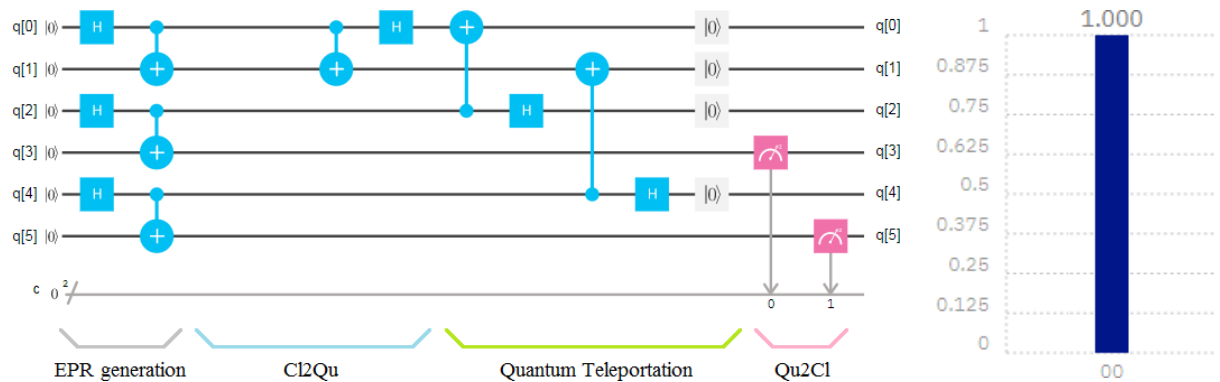- Qu2Cl interface.

Figure 49(a) Robust controlled quantum teleportation of a classical pair $\{b_1, b_2\} = \{0,0\}$ on Quirk [78].
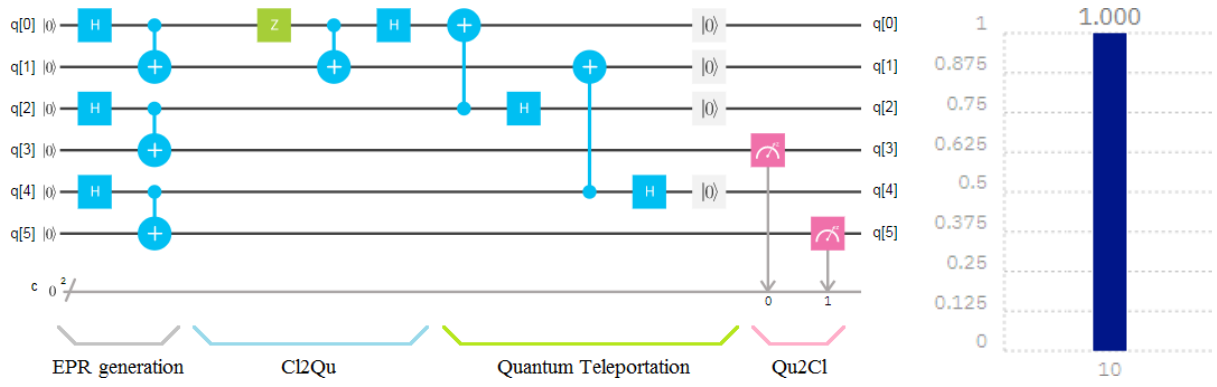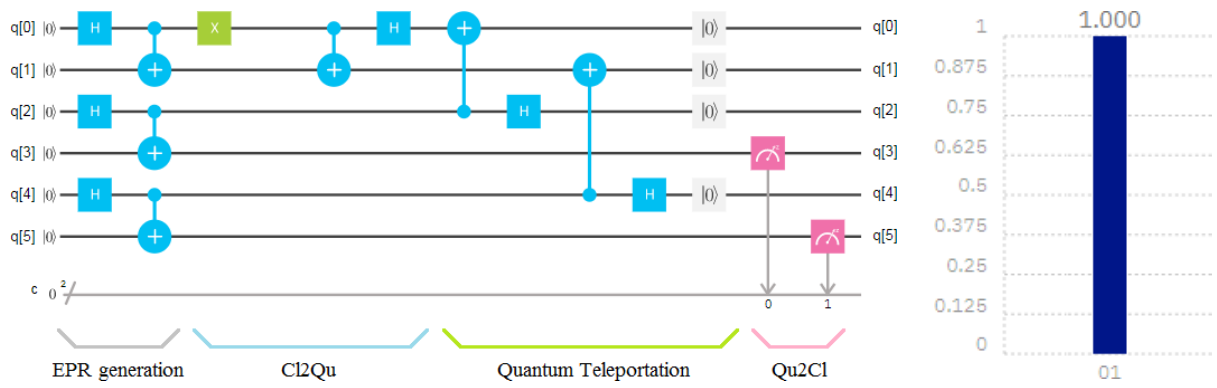

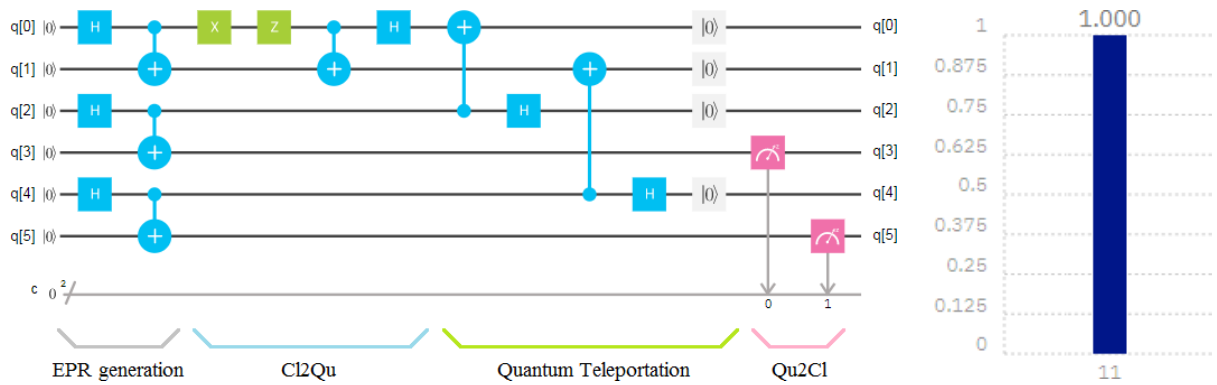**Figure 49(b)** Robust controlled quantum teleportation of a classical pair $\{b_1, b_2\} = \{0,1\}$ on Quirk [78].

Figure 49(c) Robust controlled quantum teleportation of a classical pair $\{b_1,b_2\}=\{1,0\}$ on Quirk [78].

Figure 49(d) Robust controlled quantum teleportation of a classical pair $\{b_1,b_2\}=\{1,1\}$ on Quirk [78].

The four options of **Figure 49** show all four possible combinations of classical bits to be teleported, i.e., $(b_1,b_2) \in \{(0,0); (0,1); (1,0); (1,1)\}$. On the right side of **Figures 49**, we can see that at the end of the Qu2Cl interface (i.e., the threads corresponding to q[5] and q[7]) we have exactly the same bits that those at the end of quantum measurement corresponding to q[0] and q[1] at the left side of the same figure, which indicates that the teleportation was perfectly done. The best witness of this are the Bloch's sphere (showing spin up for 0 and spin down for 1) and the Po|1> or Chance blocks (showing OFF for 0 and ON for 1) in each case. We must note that all quantum measurement are always at the end of each thread.

Figure 50 represents the same implementation of **Figure 49** but on IBM Q platform [79].

Figure 50(a) Robust controlled quantum teleportation of a classical pair $\{b_1,b_2\}=\{0,0\}$ on IBM Q [79].

Figure 50(b) Robust controlled quantum teleportation of a classical pair $\{b_1,b_2\}=\{1,0\}$ on IBM Q [79].

Figure 50(c) Robust controlled quantum teleportation of a classical pair $\{b_1,b_2\}=\{0,1\}$ on IBM Q [79].

Figure 50(d) Robust controlled quantum teleportation of a classical pair $\{b_1,b_2\}=\{1,1\}$ on IBM Q [79].

Unlike the implementation on Quirk platform[78] of **Figures 49** that represent everything on the same graph, **Figures 50** show the result of the teleportation of two classical bits on IBM Q platform [79] in two graphs: on the left we have the quantum circuit, while, on the right, we have the probability bars. Although with fewer witness tools than in the case of Quirk, the implementation on IBM Q gives similar results, allowing us to check the success in the teleportation of classical information. The experiment parameters were: shots = 1024, and seed = 7. A fundamental fact to keep in mind is that we do not have the possibility of using quantum measurement in any arbitrary point of the quantum circuit on IBM Q platform, but in the end only. Besides, we cannot create pairs of classical bits in a so ductile way as we did on Quirk platform. Therefore, the action of the classical bits is interpreted here as the appearance and disappearance of Pauli's X and Z gates in **Figures 50**.

The success of these implementations will allow us to use these tools in Quantum Key Distribution (QKD) [96, 97], which will play a fundamental role in Quantum Internet [88-94].

4.3.2. Instantaneous QKD based on entanglement

Clearly, the problem of quantum teleportation, in all its forms, lies in the difficulties of logistics and distribution of EPR pairs, therefore, it is impractical to use it to teleport large volumes of data, since we must distribute an EPR pair by every qubit to teleport. Although in this work we have shown that teleportation has an instantaneous version, it can only be true once the EPR pair that holds the channel (link by entanglement) has been distributed. Something that we have not mentioned so far is that this distribution will always be subject to the natural limit that implies the speed of light in the form of a photon emitted by the air, optical fiber, among other means. With this background, we can only think of a practical use of teleportation in information security. In addition, one thing is to think quantum internet between cities of a continent and another very different is to try to get quantum internet to Mars from Earth.

In other words, until solving the problem of distribution of the EPR pairs, the only argument that supports quantum internet is security. With the controlled quantum teleportation presented in this work we eliminate a channel, the classical channel, and thus automatically raise the level of security. With the uncontrolled quantum teleportation scheme, the only route exposed to hackers is the classical channel that transports the classical bits of disambiguation with which Bob reconstructs the teleported state thanks to a unitary transformation on the EPR channel. Then, the hacker cannot get the information but can alter the classical bits of the classical channel preventing Bob from having the correct information either.

The problem of the distribution of the EPR pairs is not a trivial issue at all, because we must remember that in all the versions of quantum teleportation the entanglement is eliminated to be able to complete the teleportation and not to violate the No-Cloning Theorem [85]. In fact, to date, there is not even any procedure under study in the world that can lead to avoid a new distribution of an EPR pair once the entanglement has died when wanting to teleport the next qubit of information. We can think of the entanglement is like a cow, to take advantage of its meat, first we have to kill it and if we want to make another barbecue we need another cow to kill.

The procedure for the teleportation of classical information named in the previous subsection is, in itself, a new method of quantum key distribution (QKD), where entangled photons are sent by some optical channel without useful information inside and at the speed of light. Instead, the message with the useful information travels secretly and instantaneously through a single channel, the EPR channel.

Notwithstanding what has been said, we must always transmit an element of the EPR pair just before the distribution of the key, to generate the secure and instantaneous EPR channel that allows such distribution. Next, we will test a procedure, which requires transmitting an element of the EPR pair only the first time for the distribution of the first key. From the second case onwards, we will resort to a process of virtualization of the entanglement, which will free us from the repeated, uncomfortable and impractical transmission of an element of the EPR pair before the distribution of the next key.

4.3.3. Entanglement virtualization for a more practical QKD

In every process of QKD, we identify two aspects: the tactical and the strategic. The tactical aspect is typically represented by the transmission of the key itself, which can be done by:

- an uncontrolled quantum teleportation, at the speed of light due to the transmission of the classical bits of disambiguation through a channel that is also classical, or

- a controlled quantum teleportation, which is instantaneous, without classical bits of disambiguation traveling at the speed of light, and that was already presented in this work,

and the strategic one, which puts the whole QKD procedure in a more general context, but always limited to the speed of light because of the distribution of the EPR pair by air or optical fibers.

In the strategic aspect, we are always limited by the speed of light, then, we will take advantage of this situation in the most practical way possible using the best version of the tools seen. This simply means, to continue using a classical channel for sending encrypted information, but with a series of important differences based on **Figure 51**:

- we distribute an EPR pair, then the first and only key k_0 is teleported safely and unalterably thanks to a controlled teleportation. The key can be at both ends of the link simultaneously without violating the No-Cloning theorem because it is composed of CBSs exclusively [98].

- On Alice's side:
  • with the plaintext PT_i and the previous key k_{i-1} function F builds the new key k_i,
  • with the plaintext PT_i and the new key k_i function G builds the ciphertext CT_i,

- On Bob's side:
  • with the ciphertext CT_i and the previous key k_{i-1} function F builds the new key k_i,
  • with the ciphertext CT_i and the new key k_i function G rebuilds the plaintext PT_i.

It is evident that there is an entanglement between functions F and G on both sides of the classical channel according to the four equivalent bases of Bell in this new context:

$$\left|B_{FF}\right\rangle=\left|F^A\cap F^B\right\rangle\cup\left|G^A\cap G^B\right\rangle \tag{115}$$

$$\left|B_{FG}\right\rangle=\left|F^A\cap F^B\right\rangle\underline{\cup}\left|G^A\cap G^B\right\rangle \tag{116}$$

$$\left|B_{GF}\right\rangle=\left|F^A\cap G^B\right\rangle\cup\left|G^A\cap F^B\right\rangle \tag{117}$$

$$\left|B_{GG}\right\rangle=\left|F^A\cap G^B\right\rangle\underline{\cup}\left|G^A\cap F^B\right\rangle \tag{118}$$

where, $a\cap b$ means *interaction between a and b*, $c\cup d$ means *complementation between c and d*, and, $c\underline{\cup}d$ means *anti-complementation between c and d*, i.e., they are not the known operators of union and intersection in sets theory. The action of the operators: interaction, complementation and anti-complementation, allows a satisfactory encryption and a perfect recovery of the plaintext in a perfect deterministic synchrony, which raises the level of sensitivity of the channel, in such a way that an apocryphal presence would be detected as a lack of coherence in the received message.
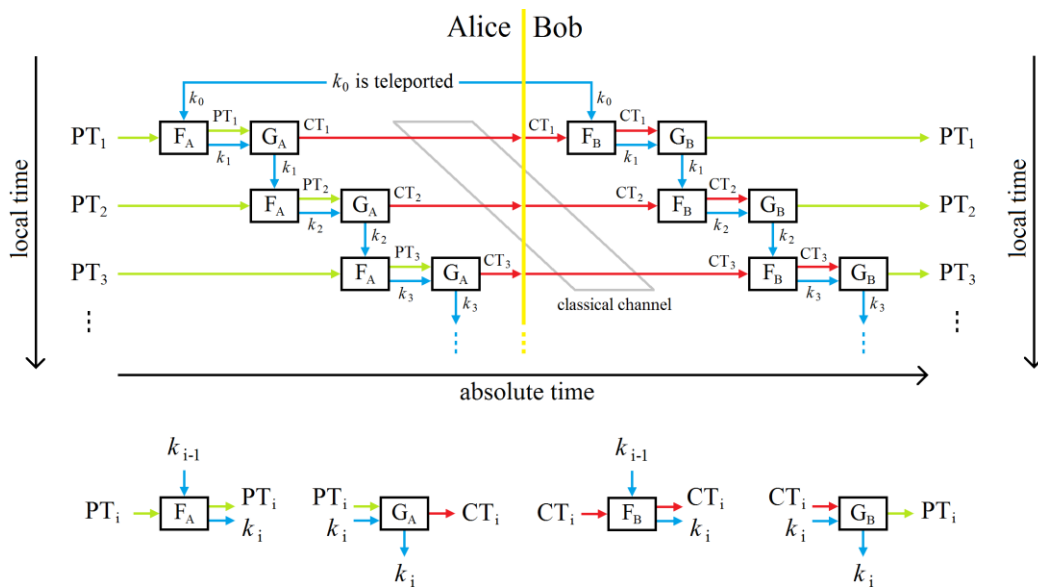

Figure 51 Virtualization of entanglement after the real quantum teleportation of the first key.

That elevation in the sensitivity level imitates the action of an observer in a quantum measurement context, where, we must remember that every quantum measurement alters what is measured. In other words, we are creating an artificial entanglement and we are keeping it alive by the action of the operators $\{\cap, \cup, \underline{\cup}\}$ and functions $\{F, G\}$ as if the flow of QKD was never interrupted.

When we say that the functions $\{F, G\}$ work with the plaintext or the ciphertext, in reality what we mean is that F and G are able to use: everything, part or a characteristic of said texts within each function. The most innocent of such a feature could be some amount of something (e.g., sum of any character of the texts). Anyway, we must understand that by putting all this in its corresponding context, i.e., quantum internet, the information will definitely be organized in frames and layers (and quantum internet protocol datagrams), so that we will have a series of other tools to play with.

When a hacker acting in the middle of the classical channel, which does not have the functions $\{F, G\}$ or the strategy between them, i.e., the correct used base $\left\{\left|B_{FF}\right\rangle, \left|B_{FG}\right\rangle, \left|B_{GF}\right\rangle, \left|B_{GG}\right\rangle\right\}$, and tries to measure the message, the result of that measurement will be like a random martingale, which emulates the also random result of a quantum measurement on an entangled particle. In addition, decoherence in the plaintext recovered by Bob will indicate an apocryphal presence in the channel. Although the analysis of Bob can be done on a witness element, which is complementary to the plaintext and before obtaining it, which can acts as a flag indicating the integrity of the procedure.

Since the whole procedure depends, in some way, on a whimsical creation of the message to be transmitted, the practical effect of the whole procedure is equivalent to the permanent change of the encryption and decryption algorithms with each message. Moreover, we can configure the procedure so that everything changes with each frame or subframe. Therefore, users should not memorize keys, nor think new ones, being the security transparent to all of them, because nobody knows its key and nevertheless it always changes capriciously and randomly with each frame (or another think controlled by clocks to both sides of classical channel) of the message, i.e., permanently.

For all that said, and although the procedure in **Figure 51** is about the teleportation of keys, it is in some way also a mechanism for teleportation of messages with important information.

Perhaps the least intuitive of the three operators $\{\cap, \cup, \underline{\cup}\}$ is that of anti-complementation, freedom or compensation, however, in all three operators, we leave each future user free to select the finest identity and combination of them to obtain the best result according to the use they want to give them.

What about the impact of noise on the procedure in **Figure 51**? This question has two answers:

- *classic*: the same impact that any classical communication system has, for which we can resort to the whole arsenal of tools tending to mitigate errors such as error correcting codes, use of parity bits, etc,

- *quantum*: the same impact expected in a quantum system when we must coexist with noisy gates and decoherence as a result of quantum measurement [37, 38] at the end of the process.

Finally, we will use this procedure within a complete information security protocol in subsection 5.4.

4.4. Entanglement and teleportation swapping

Entanglement swapping [99-105] is the technique traditionally used in quantum repeaters [106-108], evidently from uncontrolled quantum teleportation [15-19]. Here, we will present both versions seen in Section 3, i.e., uncontrolled and controlled techniques working together with:

- Entanglement Swapping, properly speaking, and
- Teleportation Swapping, i.e., the exchange of two teleported qubits between Alice and Bob in order to try bidirectionality within the quantum teleportation.

4.4.1. Entanglement swapping

Figure 52 represents the entanglement swapping thanks to the uncontrolled technique on Quirk [78], where, on the left side of that figure, we can see the generation of two pairs of entangled particles. The first EPR pair results from q[0] and q[1] qubits, which are first at ground state |0>. The second EPR pair arises from q[2] and q[3] qubits, also at ground state at the beginning.
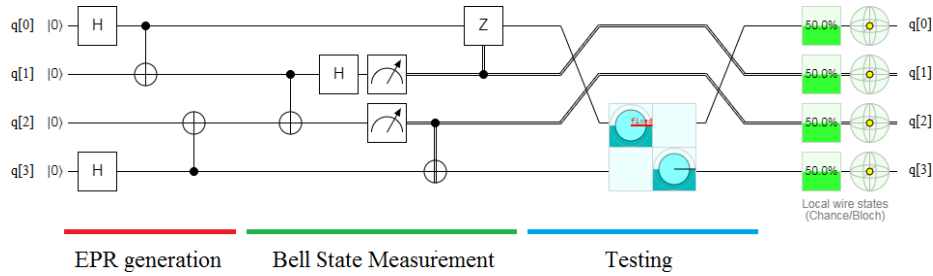

Figure 52 Entanglement swapping via the uncontrolled technique on Quirk platform [78].

After the blocks that generate the EPR pairs, we can see a BSM block. Finally, to the right of **Figure 52**, qubits q[0] and q[3] end up being entangled. Instead, **Figure 53** shows the same configuration of **Figure 52** but implemented on IBM Q [79]. **Figure 54** represents the distribution of probabilities for this experiment where the results were: 0.132+0.126+0.124+0.109 = 0.491 ~ 0.5 for |00> on the right, and 0.133+0.131+0.124+0.121 = 0.509 ~ 0.5 for |11> on the right side too, with the following experiment parameters: shots = 1024, and seed = 7. Although the action of decoherence is evident, given that the outcomes are not exactly 0.5, however, the results obtained are quite good. We must bear in mind that in every real physical implementation, a very important factor in relation to quantum internet will appear being the coherence time of the EPR pairs, and their relation with the distances to be covered during the distribution of these, which will further degrade the outcomes.

Figure 53 Entanglement swapping via the uncontrolled technique on IBM Q platform [79].

Figure 54 Distribution of probabilities for the experiment of **Figure 53**.

Figure 55 shows the entanglement swapping thanks to the controlled technique on Quirk [78]. The only difference with **Figure 52** is to replace the BSM with the BSC based on the use of the qubit reset gates [|0>]. Here also and clearly, q[0] and q[3] end up entangled as can be seen on the right of **Figure 55**. **Figure 56** represents the same configuration of **Figure 55** but on IBM Q platform [79]. This implementation is much more robust than that of **Figure 53**, as can be seen in the probability distribution of **Figure 57** with values of 0.498 for |00> and 0.502 for |11>, that is, both closer to 0.5 than those of the uncontrolled version. The experiment parameters were: shots = 1024, and seed = 7.

Figure 55 Entanglement swapping via the controlled technique on Quirk platform [78].

Figure 56 Entanglement swapping via the controlled technique on IBM Q platform [79].

Figure 57 Probability distribution for the experiment of **Figure 56**.

4.4.2. Teleportation swapping

As we have mentioned before, this technique represents an effort to give bidirectionality to quantum teleportation. That is Alice and Bob interexchange qubits at the end of the process. We are going to start with the implementation of the uncontrolled protocol on Quirk platform [78], as we can see in **Figure 58**. Now, let us suppose that Alice generates a qubit q[0] = (85.4 % |0>, 14.6 % |1>), and Bob generates another qubit q[5] = (14.6 % |0>, 85.4 % |1>). Then we have a block for the generation of two EPR pairs and then another module with a pair of SWAP gates. The following two uncontrolled quantum teleports will cross-transmit the corresponding qubits in such a way that at the end of the whole process Alice will receive in q[0] the qubit generated by Bob, while Bob will receive in q[5] the qubit generated by Alice. **Figure 59** shows us the uncontrolled protocol implemented on IBM Q platform [79], while **Figure 60** represents the probability distribution for the experiment of **Figure 59**.
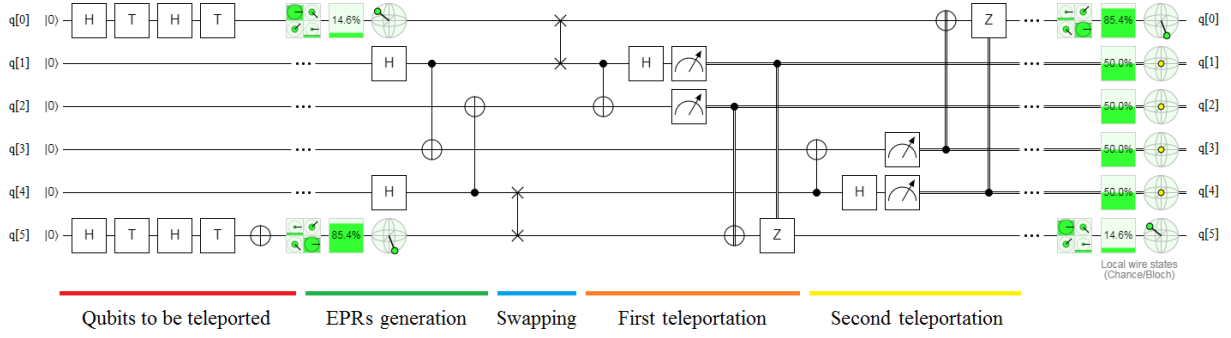
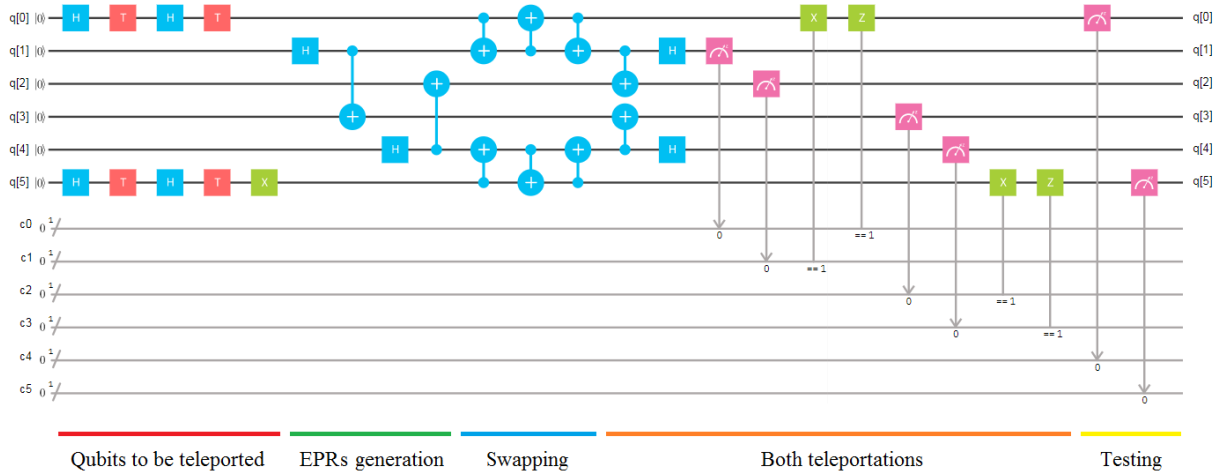**Figure 58** Uncontrolled teleportation swapping on Quirk platform [78].

Figure 59 Uncontrolled teleportation swapping on IBM Q platform [79].

Figure 60 Probability distribution for the experiment of **Figure 59**.

The results of **Figure 60** are: q[0] = (16.4 % |0>, 83.6 % |1>), and q[5] = (83.6 % |0>, 16.4 % |1>), where the experiment parameters are: shots = 1024, and seed = 7. The impact of decoherence in this experiment is evident as the number of quantum measurements [37, 38] needed increases.

As a superior alternative, **Figure 61** shows the controlled teleportation swapping on Quirk platform. The simplicity of implementation for this version versus that of **Figure 58**, is visually obvious. In fact, we expect less decoherence here than with the uncontrolled version, since the controlled version uses a smaller quantity of quantum measurements, although this cannot be verified on Quirk, then, we resort to IBM Q platform of **Figure 62**, where **Figure 63** gives us its probability distribution. This last figure gives us the following results: q[0] = (15.1 % |0>, 84.8 % |1>), and q[5] = (84.8 % |0>, 15.1 % |1>), where the experiment parameters are: shots = 1024, and seed = 7. As we had predicted, the impact of decoherence in this experiment is evidently less than the previous case (uncontrolled) since 2 quantum measurements were used instead of 6 as in the uncontrolled case of **Figure 59**. This implies the superiority of the controlled version of **Figure 62** over the uncontrolled version of **Figure 59** not only by the instantaneity but also by the accuracy.
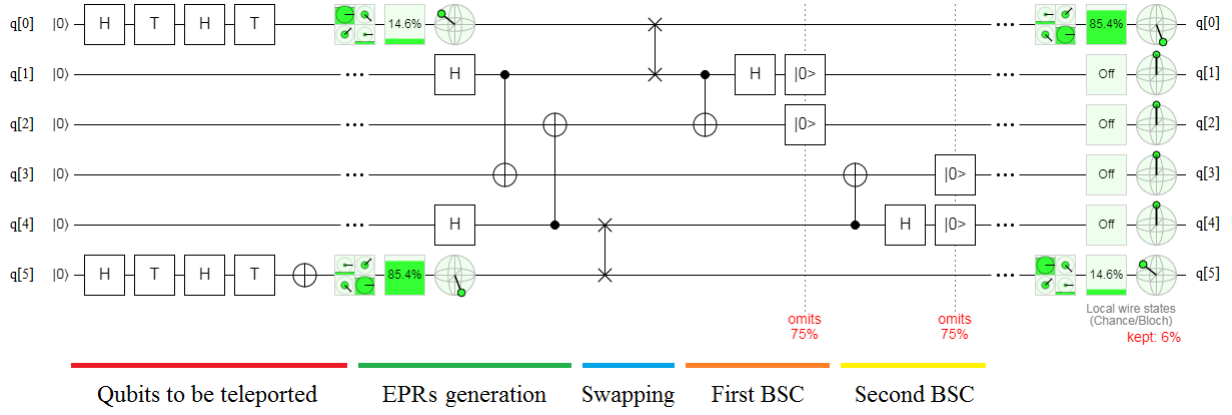
57

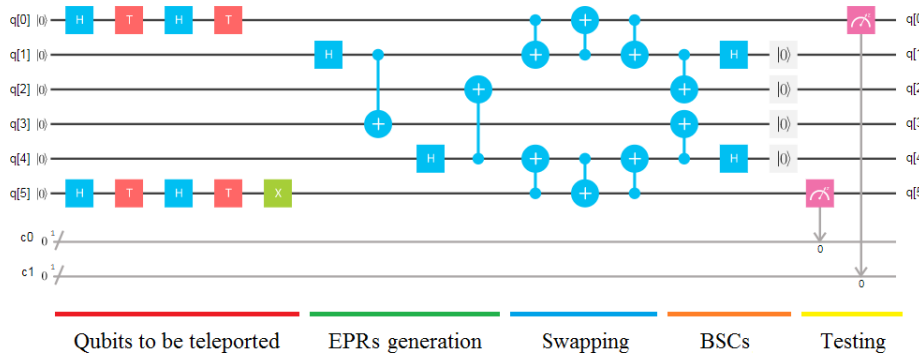**Figure 61** Controlled teleportation swapping on Quirk platform [78].

Figure 62 Controlled teleportation swapping on IBM Q platform [79].
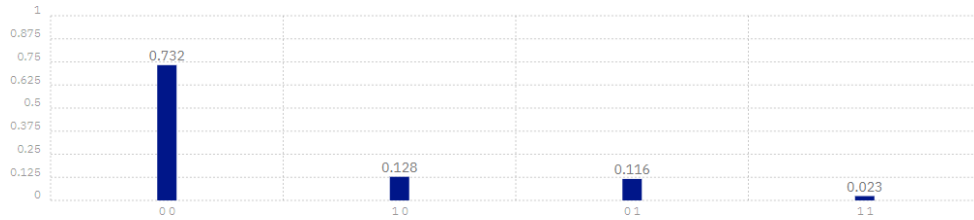

Figure 63 Probability distribution for the experiment of **Figure 62**.

5. Quantum repeaters for quantum internet

In this section we will present three protocols of quantum repeaters, namely:

- *Relay race or satellite posts*: it is a sequential protocol, which allows us to chain satellites in order to take the qubit to be teleported to any arbitrary distance,

- *Teleportation of EPRs*: in this protocol we first teleport an EPR pair (which arise from a pivot point) to two satellites in two diametrically opposed locations of the space, so that at one end we introduce the qubit to be teleported, while at the other end we receive it. It is a parallel system, which works across the width in order to divide the distribution time of the EPRs by half, taking better advantage of the coherence time. On the other hand, multiplying the number of pivot points, the range has no limits, assuring us that the complete procedure will always be within the coherence time. Finally, the pivot points can be on a planet, or on other satellites.

- *Hybridization*: It is a mix between the previous two versions.

5.1. Relay race or satellite posts

This protocol is clearly sequential and works just like a relay race, and just like in rugby the pass of information is always forward, in an exclusive manner. According to **Figure 64**, which represents the implementation of this protocol on Quirk platform [78], the qubit q[0] to be teleported is prepared to act on point (1). The first qubit teleporter puts the qubit on point (2), then, the second qubit teleporter puts the qubit on point (3), i.e., the final destination on q[4].

Figure 64 Uncontrolled *satellite post* on Quirk platform.

Notwithstanding the above, the segmentation of the quantum circuit that we can see in the lower part of **Figure 64** is not entirely accurate. The reality is that we must perform a regrouping of blocks more in line with reality according to the real responsibility of each actor involved: Alice on land, quantum satellite, and Bob on land, where the latter is obviously in a different location and it is very distant from Alice. We will only perform this regrouping for this case in order not to overload or complicate the subsequent figures corresponding to other protocols. This regrouping can be seen in detail in **Figure 65**. The first macro-block highlighted in red includes: the qubit to be teleported, the first EPR generation and distribution, and the first BSM which will transmit the disambiguation bits to the quantum satellite via a radio channel. This first macro-block will be labeled as *Alice on land*. The second macro-block highlighted in light green and labeled as *quantum satellite* includes: a unitary transformation thanks to which we will reconstruct the teleported state from an element of the first EPR pair and the classical bits received by radio, and the generation of a second entangled pair and a second BSM, which will transmit the disambiguation bits to Bob on land via another radio channel. Finally, the third macro-block highlighted in blue and labeled as *Bob on land* includes a second unitary transformation, which received the second element of the second EPR pair as well as the disambiguation bits thanks to which Bob can reconstruct the teleported state.
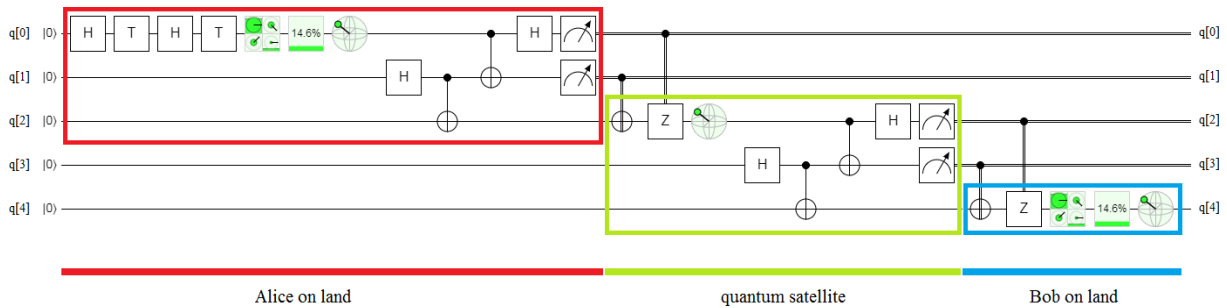

Figure 65 Reconfiguration of the layout belongs to the uncontrolled *satellite post* on Quirk platform.

Figure 66 allows us to see a practical representation of the regrouping of **Figure 65** with a clear correspondence between all the involved blocks. All begins on point A (on land), where the block labeled as BSM is inside macro-block highlighted in red in **Figure 65**, while the second BSM block

will be on board inside quantum satellite. The point B (on land) receives an element of the EPR pair and the classical bits of disambiguation emitted by the quantum satellite with which Bob applies a unitary transformation and thus reconstructs the teleported state.
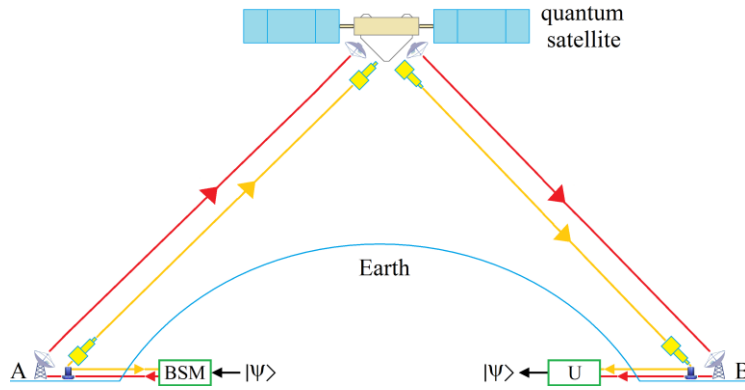

Figure 66 Detailed allocation of all elements of **Figure 65**.

Figure 67 represents the same protocol of **Figure 64** but on IBM platform, while **Figure 68** shows the probability distribution for this experiment with the next result: q[4] = (84.78 % |0>, 15.22 % |1>) where the experiment parameters were: shots = 1024, seed = 7.

Figure 67 Uncontrolled *satellite post* on IBM Q platform [79].
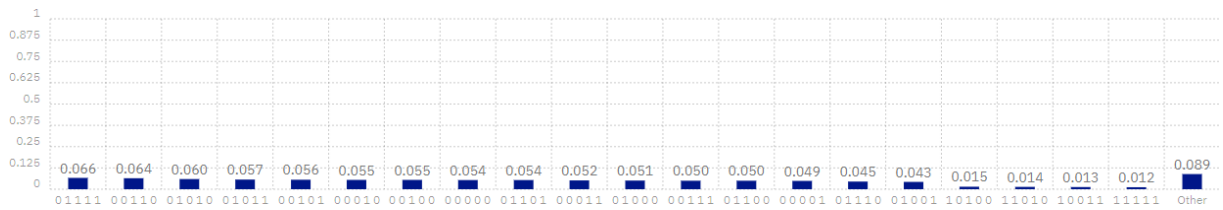

Figure 68 Probability distribution for the experiment of **Figure 67**.

We can see an implementation of the controlled *satellite post* on Quirk platform in **Figure 69**. The only difference with the uncontrolled implementation of **Figure 64**, also on Quirk, is the replacement of the BSM blocks with the BSC blocks, with all that this entails, namely: instantaneity and greater accuracy of the teleported state.
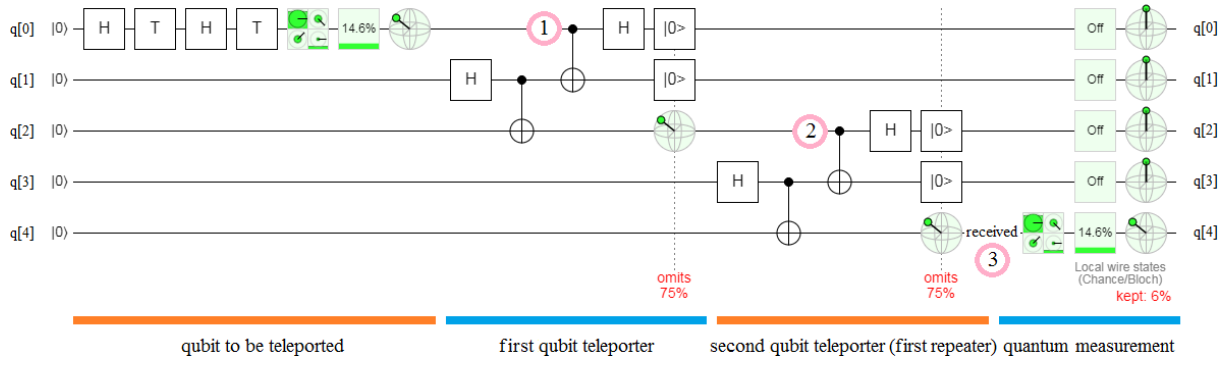
Figure 69 Controlled *satellite post* on Quirk platform [78].

Figure 70 represents the satellite scheme of Figure 69. We can check the comparative simplicity of the controlled version of Figure 70 versus the uncontrolled version of Figure 66. The first thing that is evident is the absence of the classical radio channels as well as the unitary transformation at point B, in addition to the replacement of the BSM by the BSC at point A.
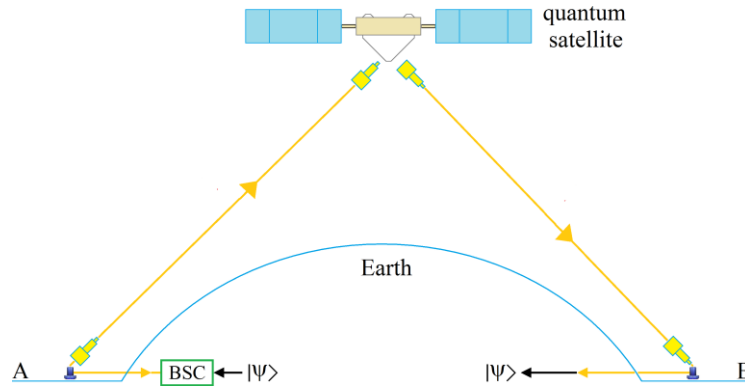

Figure 70 Detailed allocation of all elements of Figure 69.

The implementation of the controlled *satellite post* on IBM Q platform can be seen in Figure 71, with one quantum measurement instead of five like Figure 67 for the uncontrolled case. Figure 72 shows the probability distribution for this experiment with the next results: q[4] = (86 % |0>, 14 % |1>) which represents an excellent outcome for this experiment, much more accurate than the uncontrolled case. The experiment parameters were: shots = 1024, and seed = 7.
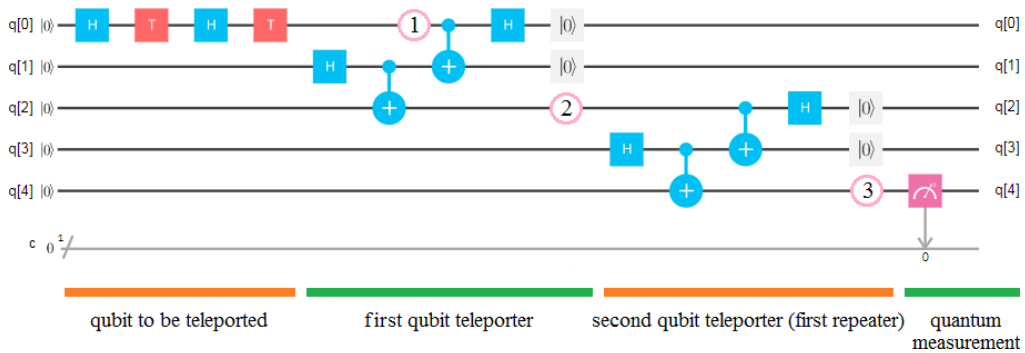

Figure 71 Controlled *satellite post* on IBM Q platform [79].

Figure 72 Probability distribution for the experiment of **Figure 71**.

5.2. Teleportation of ERPs

This protocol begins with the distribution of an EPR pair from a point called pivot (P). This pivot (P) is on the orange segment corresponding to the generation of the EPR pair, which can be seen on the left side of the Quirk implementation of **Figure 73**. Each of the elements of the EPR pair will be teleported by one of the two satellites. Said satellites will be located at an equidistant distance from the pivot (P) at opposite ends and will be responsible for teleporting the EPR pair to their two ground destinations, points (1) and (2), both on land, which make up the two ends of the communication link. Subsequently, the element of the EPR pair in point (1) and the qubit to be teleported in point (3) enter the BSM on the right of **Figure 73** on the segment labeled as qubit teleporter, whereupon the teleportation process begins. At the other end of the link (also on the ground) two sets of unitary transformations reconstruct the teleported qubit.
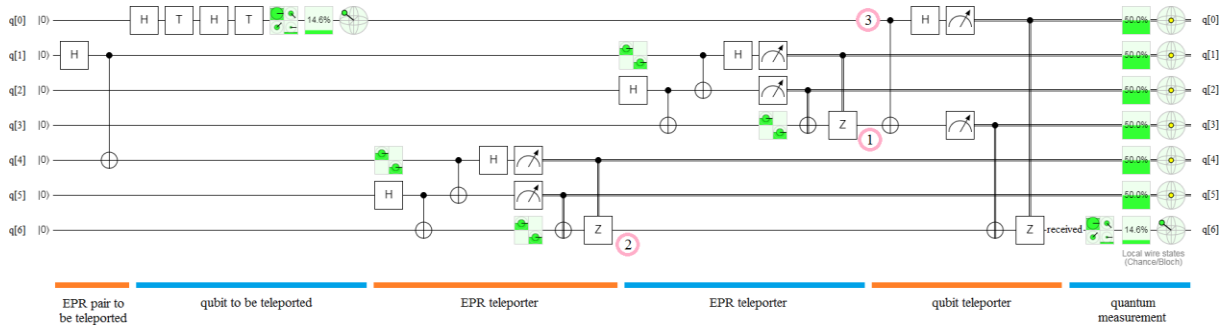

Figure 73 Uncontrolled *teleportation of EPRs* on Quirk platform.

The main reason for this protocol is to halve the distribution time of the EPRs to try to make the most of the coherence time. It is a parallel and simultaneous procedure, however, **Figure 73** does not do justice to the true protagonists of this protocol. Instead, **Figure 74** shows that in this protocol there are actually five very well-defined actors, which are macro-blocks labeled as:

- *Alice on land* (in red): this macro-block includes the qubit generation block (i.e., the qubit to be teleported), and the last BSM for the final qubit teleportation,
- *EPRs to be teleported* (in green): it is simply a block for the generation of an EPR pair, which are distributed from land,
- *Quantum satellites* (in blue): they are two, each with its own block of EPR pair generation, and BSM, and
- *Bob on land* (in yellow): which includes two sets of unitary transformations for the reconstruction of the teleported state and the final measurement process.

The reconfiguration of the layout which belongs to the controlled *teleportation of EPRs* on Quirk of **Figure 74** can be understood better from **Figure 75**, where we can see: the pivot (P) on the north pole of Earth, both quantum satellites, and the points A (emitter) and B (receiver). The last unitary transformation at the point B receives the classical bits for disambiguation from Internet. Both quantum satellites contain their own EPR pair generation and BSM blocks.
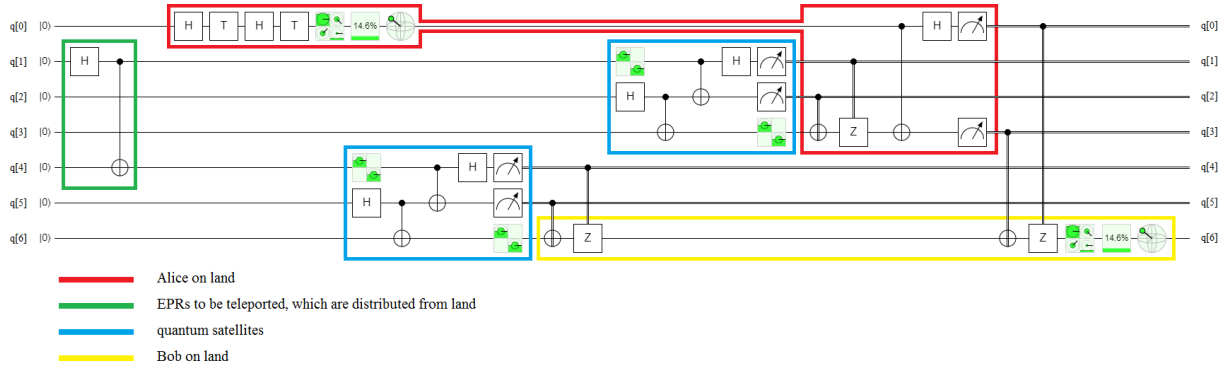
Figure 74 Reconfiguration of the layout belongs to the uncontrolled *teleportation of EPRs* on Quirk.
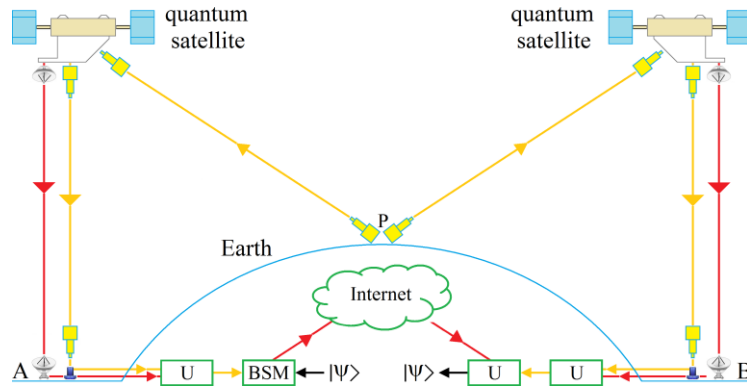

Figure 75 Detailed allocation of all elements of **Figure 74**.

The uncontrolled *teleportation of EPRs* on IBM Q platform can be seen in **Figure 76**. It is an identical scheme to that of **Figure 73** for the Quirk platform. **Figure 77** shows the probability distribution for this experiment with the next result: q[4] = (83.19 % |0>, 16.80 % |1>), where the experiment parameters were: shots = 1024, seed = 7. The obtained results are clearly of inferior quality to those of **Figures 67** and **68** for the case of uncontrolled *satellite post*, which is reasonable because in that experiment five quantum measurements were used, while in this experiment with *teleportation of EPRs*, as shown in **Figure 76**, we had to use seven. The increase in the quantum measurement number automatically increases decoherence [37, 38].
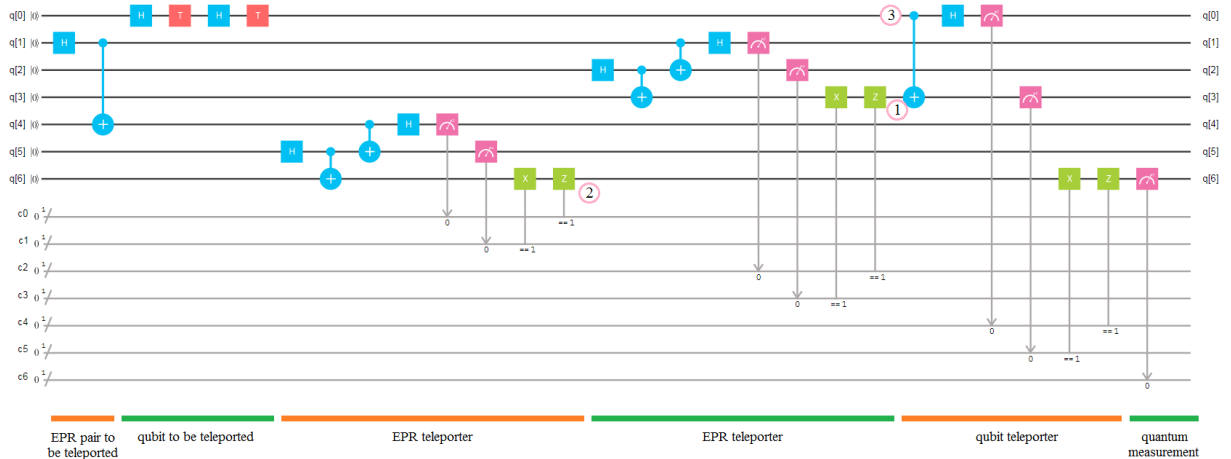

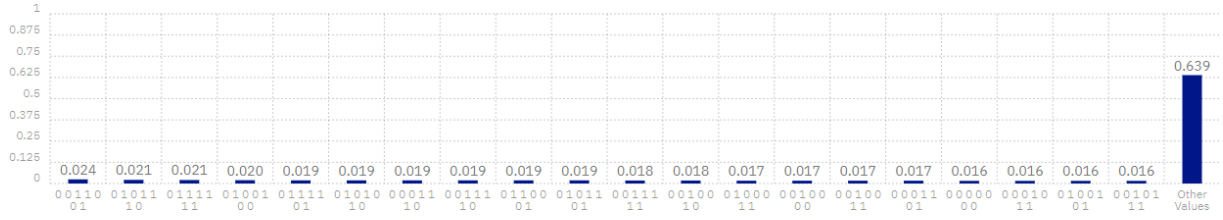**Figure 76** Uncontrolled *teleportation of EPRs* on IBM Q platform [79].

Figure 77 Probability distribution for the experiment of **Figure 76**.

Now, we present the controlled *teleportation of EPRs* protocol on Quirk platform, which can be seen in **Figure 78**. The only difference between the controlled version of **Figure 78** and the uncontrolled version of **Figure 73** is in the replacement of the three BSMs (two corresponding to the quantum satellites, and the last one on land held by Bob) with three BSCs. The coincidence between the qubit q[0] at the output of the four generation matrices of the qubit to be teleported in the upper-left corner of **Figure 78** with q[6] in the lower-right corner of this figure, tells us of a perfect teleportation, though certainly, without considering decoherence.
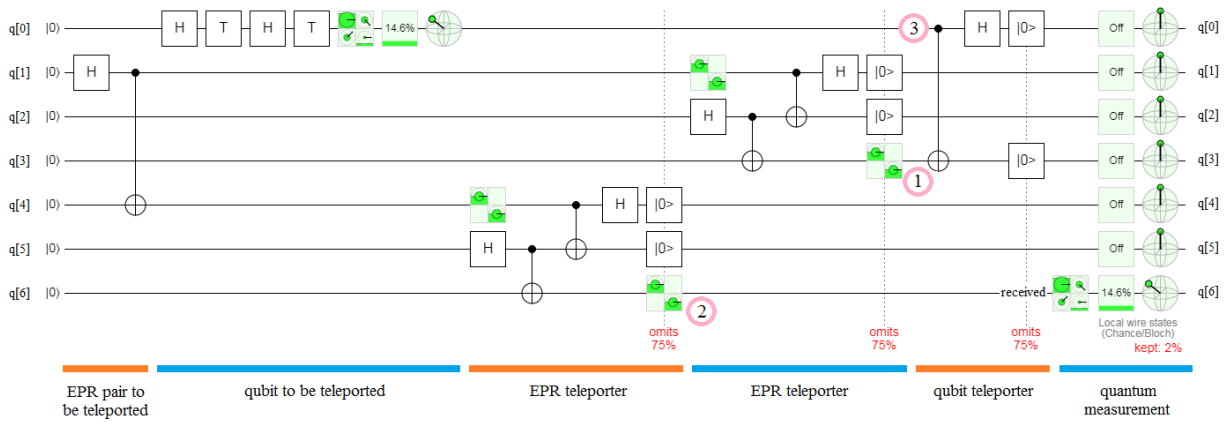

Figure 78 Controlled *teleportation of EPRs* on Quirk platform [78].

The detailed scheme about the satellite configuration of this protocol can be seen in **Figure 79**. The simplicity of this configuration compared with that of **Figure 75**, for the uncontrolled case, is remarkable. Besides, it is clearly visible, the absence of: the classical radio channels (in red) for the transmission of the classical bit of disambiguation, and the unitary transformations (in green), as well as the internet intervention.
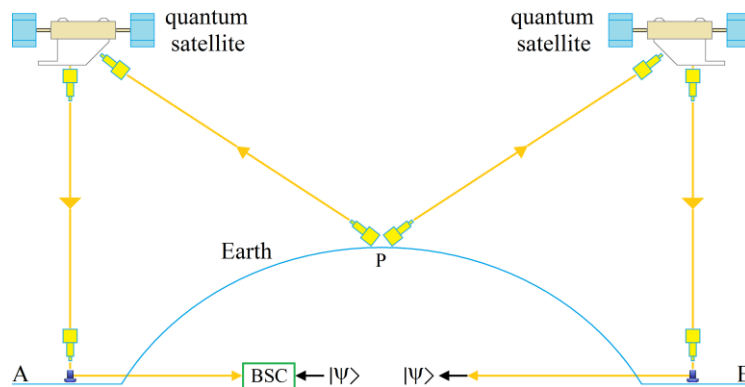

Figure 79 Detailed allocation of all elements of **Figure 78**.

Figure 80 presents this protocol implemented on IBM Q platform. **Figure 81** shows the probability bars for this experiment with the next outcome: q[6] = (86% |0>+14% |1>), which represents an absolute coincidence with the prepared qubit by this platform.

Figure 80 Controlled *teleportation of EPRs* on IBM Q platform [79].

Figure 81 Probability distribution for the experiment of **Figure 80**.

Figure 82 shows us a version of the protocol of **Figure 78** but with double pivot points (P) on Quirk, demonstrating the complete robustness of this configuration. We will have two pairs of EPR pairs to be
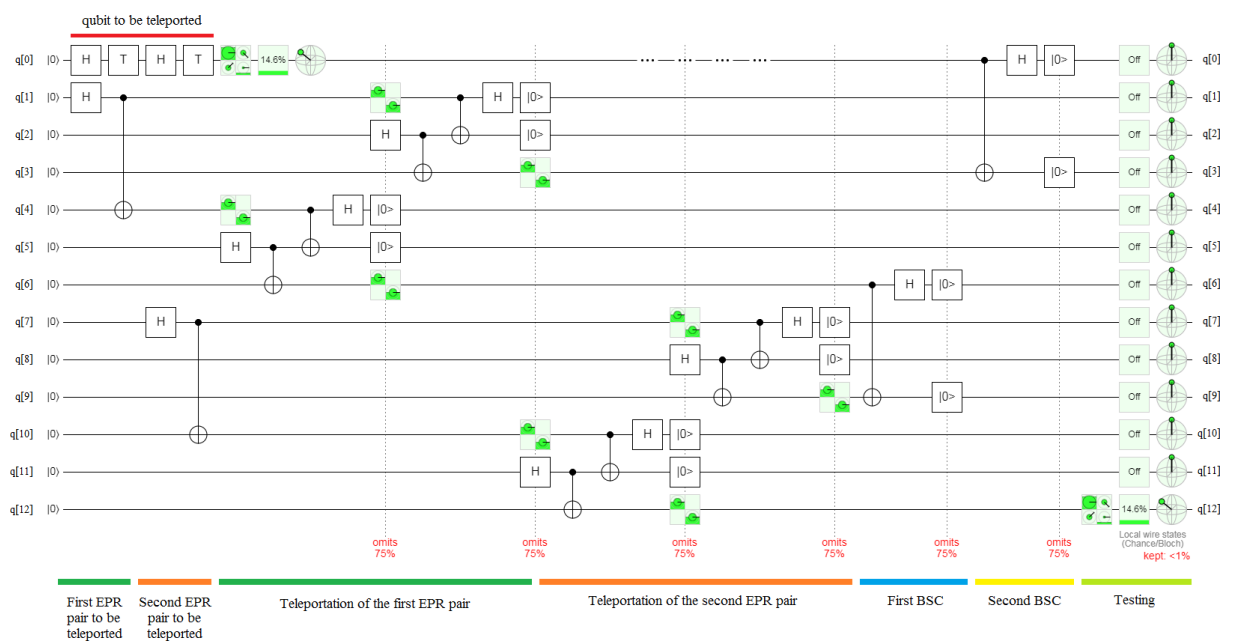

Figure 82 Controlled *teleportation of EPRs* on Quirk platform with double pivot.

distributed from land (i.e., from both pivot points) and we will need a double number of quantum satellites to teleport such EPRs. The main advantage of this protocol consists of a division by 4 of the travel itinerary of said EPRs or multiply by 4 the range of the distribution of the EPRs and thus be able to obtain a better exploitation of the coherence time. **Figure 82** shows a complete successful final teleportation, with q[0]$_{left}$ = q[12]$_{right}$. Implementations on other platforms are equally successful.

5.3. Hybridization

As we mentioned at the beginning of Section 5, hybridization consists of merging the two techniques discussed above: *satellite post* and *teleportation of EPRs*. **Figure 83** represents the uncontrolled hybridization on Quirk platform. The main difference between this layout and that one present in **Figure 73** is the duplication in the number of satellites that teleport each element of the EPR pair which arises from the pivot point (P). In other words, each EPR is sequentially teleported by two quantum satellites instead of one, thus multiplying by 2 the range of said distribution. Comparing the qubit q[0] to be teleported on the left-up corner of **Figure 83** with q[10] on the right-down corner of the same figure, we can see that the teleportation was completely successful.
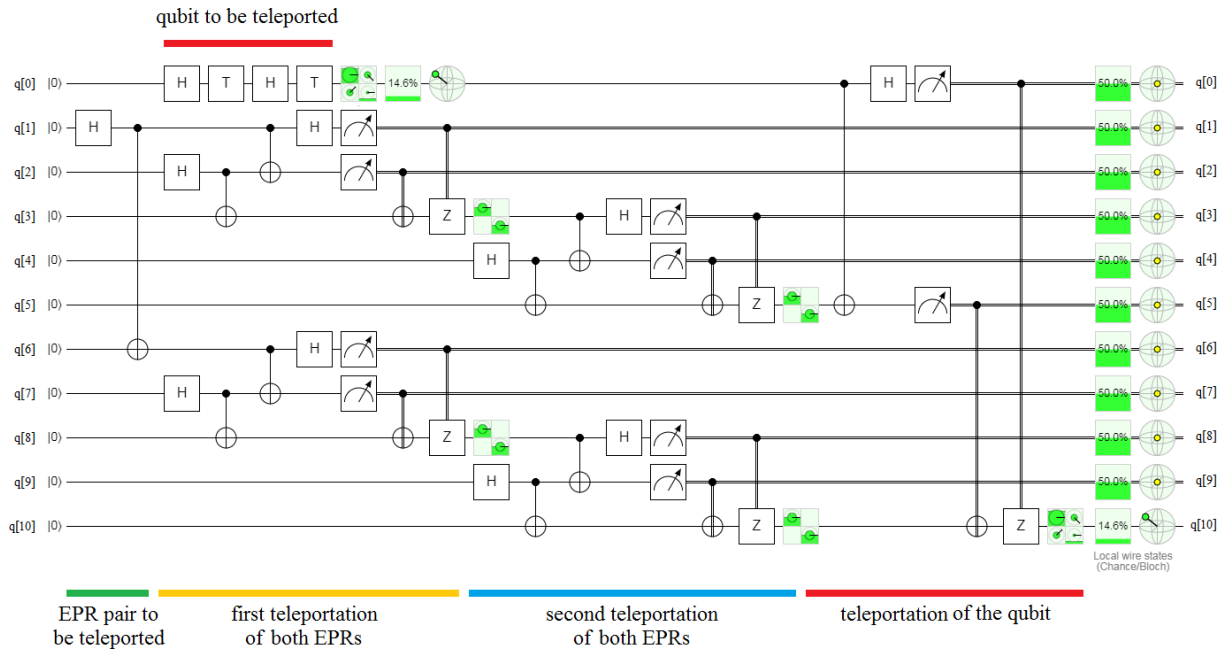

Figure 83 Uncontrolled hybridization on Quirk platform [78].

The uncontrolled hybridization on IBM Q platform [79] is presented in **Figure 84**. We can notice the absence of a figure with the probability distribution. Due to the huge number of bars of that figure, we will only give the final outcome: q[10] = (87.4% |0>+ 12.6% |1>). The presence of 11 quantum measurements explains the deterioration of the teleported qubit compared to the original value. The experiment parameters were: shots = 1024, seed = 7.

Figure 85 shows us the controlled hybridization on Quirk platform. The main difference with the configuration of **Figure 83** for the uncontrolled hybridization is the replacement of the BSM with BSC. The check point at the output of each BSC using density matrices tells us that the intermediate teleportations of the EPR pairs are developing perfectly. We could continue to add relay satellites for each element of the distributed pair and the result would still be satisfactory with a marked increase in the final teleportation range. Besides, the absence of quantum measurement and unitary transformations on Bob's side will allow us to obtain greater accuracy in the outcomes and will greatly simplify the practical implementation of this protocol.

Figure 84 Uncontrolled hybridization on IBM Q platform [79].

Figure 85 Controlled hybridization on Quirk platform [78].

Finally, **Figure 86** represents the controlled hybridization protocol on IBM Q platform, while **Figure 87** shows a very simple probability distribution for this experiment because there is only one quantum measurement. The obtained outcome is: q[10] = (86.7% |0>+13.3% |1>), which is obviously better than the outcome of **Figure 84** for the uncontrolled protocol. Moreover, the experiment parameters were: shots = 1024, and seed = 7.

Some essential elements used in every quantum repeater are the memories which are present in each BSM. We have ignored them so far because they are not part of the central axis treated incumbently in this work, however, their use in practice is necessary.

67

Figure 86 Controlled hybridization on IBM Q platform [79].

Figure 87 Probability distribution for the experiment of **Figure 86**.

5.4. Complete security protocol

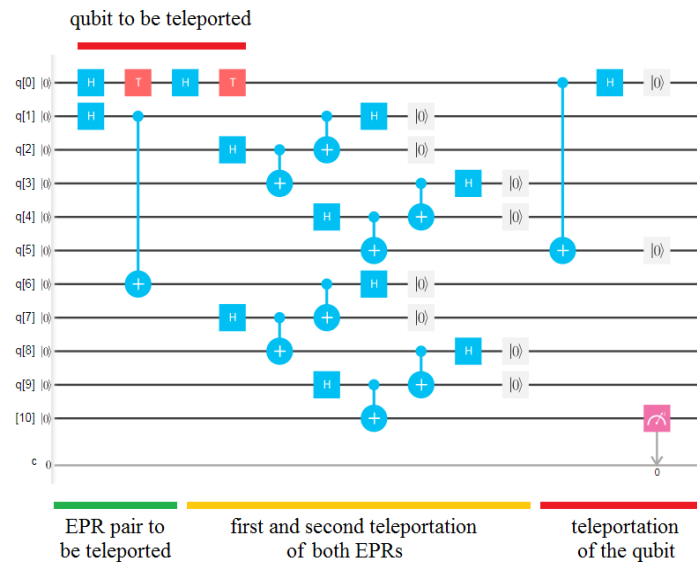Given that quantum internet uses teleportation as a fundamental tool of its toolbox and considering the need of teleportation for a redistribution of EPR pairs every time the process of reconstruction of the teleported state ends, the current quantum internet is only practical for security. Specifically, only keys are teleported. In fact, when in this context we speak of qubit to teleport, in reality we speak of the key to be distributed. This is more than evident, because if we wanted to use teleportation to disseminate messages instead of keys, the volume of information would be such that will require a distribution of EPR pairs for each qubit to teleport. This fact, by itself, would make quantum internet absolutely impractical. It is precisely in relation to what has been said that the three great challenges of the current quantum internet are:

1. a dissemination of information without violating the No-Cloning theorem [85],
2. a practical and efficient redistribution of EPR pairs each time a teleportation ends, and
3. a longer coherence time.

The three points complicate the performance of quantum internet within our planet, but the last two make it impossible to get quantum internet to Mars from Earth, although as we said before, until now. In fact, point 1 deserves further clarification. If we send by quantum internet a generic qubit, that is, a qubit with projections on the three axes of the Bloch's sphere, in order to give it discriminance against other qubits, this will have pros and cons. The pros are that only one EPR pair must be prepared to teleport said qubit, while the cons are that it cannot be disseminated to more than one destination without violating the No-Cloning Theorem [85]. On the other hand, if we want to teleport words of CBS and thus replace, even in part (since in the most general case, the same discriminance of a generic qubit would only be obtained from an infinite number of CBS), to a generic qubit, the advantage is

68

that the No-Cloning theorem is not violated because of a multi-destination distribution. However, we must prepare an EPR pair for each CBS of the word to be transmitted, which buries the efficiency of the process as a whole.

Therefore, we resign ourselves, at least for now, to the use of this fascinating tool, i.e., quantum internet, only as a surpassing version of the classical internet as far as security is concerned. For this reason, we present here a complete security protocol for quantum internet, gathering the pieces seen so far in this work, that is:

a. Cl2Qu and Qu2Cl interfaces from Subsection 4.2 (**Figures 47** and **48**),
b. Robust and controlled quantum teleportation from Subsection 4.1.6 (**Figure 41**),
c. Controlled teleportation of classical information as an improved version of QKD, from Subsection 4.3.1 (**Figure 49**),
d. Quantum repeaters from Section 5, using robust and controlled quantum teleportation, and
e. Entanglement virtualization for a more practical QKD from Subsection 4.3.3 (**Figure 51**).

In other words, taking as a frame of reference **Figure 51**, that is, the item (**e**), we take a binary key (classical), and convert it to quantum key using the Cl2Qu interface of the item (**a**). We send it to the furthest destination possible, thanks to the quantum repeaters of item (**d**), which use the controlled teleportation of classical information technique of item (**c**), which in turn uses robust and controlled teleportations of item (**b**). Once the key is received, we convert it again to binary (classical) by means of a Qu2Cl interface of item (**a**). From that moment on, the virtualization of the entanglement gives perpetual continuity to the change of key process and transmission of encrypted information.

The security procedure described above is the seed of a new quantum internet, which will be:

I. more secure, by removing the classical channel, since in the traditional technique the hacker cannot get useful information, but can alter the classical bits that circulate through the channel also classical and thus making Bob receive wrong information,
II. more robust, by removing most quantum measurements and by the simplicity of Eq.(99) versus Eq.(80),
III. instantaneous, according to what we have seen in Section 2, 3, and 4,
IV. more practical, since only the first EPR pair should be distributed, from then on the keys are reconstructed by the entanglement virtualization, and,

consequently, quantum internet will have:

V. best quantum repeaters.

6. Conclusions and future works

Next, we will develop the conclusions and the proposal for future works that derive from this work.

6.1. Conclusions

From this work, we can draw several conclusions, however before listing them, we will regroup the blocks of the controlled quantum teleportation protocol of **Figure 28** according to the upper part of **Figure 88**, which, as we can see, ends up becoming a large SWAP or big cross. As in treasure maps, the cross represents a key point. This point is of capital importance for the avatars, because for them the whole universe is a point and time is an instant. It is evident that at the exit of the great SWAP, we get again the same thing that we have introduced in its entrance. This is also a testimony to the reusability of the elements involved in the controlled protocol, which can be seen in the lower part of **Figure 88**, where the reusability can have different configurations, although the chain can be extended indefinitely with any of them, i.e.: a queue or a ring. However, as we have seen previously, reusability is not synonymous with simultaneity due to the action of the No-Cloning Theorem [85].
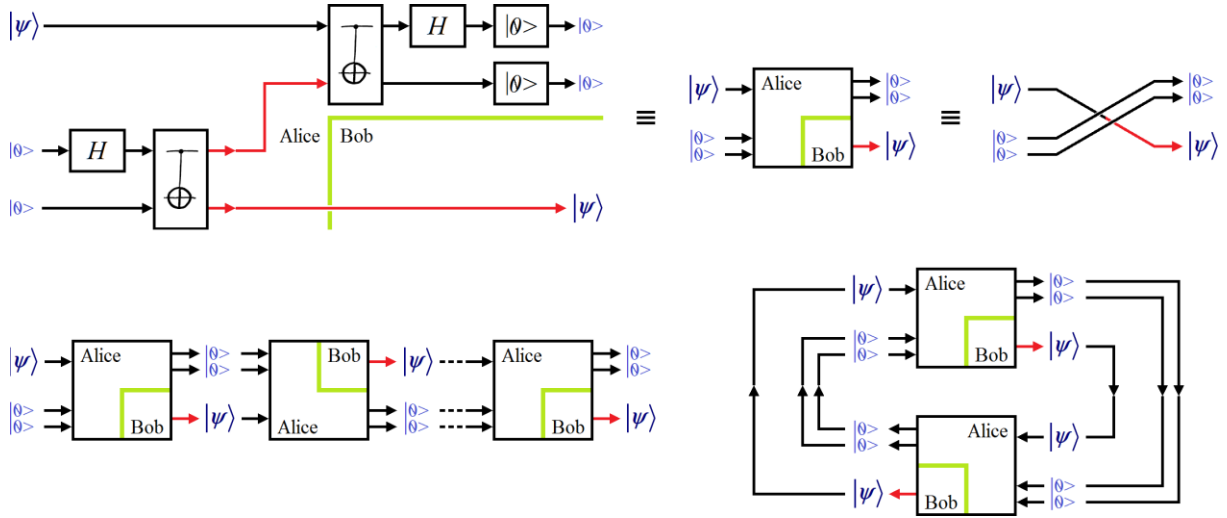
Figure 88 *Upper part*: the controlled quantum teleportation ends up in a big SWAP or cross. *Lower part*: the reusability of this protocol is evident in any configurations that involve it.

Moreover, the implementations related to the controlled quantum teleportation protocol of Section 3.2.2 (**Figure 28**) verify everything demonstrated in Section 2 regarding the avatars:

1. there is not the slightest hint of an impediment for an instantaneous communication on an EPR channel for a procedure based on the control of the experiment instead of its measurement,

2. no faster-than-light speed or superluminal signaling is required for:
   - an instantaneous communication between two entangled particles,
   - an instantaneous quantum teleportation,
   - a turtle to instantly travel a path of zero length, since, there is nothing more traversable than a zero-length path, then for
   - every wormhole created from two entangled black holes will be traversable.

3. a gap in this specialty was filled in the literature, which did not explain the instantaneous communication of nature during entanglement, alluding that the latter violated Special Relativity. In fact, not only this does not happen but in the light of this work, now we know that:
   - there is no contradiction between Special Relativity and Quantum Mechanics (Section 2), then
   - it is demonstrated that Quantum Mechanics is a complete theory, deactivating the EPR paradox [26],
   - behind-the-scenes there are elements that are reflections of the original entangled spins and that we call avatars, which, based on what was seen in Section 2, act as a hinge between Special Relativity and Quantum Mechanics,
   - the entanglement is a non-local phenomena between the original entangled spins, but local among its avatars. For the avatars everything is reduced to one point, in fact, it is a recurring theme that is repeated in everything they are involved in, and this again takes us to the upper part of **Figure 88**.

4. with the symbolic logic based on the Dirac's notation, the avatars would have never been revealed and therefore we would continue to believe that there is a contradiction between the two main pillars of Physics: Special Relativity and Quantum Mechanics, and that the second one cannot explain entanglement without violating or at least contradicting the first one.

5. we understand that any effort tending to compress data for a channel with the characteristics expressed in Section 2, that is, with an unlimited bandwidth is unnecessary, in virtue of what was demonstrated in Section 2 and its verification through the subsequent implementations of Sections 3, 4 and 5, thanks to robust and controlled quantum teleportation,

6. that by becoming a hinge between Special Relativity and Quantum Mechanics the avatars are a first approximation to the Theory of Everything (TOE) [62].

Summing-up, the present work theoretically and experimentally explores what has been established by Section 2, which tries to reconcile Special Relativity with Quantum Mechanics and at the same time states that: some byproducts resulting from entanglement, called avatars, are located halfway between the entangled particles at a single intermediate point and are mutually local at that point, i.e., their locations overlap. Each entangled particle has its own avatar, which represents that entangled particle at midpoint. In fact, it is the avatars who actually communicate, given that since the distance between avatars is null, the channel of communication between them will also be. As obvious as it is, a superluminal signal is not needed to travel through a null path in a null time. Consequently, avatars act as a hinge that links both theories (Special Relativity and Quantum Mechanics) making the completeness of Quantum Mechanics clear. Moreover, a thorough analysis of the non-locality of this effect will be carried out while demonstrating that entanglement is an instantaneous phenomenon of infinite range, and that it does not require the use of a superluminal signaling for this purpose, i.e., entanglement does not violate local realism or causality. Finally, the theoretical and experimental verifications presented in Sections 3, 4 and 5 act as a notary of the validity of such new focus as well as the very existence of the avatars.

On the other hand, we know that the result of the quantum measurement of one of two entangled particles is random, but the synchronization with the other entangled particle is instantaneous and deterministic. So, obviously nature is communicating instantaneously. The problem lies in the eventual control of that resource. The response of the literature later to the EPR paradox paper [26] to this topic has been: there may be such instantaneous communication for this non-local phenomenon, however, it cannot be used to send useful information. Clearly, this response represents a cold water cloth on an infected wound, that is, nothing cures, nothing resolves, because, it is not relevant whether man can or cannot take advantage of this resource. What is important here is to find out how it is that nature communicates instantaneously. EPR paradox is not opposed to the human use of the resource, but to the very existence of that instantaneous and deterministic communication as it collides head-on with Special Relativity. Control over the resource is a completely separate argument. But if nature can communicate instantaneously, then: why cannot man? In this work, we have seen that man can effectively take advantage of this resource with total control over it.

Focusing now on Quantum Internet, and trying to answer the question in the title of this work, which is: is instantaneous quantum internet possible? The answer is: *prima facie no*, at least not for now, but not for the reasons stated in the literature [26, 35, 36], cited by the creators of the quantum teleportation in their paper [15], or remarked by Penrose in his book [109] (where, quanglement is entanglement), i.e.,

"*Not being capable directly of carrying information, quanglement does not respect the normal restrictions of relativistic causality.*" ([109], p.636),

but for the coherence time and the redistribution of a new EPR pair, that is, the need to redistribute an EPR pair each time the teleportation of a qubit ends in order to transport the next qubit, since all distribution is subject to the speed of light, i.e., it is not instantaneous.

Deepening further what Penrose remarked in his book, let us consider the experiment of **Figure 89** which consists of a regrouping of the blocks of **Figure 28** corresponding to controlled quantum teleportation. In the lower part of **Figure 89**, we see the generator block of the EPR pair. Each element of said pair takes opposite courses of a channel, which *ipso facto* is generated by the same distribution of the entangled elements. On the left of **Figure 89**, one of the elements of the EPR pair enters the Bell State Control (BSC) block, composed of the gates: CNOT, Hadamard's (H) and qubit reset. The qubit to be teleported $|\psi\rangle$ also enters the same BSC block. So, as we have seen throughout this work, the capacity of entanglement to transport information directly and instantaneously allows us to obtain the qubit $|\psi\rangle$ on the right of **Figure 89**.
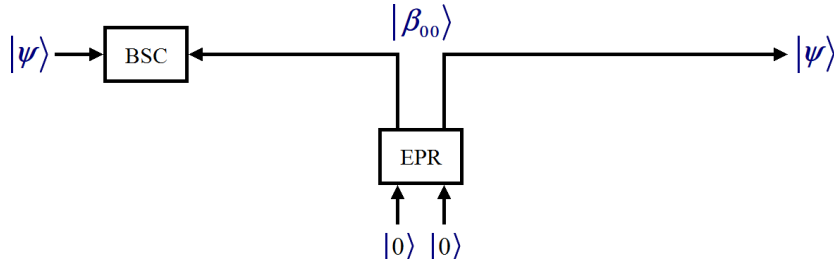
Figure 89 Experiment that contradicts what was remarked by Penrose ([109], p.636).

The control action via two qubit reset gates at the output of qubits q[0] and q[1] of **Figure 32** directly and instantly causes the qubit to be teleported to appear in Bob's hands on the right of **Figure 89**, i.e., in the thread of the qubit q[2] on the right of **Figure 32**. That is, entanglement is capable directly (and instantaneously) of carrying information, in fact, respecting the normal restrictions of relativistic causality, as demonstrated in Section 2, and contradicting what is remarked by Penrose ([109], p.636). It happens that Penrose's comment does not contemplate the control action that is the subject of the present work for entangled pairs and quantum teleportation.

Therefore, quantum internet is instantaneous from a tactical point of view because controlled quantum teleportation is, however it is not yet strategically instantaneous. The problem is that the same thing that gives instantaneity in the tactical realm (i.e., the control action of qubit reset gate), takes away in the strategic one because to be able to teleport we have to kill the entanglement first, so as not to violate the No-Cloning Theorem, and thus everything has to start again, continuously.

The problem of the redistribution of the EPR pairs is of such severity that in Subsection 4.3.3 (**Figure 51**) desperate measures have been taken to keep the entanglement alive or to fictitiously extend the lifetime of the EPRs in the context of QKD even when it has actually ended. However, this technique represents a formidable and practical tool that only requires distributing the EPRs for the first and only time in this context, i.e., QKD. What else can we do? The excessive anxiety to solve this serious problem leads us to try to climb a tree which is still a simple seed.

A solution to the controversial issue of redistribution of EPR pairs will reach all those protocols that base their operation on entanglement. It is obvious that alternatives to the Classical-to-Quantum interface of Subsection 4.2 and the controlled quantum teleportation of Subsection 3.2.2 that do not need to distribute an EPR pair for each qubit to be manipulated are required. We may conclude that a mechanism to reconstruct entanglement once the teleported qubit has been recovered is needed locally from Bob and Alice's side, simultaneously. Anyway, this is the great challenge ahead that quantum internet has.

On the other hand, the distribution of the EPR pair can be interrupted by any factor that blocks the optical link, or any other means used for distribution, but once the distribution is established, nothing will interrupt the entanglement, since the avatars are all together at the same point, therefore, a link based entanglement does not suffer fading, vanishing, nothing interrupts it, it does not need antennas, or high power transmission systems. Also, it is important to mention that the entanglement is a monogamous process [1-3]. Summing up, a link based on entanglement is then the epitome of communications making data compression and security unnecessary. Indeed, if we managed to solve the problem of the redistribution of the pairs EPRs and extend the coherence time, any security scheme such as QKD would be absolutely unnecessary compared to the intrinsic security of entanglement.

Finally, it is incredible, and at the same time, impressive how the power of something that we cannot see has given rise to everything developed in this work, that is, the avatars. Maybe, that power has to do with the famous Antoine de Saint-Exupery quote [110]:

"It is only with the heart that one can see rightly; what is essential is invisible to the eye".

6.2. Future works

It is up to companies like IBM or Rigetti to implement the qubit reset gate [|0>] on their QPU in coherence time. Whoever achieves it first, will dominate the world of quantum communications, in general, and quantum internet, in particular.

It remains for us:
- to try to solve the problem of the redistribution of EPR pairs every time a teleportation ends,
- to increase the coherence time,
- to develop a type of distribution of information that does not violate the No-Cloning Theorem,
- to evaluate on a QPU which of the two versions of controlled quantum teleportation is more robust: **Figure 28** or **41**, and
- to analyze more deeply if the avatars are some kind of non-local hidden variable.

References

1. Audretsch, J.: Entangled Systems: New Directions in Quantum Physics. Wiley-VCH Verlag GmbH & Co., Weinheim, Germany. (2007)
2. Jaeger, G.: Entanglement, Information, and the Interpretation of Quantum Mechanics. The Frontiers Collection. Springer-Verlag. Berlin, Germany. (2009)
3. Horodecki R, *et al*.: Quantum entanglement. (2007) arXiv:quant-ph/0702225
4. Abellán C, *et al*.: Challenging local realism with human choices: The BIG Bell Test Collaboration. *Nature*, 557, 212–216. (2018)
5. Popescu S, Rohrlich D.: Causality and Nonlocality as Axioms for Quantum Mechanics. (1997) arXiv.org:quant-ph/9709026
6. Ghirardi, G.C., *et al*.: Experiments of the EPR Type Involving CP-Violation Do not Allow Faster-than-Light Communication between Distant Observers. *Europhys. Lett.* 6, 2, 95-100. (1988)
7. Eberhard, P.H., Ross, R.R.: Quantum field theory cannot provide faster-than-light communication. *Found. Physics Letters*. 2, 2, 127-149. (1989)
8. Einstein, A., *et al*.: The Principle of Relativity: a collection of original memoirs on the special and general theory of relativity. Courier Dover Publications, N.Y. (1952)
9. Phillips, A.C.: Introduction to Quantum Mechanics. Wiley, N.Y. (2003)
10. Bell, J.S.: Speakable and unspeakable in quantum mechanics. 52-62. Cambridge University Press, Cambridge. (2004)
11. Bancal, J.-D., *et al*.: Quantum non-locality based on finite-speed causal influences leads to superluminal signaling. *Nature Physics*. 8, 867-870. (2012)
12. Herbert, N.: FLASH-A superluminal communicator based upon a new kind of quantum measurement. *Found. Physics*. 12, 12, 1171-1179. (1982)
13. Weinstein, S.: Superluminal Signaling and Relativity. *Synthese*, 148:2, 381-399. (2006)
14. Weinstein, G.: Einstein on the Impossibility of Superluminal Velocities. (2012) arXiv: physics.hist-ph/1203.4954
15. Bennett, C.H., *et al*.: Teleporting an Unknown Quantum State via Dual Classical and Einstein-Podolsky-Rosen Channels. *Phys. Rev. Lett*. 70, 1895. (1993)
16. Bouwmeester, B.D., *et al*.: Experimental quantum teleportation, *Phil. Trans. R. Soc. Lond. A*, 356, 1733-1737. (1998)
17. Bouwmeester, D., *et al*.: Experimental Quantum Teleportation. *Nature*, 390, 575–579. (1997)

18. Boschi, D., *et al*.: Experimental Realization of Teleporting an Unknown Pure Quantum State via Dual Classical and Einstein-Podolsky-Rosen Channels. *Phys. Rev. Lett.*, 80, 1121. (1998)
19. Kurucz, Z., Koniorczyk, Z., Janszky, J.: Teleportation with partially entangled states. *Fortschr. Phys.* 49:10–11, 1019–1025. (2001)
20. Walleczek, J., Grössing, G.: The Non-Signalling theorem in generalizations of Bell's theorem. (2014).
21. Bacciagaluppi, G.: Insolubility from No-Signalling. *Int. J. Theo. Phys*. 53, 3465-3474. (2013)
22. De Martini, F., Santamato, E.: Nonlocality, No-Signalling and Bell's Theorem investigated by Weyl's Conformal Differential Geometry, *Physica Scripta*, T163, 014015. (2014)
23. Abramsky, S., Brandenburger, A., Savochkin, A.: No-Signalling is Equivalent to Free Choice of Measurements. (2014)
24. Walleczek, J., Grössing, G.: Nonlocal Quantum Information Transfer Without Superluminal Signalling and Communication, *Found Phys*, 46, 1208–1228. (2016)
25. Ghirardi, G.C., *et al*.: A General Argument against Superluminal Transmission through the Quantum Mechanical Measurement. Process. *Lettere al Nuovo Cimento*, 27:10, 293-298. (1980)
26. Einstein, A., Podolsky, B., Rosen, N.: Can Quantum-Mechanical Description of Physical Reality Be Considered Complete? *Phys. Rev.* 47:10, 777–780. (1935)
27. Mayers, D., Tourenne, C.: Violation of Locality and Self-Checking Source: A Brief Account. In: Tombesi P, Hirota O. (eds) Quantum Communication, Computing, and Measurement 3, 269-276. Springer, Boston, MA. (2002)
28. Chen, Z.-B., Yu, S., Zhang, Y.-D.: Violations of Locality Beyond Bell's Theorem. (2003) arXiv:quant-ph/0307143
29. Dalton, B.J., Reid, M.D.: Quantum Theory and Local Hidden Variable Theory: General Features and Tests for EPR Steering. (2016) arXiv:quant-ph/1611.09101
30. Bell, J.: On the Einstein Podolsky Rosen paradox. *Physics Physique Fizika*. 1:3, 195-200. (1969)
31. Clauser, J.F., *et al*.: Proposed experiment to test local hidden-variable theories. *Phys. Rev. Lett*., 23, 15, 880-884. (1969)
32. Leggett, A.J.: Nonlocal Hidden-Variable Theories and Quantum Mechanics: An Incompatibility Theorem, *Found. Phys.*, 33, 10, 1469-1493. (2003)
33. Bera, M.N., *et al*.: Randomness in Quantum Mechanics: Philosophy, Physics and Technology. (2017) arXiv:quant-ph/1611.02176
34. Bohm, D.: A Suggested Interpretation of the Quantum Theory in Terms of "Hidden" Variables. I. *Phys. Rev.* 85, 2, 166–179. (1952)
35. Einstein, A.: in Albert Einstein, Philosopher Scientist, edited by P. A. Schilpp, Evanston, Library of Living Philosophers, 85. (1949)
36. Shimony, A.: in Proceedings of the International Symposium on Foundations of Quantum Theory, Physical Society of Japan, Tokyo. (1984)
37. Busch, P., Lahti, P., Pellonpää, J.P., Ylinen, K.: Quantum Measurement. Springer, N.Y. (2016)
38. Schlosshauer, M.: Decoherence, the measurement problem, and interpretations of quantum mechanics. *Reviews of Modern Physics*. 76:4, 1267–1305. (2005)
39. Nielsen, M.A., Chuang, I.L.: Quantum Computation and Quantum Information. Cambridge University Press, Cambridge. (2004)
40. Kaye, P., Laflamme, R., Mosca, M.: An Introduction to Quantum Computing. Oxford University Press, Oxford. (2004)
41. Stolze, J., Suter, D.: Quantum Computing: A Short Course from Theory to Experiment. WILEY-VCH Verlag GmbH & Co. KGaA. Weinheim, Germany. (2007)
42. Dieks, D.: Communication by EPR devices. *Physics Letters A*, 92:6, 271-272. (1982)
43. Yu, X.-T., Zhang, Z.-C., Xu, J.: Distributed wireless quantum communication networks with partially entangled pairs. *Chin. Phys. B*, 23:1, 010303. (2014)
44. NIST: Quantum Computing and Communication. CreateSpace Independent Publishing Platform. (2014)
45. Hadamard, J.: Lessons in Geometry: I. Plane Geometry. American Mathematical Society. Providence, R.I. (2008)
46. Meserve, B.E.: Homothetic transformations: Fundamental Concepts of Geometry, 166-169. Addison-Wesley, N.Y. (1955)

47. Tuller, A.: A Modern Introduction to Geometries, University Series in Undergraduate Mathematics, D. Van Nostrand Co., Princeton, N.J. (1967)

48. Aspect, A., Grangier, P., Roger, G.: Experimental Realization of Einstein-Podolsky-Rosen-Bohm Gedankenexperiment: A New Violation of Bell's Inequalities. *Phys. Rev. Lett*. 49:2, 91-94. (1982)

49. Tittel, W., *et al.*: Experimental demonstration of quantum correlations over more than 10 km. *Phys. Rev. A*, 57:5, 3229-3232. (1998)

50. Einstein, A., Lorentz, H.A., Minkowski, H., Weyl, H.: The Principle of Relativity: a collection of original memoirs on the special and general theory of relativity. Courier Dover Publications. N.Y. (1952)

51. Gao, P., Jafferis, D.L., Wall, A.C.: Traversable Wormholes via a Double Trace Deformation. (2017) arXiv:hep-th/1608.05687

52. Maldacena, J., Stanford, D., Yang, Z.: Diving into traversable wormholes. (2017) arXiv:hep-th/1704.05333

53. Susskind, L., Zhao, Y.: Teleportation Through the Wormhole. (2017) arXiv:hep-th/1707.04354

54. Nandi, K.K., Zhangb, Y.-Z., Kumar, K.B.V.: Semiclassical and Quantum Field Theoretic bounds for traversable Lorentzian Stringy Wormholes. (2004) arXiv:gr-qc/0407032

55. Baggott, J.: *The Quantum Story: A History in*. p.97. Oxford University Press, Oxford. (2011)

56. Saunders, S.: Complementarity and Scientific Rationality. *Foundations of Physics*. 35:3, 417-447. (2005)

57. Selleri, F.: *Wave-Particle Duality*. p.55. Springer, N.Y. (2012)

58. Bohr, N.: Can Quantum-Mechanical Description of Physical Reality be Considered Complete? *Phys. Rev.*, 48:8, 696-702. (1935)

59. Eisberg, R., Resnick, R.: Quantum Physics of atoms, molecules, solids, nuclei, and particles. 2nd edition, John Wiley and Sons, N.Y. (1985)

60. MacKay, D.J.C.: Information Theory, Inference, and Learning Algorithms. Cambridge University Press, Cambridge. (2003)

61. Zeilinger, A.: Quantum teleportation and the non-locality of information, *Phil. Trans. R. Soc. Lond. A*, 355, 2401-2404. (1997)

62. De Aquino, F.: TOE: Theory of Everything. (2012) arXiv:gr-qc/9910036

63. Gambetta, J.M., Chow, J.M., Steffen, M.: Building logical qubits in a superconducting quantum computing system, npj Quantum Information, 3:2. doi:10.1038/s41534-016-0004-0 (2017)

64. Ristè, D., Bultink, C.C., Lehnert, K.W., DiCarlo, L.: Feedback control of a solid-state qubit using high-fidelity projective measurement. (2012) arXiv:cond-mat.mes-hall/1207.2944

65. Magnard, P., *et al.*: Fast and Unconditional All-Microwave Reset of a Superconducting Qubit. (2018) arXiv:quant-ph/1801.07689

66. Chou, K.S., *et al.*: Deterministic teleportation of a quantum gate between two logical qubits. (2018) arXiv:quant-ph/1801.05283

67. Geerlings, K., *et al.*: Demonstrating a Driven Reset Protocol for a Superconducting Qubit. (2013) arXiv:cond-mat.mes-hall/1211.0491

68. Ristè, D.: Feedback control of superconducting quantum circuits, Ph.D. Thesis, Technische Universtiteit Delft. (2014)

69. Erker, P., *et al.*: Autonomous Quantum Clocks: Does Thermodynamics Limit Our Ability to Measure Time? *Phys. Rev. X* 7, 031022. (2017)

70. Nigg, D.: Towards fault tolerant quantum computation. Ph.D. Thesis, Universität Innsbruck. (2016)

71. Basilewitsch, D., *et al.*: Beating the Limits in Qubit Reset with Initial Correlations. 3rd International Conference for Young Quantum Information Scientists (YQIS'2017). Max Planck Institute, page 60. (2017)

72. Wilhelm, F.K., *et al.*: Entwicklungsstand Quantencomputer. Federal Office for Information Security, Bonn, Germany. (2018)

73. Poschinger, U.G.: Quantum Optics Experiments in a Microstructured Ion Trap. Ph.D. Thesis, Ulm university, Berlin, Germany. (2010)

74. Huard, B.: Quantum information with superconducting circuits. Systèmes mésoscopiques et effet Hall quantique [cond-mat.mes-hall]. Ecole Normale Supérieure de Paris - ENS Paris. <tel-01011096> (2014)

75. Salathé, Y.D.: Toolbox for quantum computing and digital quantum simulation with superconducting qubits. Ph.D. Thesis, ETH Zurich, Switzerland. (2018)

76. Harrison, K., Munro, W.: Method and apparatus for selectively routing entanglement building. US 9.264.226 B2, USPAT. (2016)

77. Baggio, G.: Discrete - time feedback control strategies for quantum states preparation. Ph.D. Thesis, Università degli Studi di Padova, Facoltà di Ingegneria. (2011)

78. https://algassert.com/quirk

79. https://quantumexperience.ng.bluemix.net/qx/editor

80. https://quantum-circuit.com/

81. https://www.microsoft.com/en-us/quantum/development-kit

82. https://www.rigetti.com/

83. https://www.quantum-inspire.com/

84. Herbst, T., et al.: Quantum teleportation over a 143 km free-space link, International Conference on Space Optics (ICSO'2014) Tenerife, Canary Islands, Spain. (2014)

85. Wootters, W.K., Zurek, W.H.: A single quantum cannot be cloned. *Nature*, 299, 802-803. (1982)

86. Valivarthi, R., et al.: Quantum teleportation across a metropolitan fibre network. (2016) arXiv: quant-ph/1605.08814

87. https://algassert.com/post/1623

88. Kimble, H.J.: The quantum internet. Nature 453, 1023–1030. (2008)

89. Lloyd, S., et al.: Infrastructure for the Quantum Internet. ACM SIGCOMM Computer Communications Review, 34:5, 9-20. (2004) doi: 10.1145/1039111.1039118

90. Azuma, K., Kato, G.: Aggregating quantum repeaters for the quantum internet. *Phys. Rev. A*. 96, 032332. (2017)

91. Bradler, K., Siopsis, G., Wozniakowski, A.: Covert Quantum Internet. (2017) arXiv:quant-ph/1704.07281

92. Yu, N., Lai, C.-Y., Zhou, L.: Protocols for Packet Quantum Network Intercommunication. (2019) arXiv:quant-ph/1903.10685

93. Pant, M., et al.: Routing entanglement in the quantum internet, *npj Quantum Information*, 5:25. (2019) doi:10.1038/s41534-019-0139-x

94. Hellemans, A.: Two steps closer to a quantum Internet. *IEEE Spectrum*, 53:1, 11–13. (2016)

95. http://www.fi.uba.ar

96. Cariolaro, G.: Quantum Communications. Springer International Publishing, N.Y. (2015)

97. ETSI: Quantum Key Distribution (QKD); Component characterization: characterizing optical components for QKD systems. ETSI GS QKD 011 V1.1.1. (2016)

98. Arul, A.J.: Impossibility of comparing and sorting quantum states. (2001) arXiv:quant-ph/0107085

99. Żukowski, M., et al.: Event-ready-detectors bell experiment via entanglement swapping. *Phys. Rev. Lett.* 71, 4287–4290. (1993)

100. Pan, J.-W., et al.: Experimental entanglement swapping: Entangling photons that never interacted. *Phys. Rev. Lett.* 80, 3891–3894. (1998)

101. Jennewein, T., et al.: Experimental nonlocality proof of quantum teleportation and entanglement swapping. *Phys. Rev. Lett.* 88, 017903. (2001)

102. Tsujimoto, Y., et al.: High-fidelity entanglement swapping and generation of three-qubit GHZ state using asynchronous telecom photon pair sources. *Scientific Reports*, 8:1446. (2018)

103. Jin, R.-B., et al.: Highly efficient entanglement swapping and teleportation at telecom wavelength. *Scientific Reports* 5, 9333. (2015)

104. Schmid, C., et al.: Quantum teleportation and entanglement swapping with linear optics logic gates. *New Journal of Physics* 11, 033008. (2009)

105. de Riedmatten, H., et al.: Long-distance entanglement swapping with photons from separated sources. *Phys. Rev. A* 71, 050302. (2005)

106. Bechmann-Pasquinucci, H., Pasquinucci, A.: Quantum key distribution with trusted quantum relay. (2018) arXiv:quant-ph/0505089

107. Lloyd, S., et al.: Long Distance, Unconditional Teleportation of Atomic States via Complete Bell-state Measurements, *Phys. Rev. Lett.* 87, 167903. (2001)

108. Sangouard, N., *et al.*: Quantum repeaters based on atomic ensembles and linear optics. *Rev. Mod. Phys.*, 83:33-80. (2011)
109. Penrose, R.: The road to reality: A complete guide to the laws of the universe. Johathan Cape. London, UK. (2004)
110. de Saint-Exupéry, A.: The Little Prince. Samaira Book Publishers. Plano, Texas. (2018)